SYNTHESIS AND CHARACTERIZATION OF N-HYDROXYMETHYLACRYLAMIDE BASED SELF-HEALABLE HYDROGELS FOR SUPERCAPACITOR

SILVARAJ A/L DAVID

FACULTY OF SCIENCE

UNIVERSITI MALAYA

KUALA LUMPUR

2022

SYNTHESIS AND CHARACTERIZATION OF N-HYDROXYMETHYLACRYLAMIDE BASED SELF-HEALABLE HYDROGELS FOR SUPERCAPACITOR

SILVARAJ A/L DAVID

DISSERTATION SUBMITTED IN FULLFILLMENT OF THE REQUIREMENTS FOR THE DEGREE OF MASTER OF SCIENCE

DEPARTMENT OF PHYSICS

FACULTY OF SCIENCE

UNIVERSITI MALAYA

KUALA LUMPUR

2022

UNIVERSITI MALAYA

ORIGINAL LITERARY WORK DECLARATION

Name of Candidate: **SILVARAJ A/L DAVID**

Matric No: **17198303/1**

Name of Degree: **MASTER OF SCIENCE**

Title of Dissertation ("this Work"):

SYNTHESIS AND CHARACTERIZATION OF N-HYDROXYMETHYLACRYLAMIDE BASED SELF-HEALABLE HYDROGELS FOR SUPERCAPACITOR

Field of Study:

EXPERIMENTAL PHYSICS

I do solemnly and sincerely declare that:

(1) I am the sole author/writer of this Work;
(2) This Work is original;
(3) Any use of any work in which copyright exists was done by way of fair dealing and for permitted purposes and any excerpt or extract from, or reference to or reproduction of any copyright work has been disclosed expressly and sufficiently and the title of the Work and its authorship have been acknowledged in this Work;
(4) I do not have any actual knowledge nor do I ought reasonably to know that the making of this work constitutes an infringement of any copyright work;
(5) I hereby assign all and every rights in the copyright to this Work to the University of Malaya ("UM"), who henceforth shall be owner of the copyright in this Work and that any reproduction or use in any form or by any means whatsoever is prohibited without the written consent of UM having been first had and obtained;
(6) I am fully aware that if in the course of making this Work I have infringed any copyright whether intentionally or otherwise, I may be subject to legal action or any other action as may be determined by UM.

Candidate's Signature Date:

Subscribed and solemnly declared before,

Witness's Signature Date:

Name:

Designation:

SYNTHESIS AND CHARACTERIZATION OF N-HYDROXYMETHYLACRYLAMIDE BASED SELF-HEALABLE HYDROGELS FOR SUPERCAPACITOR

ABSTRACT

Hydrogels are garnering increasing interest in scientific and technological development as a result of their ability to be able to hold a large volume of water. This characteristic is possible due to the presence of a hydrophilic polymer strain, which results in the material's widespread use. Due to their soft physical properties, they are an attractive material for use as electrolytes in supercapacitors. However, when hydrogels are used as the electrolyte in supercapacitors, critical issues such as electrochemical performance, stability, and a small potential window are raised in comparison to supercapacitors constructed using organic electrolytes. Recent advancements in the development of a unique water-in-salt hydrogel electrolyte supercapacitor with a broad potential window has sparked attention. As a result, the present work utilised the free radical method to synthesize poly (N-hydroxymethylacrylamide) (PNHMA) hydrogel and lithium salt-containing hydrogel electrolytes. The free radical initiator was ammonium persulfate, while the crosslinking agent was sodium montmorillonite (clay). Lithium trifluoromethanesulfonate (LiTF) salt was introduced as an ion source due to the salt's ionization producing free-moving ions. Fourier transform infrared spectroscopy (FTIR), X-ray diffraction analysis (XRD), and field emission scanning electron microscopy (FESEM) were used to analyse the produced hydrogel electrolytes. The ionic conductivity of the produced hydrogel electrolytes was determined using electrochemical impedance spectroscopy (EIS). The hydrogel electrolyte containing 30 wt.% LiTF (NHMA3) demonstrated the maximum ionic conductivity of 6.6 x 10^{-3} S/cm and the lowest activation energy (E_a) of 0.085 eV. The hydrogel electrolytes were embedded in an

electric double layer capacitor (EDLC) using an activated carbon electrode and then characterized using cyclic voltammetry (CV) and galvanostatic charge discharge (GCD). These two approaches demonstrated that the hydrogel based supercapacitor with the setup of AC/NHMA3/AC exhibited a maximum specific capacitance of 165.19 F/g at 5 mV/s and 287.96 F/g at 200 mA/g, as well as a specific energy of 39.63 W h/kg and a specific power of 199.16 W/kg. Additionally, after 5000 cycles at a current density of 5 A/g, the supercapacitor retained 98.5 percent capacitance. As a result, it can be concluded that hydrogel electrolytes created in this study have tremendous potential for smart, lightweight, and flexible electronic devices.

Keywords : N-hydroxymethylacrylamide, Lithium trifluoromethanesulfonate, Hydrogel electrolytes, Sodium montmorillonite, Symmetric supercapacitor

SINTESIS DAN PENCIRIAN HIDROGEL BERASASKAN N-HYDROXYMETHILACRYLAMIDE BOLEH SEMBUH DIRI UNTUK SUPERKAPASITOR

ABSTRAK

Hidrogel semakin menarik minat dalam pembangunan saintifik dan teknologi hasil daripada keupayaan mereka untuk dapat menampung jumlah air yang besar. Ciri ini mungkin disebabkan oleh kehadiran terikan polimer hidrofilik, yang mengakibatkan penggunaan bahan yang meluas. Oleh kerana sifat fizikalnya yang lembut, ia adalah bahan yang menarik untuk digunakan sebagai elektrolit dalam superkapasitor. Walau bagaimanapun, apabila hidrogel digunakan sebagai elektrolit dalam superkapasitor, isu kritikal seperti prestasi elektrokimia, kestabilan, dan tetingkap berpotensi kecil dinaikkan berbanding dengan supercapacitors yang dibina menggunakan elektrolit organik. Kemajuan terkini dalam pembangunan superkapasitor elektrolit hidrogel air dalam garam yang unik dengan tetingkap berpotensi yang luas telah mencetuskan perhatian. Air bendalir dan ion garam cepat tidak bergerak dalam rangkaian hidrogel polimer, menjadi komponen perancah polimer dan meningkatkan prestasi keseluruhan supercapacitor. Hasilnya, kerja ini menggunakan kaedah radikal bebas untuk mensintesis hidrogel poli (N-hydroxymethylacrylamide) (NHMA) dan elektrolit hidrogel yang mengandungi garam litium. Inisiator radikal bebas ialah ammonium persulfat, manakala agen penghubung silang ialah natrium montmorilonit (tanah liat). Garam litium trifluoromethanesulfonate (LiTF) diperkenalkan sebagai sumber ion kerana pengionan garam menghasilkan ion bergerak bebas. Spektroskopi inframerah transformasi Fourier (FTIR), analisis pembelauan sinar-X (XRD), dan mikroskop elektron pengimbasan pelepasan medan digunakan untuk menganalisis elektrolit hidrogel (FESEM) yang dihasilkan. Kekonduksian ionik elektrolit hidrogel yang dihasilkan ditentukan menggunakan spektroskopi impedans elektrokimia (EIS). Elektrolit hidrogel yang

mengandungi 30% LiTF (NHMA3) menunjukkan kekonduksian ionik maksimum 6.6 x 10^{-3} S/cm dan tenaga pengaktifan (Ea) terendah sebanyak 0.085 eV. Elektrolit hidrogel telah dibenamkan dalam kapasitor lapisan dua elektrik (EDLC) menggunakan elektrod karbon teraktif dan kemudian dicirikan menggunakan voltammetri kitaran (CV) dan nyahcas cas galvanostatik (GCD). Kedua-dua pendekatan ini menunjukkan bahawa hidrogel AC/NHMA3/AC mempamerkan kapasiti spesifik maksimum 165.19 F/g pada 5 mV/s dan 287.96 F/g pada 200 mA/g, serta tenaga khusus 39.63 W h/kg dan kuasa khusus 199.16 W/kg. Selain itu, selepas 5000 kitaran pada ketumpatan arus 5 A/g, supercapacitor mengekalkan 98.5 peratus kapasiti. Hasilnya, dapat disimpulkan bahawa elektrolit hidrogel yang dicipta dalam kajian ini mempunyai potensi yang besar untuk peranti elektronik pintar, ringan, dan fleksibel.

Kata kunci : N-hydroxymethylacrylamide, Lithium trifluoromethanesulfonate, Hydrogel electrolytes, Sodium montmorillonite, Superkapasitor simetri

ACKNOWLEDGEMENTS

My wonderful supervisors, Prof. Dr. Ramesh A/L T. Subramaniam and Associate Prof. Dr. Ramesh Kasi, provided invaluable assistance and clear direction in the completion of my thesis. Prof. Ramesh and Dr. Ramesh were always delighted and willing to assist me in resolving my doubts and directing my approach to the thesis' final outcome.

Furthermore, Dr. Shahid Bashir was really helpful in explaining to me in detail how to execute various experiments under a tight deadline. Dr. Shahid, who is also a dear friend of mine and is a laid-back, open-minded individual. I would not have finished this without their constant encouragement. . Thank you very much!

To add to the list, I'd want to express my gratitude to all of my family members and my wife, who have provided me with tremendous incentive to complete this project.

TABLE OF CONTENTS

LIST OF FIGURES

LIST OF TABLES

CHAPTER 1 : INTRODUCTION

1.1 Background studies

The momentum of the growth of technology and modernization is happening at a rapid rate. This growth doesn't grow by itself, and it needs fuel/energy to support the growth and it is also very important to notice the importance of mobile machines, electronics, handphones and so on needs to have a worthwhile energy storage to uphold the growth mentioned above. Research shows that since the late 1980's the growth of population and consumption also contributes to price increase and demand of energy (Taylor et al., 2019). Because of the rise environmental concerns, the importance and need for renewable energy has increased. This has prompted many companies to explore various forms of energy sources such as wind and solar. Using green energy instead of fossil fuels is a cost-effective and efficient strategy to minimise our dependence on foreign oil.. However, transitioning to green energy requires the proper storage to ensure its continuous and reliable supply (Noori et al., 2019). Energy storage refers to various technologies that can be used for various applications such as electric vehicles, grid storage, and backup power (Tiruye, 2016; R. Zhang, 2016).

The rapid emergence and evolution of energy storage technologies such as supercapacitors, fuel cells, and electric vehicles, environmental-friendly energy storage technologies have been developed as a result . Although supercapacitors have high energy density, their low power densities restrict their effectiveness in high-power applications. Supercapacitors are capable of storing up to 10 times more energy than standard batteries. They can also provide fast and continuous energy supply. The exceptional properties of nanoscale capacitors can be attributed to their unique composition. This is due to the presence of a layer of attracted ions on their surface. Electrode-electrolyte's thickness are

dependent on the size of ions, the bigger the size of ions, the bigger the thickness of electrode-electrolyte interface will be (Gao, 2013).

Supercapacitors (SCs) are devices that is capable of storing energy that have numerous advantageous properties such as high power capacity, long life cycle, and reversibility. For supercapacitors, generally there are two main mechanisms which are electric double layer capacitors (EDLC) and pseudocapacitors(PC).

Electrode-electrolyte interface charge separation results in EDLC's capacitance. Whereas for pseudocapacitors this characteristic arises from the faradic reactions that occur on the electrode surface, such as transitional metal oxide based supercapacitors (Gao, 2013). SCs are commonly used as backup sources for various consumer electronic devices. They are also used as energy storage devices in hybrid vehicles and industrial equipment (Kö Tz & Carlen, 2000; Miller & Simon, 2008)

While electrochemical capacitors and batteries are similar in design, electrochemical capacitors have a higher capacitive charge storage than Faradaic capacitors (Rajeshwar, 1993). The high capacitive nature of the capacitor is responsible for the high power density, which is achieved entirely through relatively high charging and also discharging rates. These occurred solely as a function of the active material's ionic and electronic transport rates. Electrochemical capacitors are also referred to as "double-layer capacitors" due to the charging process utilising high surface area double-layer carbon electrodes (Mayer et al., 1993). However, SCs are more efficient than conventional capacitors but less efficient than a battery. On the other hand, SCs have a larger energy density than batteries (Meng et al., 2017). The electrode and electrolyte are the two primary components of a supercapacitor. There are several different types of electrolytes used in these supercapacitors. These include liquid electrolytes, gel polymer electrolytes, and solid polymer electrolytes (Zeng et al., 2020). Cost effectiveness, environmental

friendliness, high ionic conductivity, nonflammability, nontoxicity, and stability are frequently cited as criteria for selecting an electrolyte. Several electrolytes have been studied during the last decade, including aqueous electrolytes, organic electrolytes, ionic liquid electrolytes, redox electrolytes, and solid or semi-solid electrolytes. Leakage is a significant disadvantage of liquid electrolytes in systems that demand durability and extensive use. Polymer electrolytes are an alternative to liquid electrolytes. Dry solid polymer electrolytes (SPEs) and gel polymer electrolytes are two types of polymer electrolytes. Electrolytes that are semi-solid or solid are extremely promising since they possess the majority of desirable physical and chemical features. Solid polymer electrolytes (SPEs) using ceramic nanofillers are solid electrolytes that exhibit no crystallisation propensity. SPEs, on the other hand, have a low ionic conductivity. On the other hand, gel polymer electrolytes in particular could combine the advantages of liquid electrolytes and the qualities of solid electrolytes that made them desirable in the first place (Poy et al., 2020). These electrolytes have a high ionic conductivity and a higher level of safety. The use of organic solvents in conjunction with a polymer host to generate gel polymer electrolytes has a number of drawbacks, including the release of volatiles and reaction with metal electrodes. Thus, a polymer electrolyte that has been inflated with water forms a huge amorphous zone that facilitates ion transport. Hydrogel polymer electrolytes are polymer electrolytes made using water as a plasticizer in the presence of a crosslinking agent (Huang et al., 2015; Park et al., 2019). Hydrogels are polymers with a crosslinked network structure that have a high capacity for absorbing and retaining water. Hydrophilic polymers obtained from natural/synthetic sources are used to create hydrogels (Bashir et al., 2018; L. Guo et al., 2020). Synthetic hydrophilic polymers have a greater capacity for water retention. Crosslinking is more favourable since it strengthens the polymer network Feng et al., 2019; Li et al., 2019). Hydrogel electrolytes-based supercapacitors raise some problems, including poor electrochemical performance, a

small potential window, and device stability. Concerns arise as a result of water breakdown and a small potential window, which restricts the selection of electrode materials. As a result of the limited electrode material selection, the produced supercapacitor's energy density is reduced. Another consideration is the selection of a polymer host and a charge carrier that are compatible with the plasticizer (water) and have a negligible effect on electrochemical performance. To solve these problems and achieve superior electrochemical performance with aqueous-based electrolytes, the hydrogel electrolyte must have a high ionic conductivity and allow for smooth ion movement for rapid charging/discharging. The hydrogel electrolyte should possess a high concentration of hydrophilic groups to efficiently absorb and retain water, as well as a high affinity and tolerance for high concentrations of charge carriers without flocculation. Lithium ion-containing hydrogel electrolytes for supercapacitors appear promising in this regard. Though there is little evidence that hydrogel electrolytes contribute to the energy density of supercapacitors, they can provide enhanced safety and likely lower fabrication costs when compared to organic electrolyte-based supercapacitors. In electronic devices where safety must be ensured, hydrogel electrolyte-based supercapacitors may be used (Z. Wang et al., 2018). The present work used free radical polymerization to create poly (N-hydroxymethylacrylamide) hydrogels and hydrogel electrolytes containing lithium ions. N-Nhydroxymethylacrylamide, APS, and sodium montmorillonite were used as monomer, initiator, and crosslinking agent, respectively, in this free radical polymerization. On the other hand, hydrogel electrolytes were prepared using Lithium trifluoromethanesulfonate (LiTF). Fourier transform infrared spectroscopy (FTIR) and X-ray diffraction (XRD) were used to characterise the produced hydrogel and hydrogel electrolytes. Field emission scanning electron microscopy (FESEM) was used to investigate the surface morphology. Electrochemical impedance spectroscopy (EIS) analysis was used to assess the ionic conductivity of the hydrogel electrolytes at room

temperature and at elevated temperatures, as well as the effect of temperature on the ionic conductivity. Additionally, electric double layer capacitors were constructed using hydrogel electrolytes (EDLCs).

1.2 Problem statement

In the category of electrochemical energy storage systems, EDLC does have quite a number of winning factors amongst the rest of the devices. As an example, compared to common capacitors, EDLC has higher energy density, while being compared with batteries it has better power density. On top of the comparisons, it is also environmentally friendly, has fast charging-discharging rates and has long cycling stability. From these traits mentioned above, EDLC definitely will to be one of the most effective energy storage systems available in the future. Therefore, it is no doubt that supercapacitors-based devices received much attention in the recent days.

Despite having many advantages, SCs also have mechanisms that need improvement, such as having low energy densities compared to lithium batteries. This particular issue might be affected due to the materials used as electrodes, electrolytes and electrode-electrolyte interactions. To address this matter, electrodes and electrolytes must be fabricated with proper materials which also have better mechanical strength and massive electrochemical window (Alexandre et al., 2019)

In electrochemical supercapacitors, adopting suitable electrolyte plays an important role as it affects the maximum operating voltage and the device's safety. Because of their strong ionic conductivity, aqueous electrolytes or organic electrolytes are commonly utilised in EDLC. This is due to the fact that they are inexpensive, but it has some drawbacks such as leakages, toilsome transportation, highly volatile and may also cause electrode corrosion (D. Wang et al., 2018)

Scientists all over the globe have spent some great amounts of effort researching about polymer electrolytes as it gains advantage in its safety and stability. Significantly safe, increased ionic conductivity and being leak proof has made Gel Polymer Electrolytes (GPEs) and microporous polymer electrolyte (MPEs) popular in the advancement of EDLCs. The gel polymers polyacrylamide (PAAM), polyethylene oxide (PEO), and polyvinyl alcohol (PVA)-based GPEs are examples of electrolytes that are extensively employed in electrolyte distribution chromatography (EDLC) (Lu et al., 2019).

1.3 Aim and objectives of the research

To synthesize a self-healable hydrogel to be embedded in EDLC as electrolytes in the following objectives

- To sythesize hydrogels and hydrogel electrolytes
- To characterize the synthesized hydrogel and hydrogel electrolytes
- To optimize the parameters for the best performance of EDLCs
- To investigate the performance of the hydrogel electrolytes for the electrochemical applications

1.4 Scope of study

Chapter 1 introduces the hydrogel polymer electrolyte and discusses the objectives. Chapter 2 discusses the history of polymer electrolytes, their development, and the parameters that control ionic transport in hydrogel polymer electrolytes. The latter section examines the rationale behind material selection and the applications of polymers in electrochemical devices. Chapter 3 discusses the sample preparation and characterization procedures, which include Fourier transform infrared spectroscopy (FTIR), X-ray diffraction (XRD), dielectric investigations, cyclic voltammetry, and the manufacture of

electrochemical devices. Chapter 4 compares and explains the outcomes of all the characterizations. Chapter 5 concludes this investigation and the subsequent study.

CHAPTER 2 : LITERATURE REVIEW

2.1 Background studies

Rapid growth in the economy is obvious in current digital world, meanwhile what happens behind the curtain is not that obvious but surely is affecting many species or areas slowly and gradually. The impact of increased greenhouse gas emissions or global warming is largely contributed by the high consumption of fossil fuels and other non-renewable energy sources. These issues can be solved or at least can be reduced by shifting from depending on non-renewable energy recourse to renewable energy resources or focusing on improving energy storage efficiency to support the energy consumption growth rate (Winter & Brodd, 2004)

There is a data (Figure 2.1) released by The United States Department of Energy in 2019 (Energy Information Administration, 2019) which predict the energy consumption of the world till the year 2050. From the data, it is expected that our world will see a whopping 50% increase in energy consumption by the year 2050. This forecast definitely needs attention as it might lead to a global energy crisis. The same department also mentioned about the factors that contributed to the energy crisis are high costs of energy storage devices, declining natural resources, negative impacts on ecology and environment which are somehow related to heavy consumption of fossil fuel. These has created an interest for scientists all over the world to research on sustainable energy development and improving the systems for renewable energy. Exploring for alternative, reliable and cost-effective energy storage devices could be the remedy for solving the future energy need (Energy Information Administration, 2019). In addition, profound advancements in energy storage technology and advanced power conversion systems are very important as we are facing a hit from the global warming and limited sources of fossil fuels.

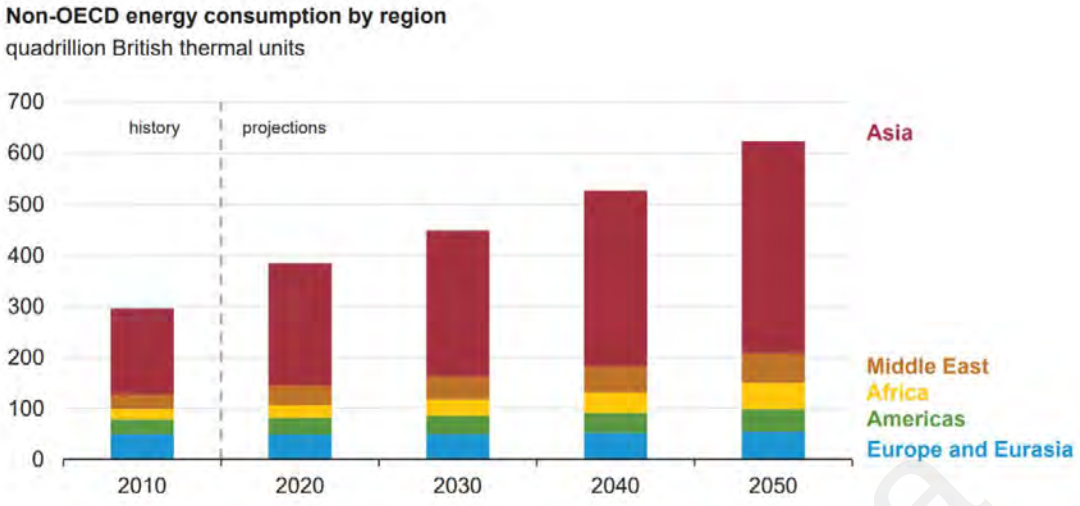

Figure 2.1 : History and projection of energy consumption from the year 2010 to 2050 (IEA, 2019)

Currently, there are a plethora of alternative energy generating technologies which are still working it's way to replace the dependence on fossil fuel. Some of the examples are solar, biomass, tidal waves, hydroelectricity, wood waste, nuclear energy, sewage gas, geothermal, landfill gas, wind etc. As good as it may sound, there are also some disadvantages coming together with these, which are the energy produced through has to be used within a short period of time, and for some specific energy forms like solar and wind energy, grid stability and managing the power takes a big toll on it. To add to it, there are consistent inconsistencies between energy generated and the demand for it. This clearly signals to scientists to research and develop efficient energy storage mechanisms or devices in order to meet the future energy demand (Energy Information Administration, 2019). Storing ample energy and supplying them with ease when needed in high quantity is the demanding technology in energy storage devices (Béguin et al., 2014). One of the main energy storage devices is capacitors, and when it is directly compared with supercapacitors, SCs surpasses the advantages (Marin Halper James C Ellenbogen, 2006). The design of supercapacitors needs immense attention such as working on the properties of electrodes, elevating the mechanisms in the electrode/electrolyte interface. The concerns on materials used play a vital role in

enhancing the technology behind SCs. The scope of improvising SCs is vital as it has huge potential in stabilizing the surging global energy need (Energy Information Administration, 2019).

2.2 Electrochemical Capacitors: Theory and Operation

In conventional capacitors, the device comprises of two metal electrodes and a dielectric material which acts as a barrier between the electrodes. Each of the metal electrodes will be filled with oppositely charged particles upon the application of voltage. The opposite charges in electrodes are set apart by the dielectric. Figure 2.2 clearly shows the description of the mentioned system (Marin Halper James C Ellenbogen, 2006).

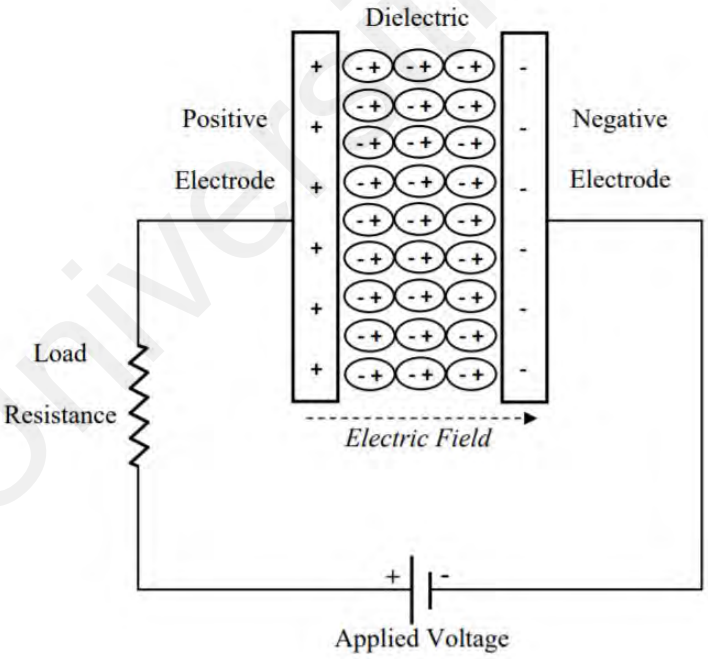

Figure 2.2 : Schematic of a conventional capacitor (R. Zhang, 2016)

Capacitance C(F) product of division of stored charge Q(Coulumb) with the applied voltage V(Volts).

$$C = \frac{Q}{V} \tag{2.1}$$

In order to calculate the Capacitance (C), the following equation below is used.

$$C = \varepsilon_0 \varepsilon_r \frac{A}{D} \tag{2.2}$$

ε_0 is the dielectric constant of free space $\left(Fm^{-1}\right)$, ε_r denotes the dielectric constant of the insulating material between the two electrodes, A represents the specific surface of each electrode $\left(m^2 g^{-1}\right)$ and D measures the distance between electrodes. The two standards in which capacitors are measured are energy density and power density. Energy (E) of capacitors are calculated as the following formula.

$$\mathrm{E} = \frac{1}{2} \mathrm{C}_{\mathrm{sp\,(GCD)}} \times (\Delta \mathrm{V})^2 \times \frac{1000}{3600} \tag{2.3}$$

Power is amount of energy transferred or converted, per unit time, when electricity is transferred. Based on Figure 2.2, to calculate P, external resistance R has to be included a factor because the capacitor mentioned mimics a circuit in series. On the other hand, the internal resistance should be included too as equivalent to series resistance (ESR) because of the internal components such as the dielectric materials, electrodes and current collectors. These resistance affects the discharge current. The maximum power P for capacitors can be evaluated by the following formula by including the impedance .(Marin S, 2006)

$$\mathrm{P} = \frac{\mathrm{E}}{\Delta \mathrm{t}} \tag{2.4}$$

From equation 2.4, we can conclude that the unit for power of a given capacitor is per unit mass or per unit volume.

Commonly, the traditional capacitors will have higher power density but lower in energy density in comparison to an electrochemical battery. This comparison is clearly shown in Figure 2.3

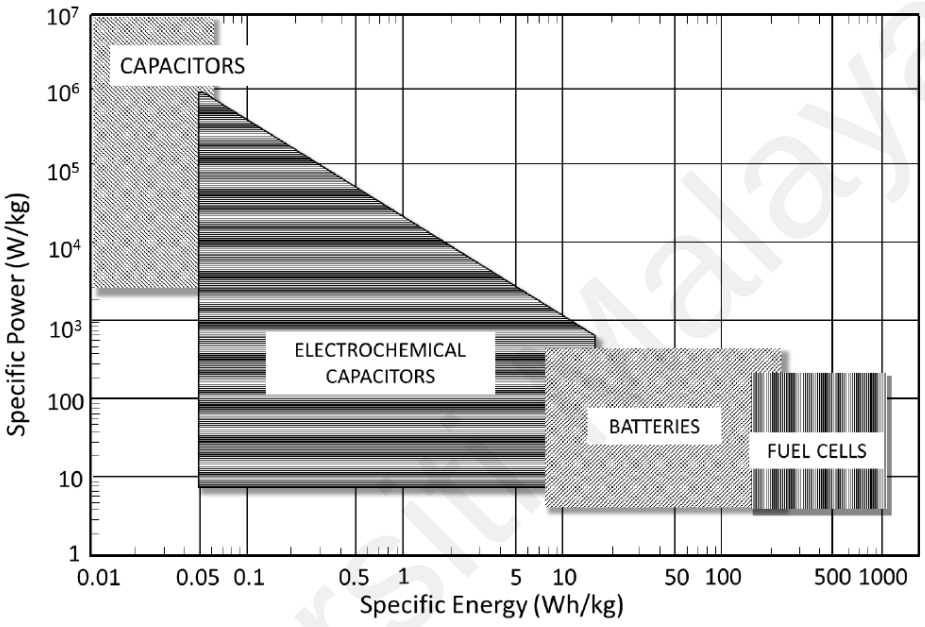

Figure 2.3 : Ragone plot for various energy storage and conversion devices (R. Zhang, 2016)

The principles on how SCs operate is almost the same. This can be clearly shown from Figure 2.2 & 2.4. Those figures, the schematic drawings of a common capacitor and a SC is portrayed. The SCs are made up by two conducting electrodes separated by a dielectric material that does not conduct electricity. Besides, SCs also have higher surface area for their conducting electrode. Due to these, capacitance and energy can be evaluated by the equation 2.2 and equation 2.4 respectively (Marin Halper James C Ellenbogen, 2006).

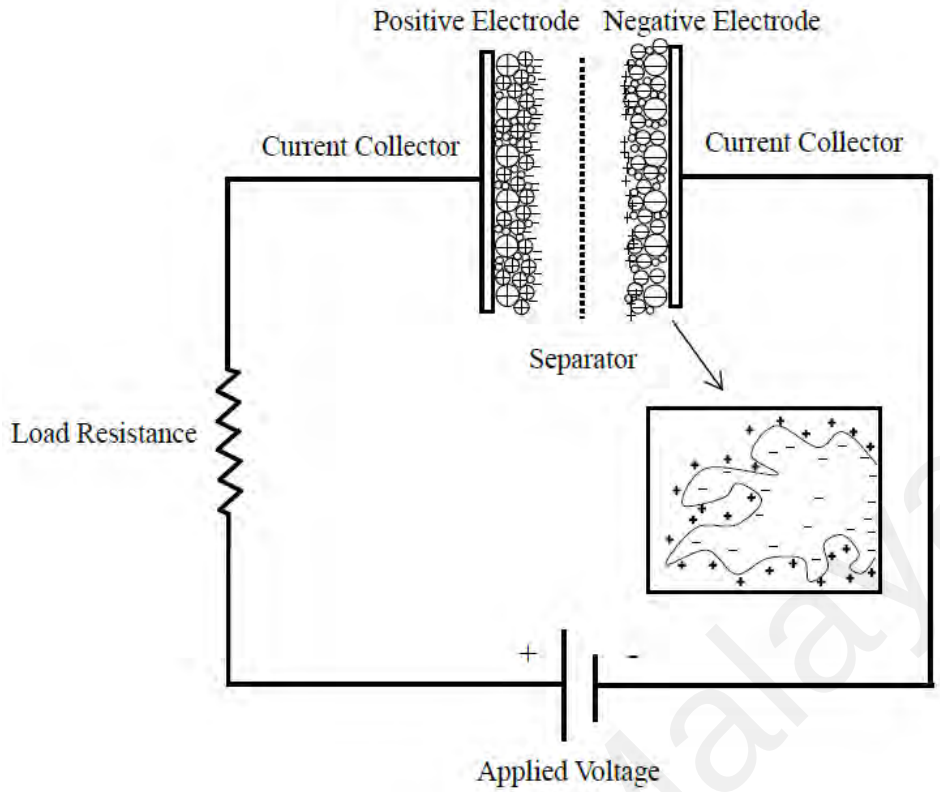

Figure 2.4 : Schematic diagram of an supercapacitor (electrochemical double-layer capacitor) (R. Zhang, 2016).

2.2.1 Principle of energy storage

Electric energy will accumulate in a electrochemical capacitor (EC) on the electrochemical double layer (Helmholtz Layer) through the interface of solid/electrolyte. The positive and negative charges which is generated in the electrolyte piles up at the surface of the electrode. The charges will then be converted to electronic charges at the electrode surface. Double layer's thickness is dependent on the size of the ions and the concentration of the electrolyte, which is in the range of 5 Å to 10 Å. The capacitance range for a standard double layer with a smooth electrode in concentrated solution will be around 10-20μFcm^{-2} which can be computed using equation 2.2. Incorporation of two electrodes in the system of electrochemical capacitors will make up an electrochemical capacitor with high capacitance (Kö Tz & Carlen, 2000).

Detailed schematic representation of an electrochemical double layer capacitor, consisting of a single cell with a high surface area electrode material filled with electrolyte and a high surface area electrode material, is shown in Figure 2.5. This depiction also shows information on the drop of potential across the cells.

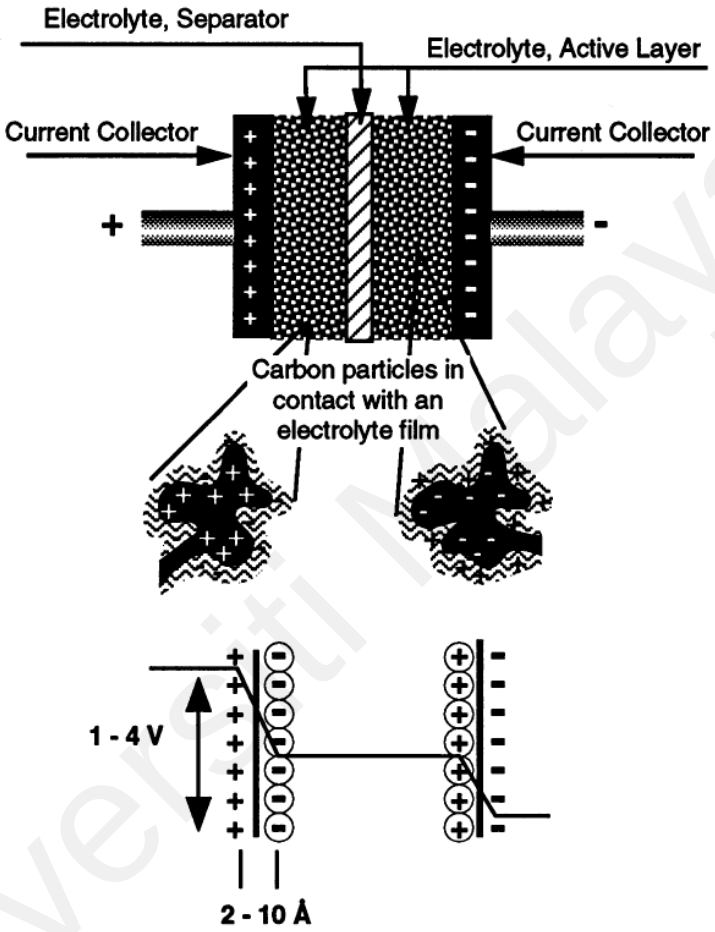

Figure 2.5 : Principle of a single-cell double-layer capacitor and illustration of the potential drop at the electrode/electrolyte interface (Kö Tz & Carlen, 2000)

By assuming that carbon has a large surface area, with 1000 $m^2g^{-1}$and capacitance of a double layer of 10 μFcm^{-2} we can complete the capacitance of a single electrode, which narrows down to $100Fg^{-1}$ for an electrode. For a given capacitor, which has two electrodes and matched with a double weight and 50% of the total capacitance $\left(C^{-1}=C_1^{-1}+C_2^{-1}\right)$ would result in $25Fg^{-1}$of active capacitor mass. Specification and details comparing single electrode values and complete capacitor is vital (Kö Tz &

Carlen, 2000). With the information available, equation 2.3 can be used to calculate the maximum energy stored in a capacitor.

2.3 Classification of supercapacitors.

There are three divisions in SCs, namely EDLCs, pseudocapacitors (PCs) and Hybrid capacitors (HCs) (Figure 2.6). SCs have some special traits which are unique mechanisms for charge storage, which are also reversible faradaic redox, electrostatic storage and sometimes both combined. PCs on the other hand has Faradaic process involving redox reactions. Energy storage in PCs is by means of chemical mechanisms, with the system of transitional metal oxide (TMO) which involve electrochemical reactions. However, in EDLCs the charges are stored at the electrode/electrolyte interface by physical means on carbon-based materials. This is a non-Faradaic mechanisms. The last of all, the HCs have the energy storage process in the faradaic and non-Faradaic combined. Carbon and transition metal oxide composite are the materials used as electrodes in the HCs (S.-M. Chen et al., 2014).

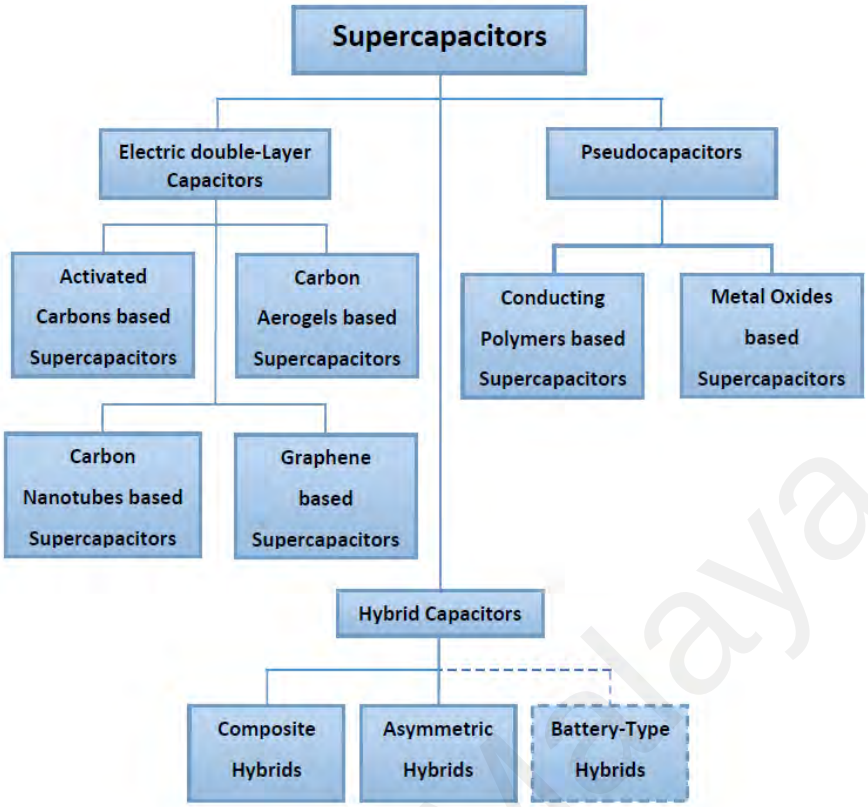

Figure 2.6 : Classification of supercapacitors

2.4 Electrochemical testing of cells

Despite having high rate of charge and discharge, PCs still have low energy storage in comparison. Since the capacitance of the PCs are dependent on the electrode material, there is a spike in interest to improve the electrode material. The tests methodology for small scale PC in a lab is quite informative and quite a norm that scientists could not test the full sized system which could also test the materials used. While different technique gives various results, to measure materials performance in an electrode for supercapacitor is not standard. The usage of electrode material is one of the most important parts in determining SC's capacitance and to also measure the system properly, a full-scale SC installed will provide more accurate, reliable and valuable date (Stoller & Ruoff, 2010).

2.4.1 Fabrication of Electrode for Testing

The capacitance, self-discharge, life expectancy, resistance of a given SC are heavily influenced by the electrode material. Due to this, the process of fabrication the electrodes are taken with high precision. An active material will be coated on a high conductive current collector base. The paste (slurry) of active material will be prepared with a binding agent and a conductive additive. (i.e. carbon). After that, the paste is applied on the current collectors to form a uniform coating. It then would be oven-dried. Commonly the thickness of the electrode can be from a few tens of micrometers to submillimeter. The mass of the substance which is the active material used must be measured.

2.4.2 Electrochemical Testing of electrode material

The methodology for conducting electrode material testing can be separated into two phases: the configuration of the test fixture and the execution of the measurement procedures (or procedures). The test fixture is equipped with all of the necessary rules and equipment components for conducting the tests. (Stoller & Ruoff, 2010).

2.4.2.1 Test Fixture Configuration

As a general rule, traditional SC is composed of two electrodes separated by a permeable separator. Various additives such as conductive low surface area carbon black is added to enhance the electrical conductivity. To channel electrical current from each electrode it is necessary to use current collectors composed of metal foil or carbon-filled polymers to collect current. An electrolyte is infused into the separator and electrodes, allowing ions pass between them while preventing electronic current from discharging the cell. A

package SC module is made consisting of many repeating units, regardless of the intended size and voltage.

A text fixture that closely resembles the configuration of a unit cell would more closely match performance of a packed cell (Conway & Pell, 2003; Stoller & Ruoff, 2010). Commercially available two electrode test rigs are available, or they can be simply made from two stainless steel plates as shown in Figure 2.7.

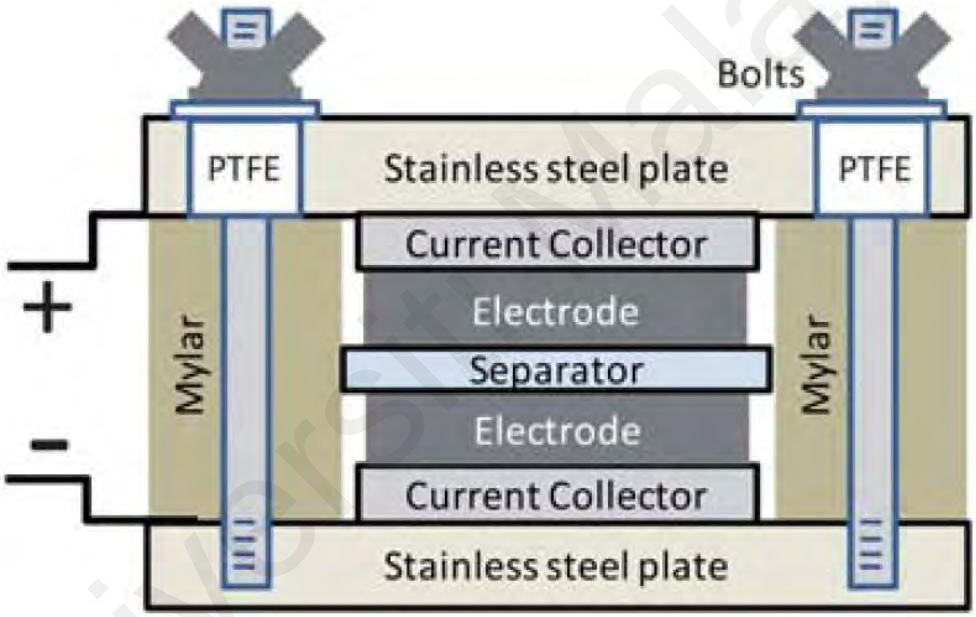

Figure 2.7 : Two-electrode test cell configuration (Stoller & Ruoff, 2010)

As shown in Figure 2.8, Electrochemical cells with three electrodes consist of a working electrode, a counter electrode, and with a reference electrode. In various ways, cells with three electrodes differ from the one with two-electrodes test and packaged cells. Only the working electrode contains the material to be examined in a three-electrode cell, and the applied charge and voltage will only transfer across the one electrode are significantly dissimilar when it is compared with the cell which has two electrodes. In a three-electrode

cell, the voltage potential applied to the working electrode is displayed on the X-axis of a cyclic voltammogram (CV) chart (and on the Y-axis of a constant current diagram) and is in relation to the reference electrode employed (Conway & Pell, 2003; Stoller & Ruoff, 2010). In a symmetrical two-electrode cell, the potential differences applied to each electrode are equal and one-half of the value for a three-electrode cell setup. Due to that, when analysed relatively, the working electrode in the cell with three electrodes has almost two times potential range when directly compared to the electrodes in the cell with two electrodes for a given potential range on the X-axis of a cyclic voltammogram (CV), resulting in a doubling of the computed capacitance value.

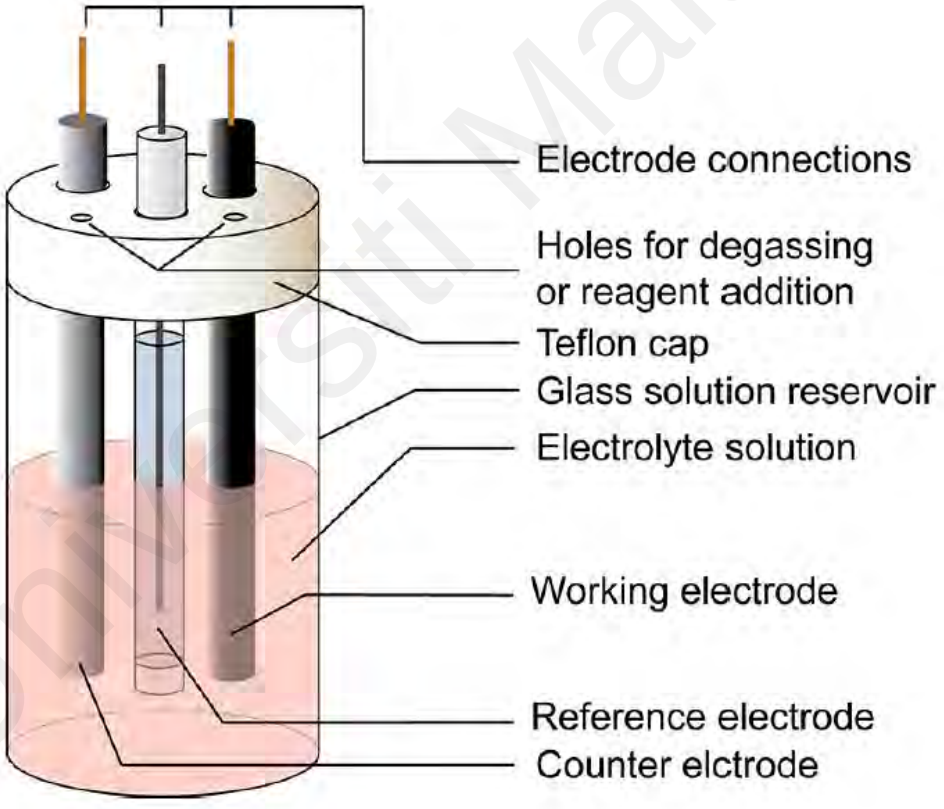

Figure 2.8 : Three-electrode test cell configuration (Elgrishi et al., 2018)

The potential difference across the counter electrode is not controlled or measured in the cell with three electrodes, and it can be an order of magnitude or less in the common case where the counter electrode is larger than the reference electrode, or nearly identical in

the case where the working and counter electrodes are the same size and material. On a CV, the point of zero charge (PZC) varies according to the reference electrode/electrolyte/material combination used, therefore the working electrode cannot truly reverse polarizations during cell operation unless the position is empirically determined and used as the minimum voltage during a CV scan (Conway & Pell, 2003; Stoller & Ruoff, 2010). The results of a three-electrode cell arrangement are twice as good as those of a two-electrode cell configuration. The mass of the active material as well as the thickness of the electrodes have an impact on the observed results. Commercial cell electrode thicknesses range from roughly 10 mm thick which translates to high power density to several hundred microns thick which is of lower power density depending on whether an ultracapacitor is a device that is designed to maximize energy or power density by exhibiting a high energy density. Aside from the fact that test electrodes should be of comparable thickness, exceptionally tiny electrodes and/or electrodes containing very small amounts of material can cause a material's performance to be exaggerated (Conway & Pell, 2003; Stoller & Ruoff, 2010).

2.4.2.2 Measurement Procedures

Charging rates, voltage ranges, and metric calculation methods all have an effect on the provided results and should be repeated using current, well-established approaches for packed cells. Gravimetric energy, power density, and life cycle testing are the most important performance parameters for packaged PC SCs. The power in a SC is proportional to the voltage's square divided by the equivalent series resistance (ESR). Each component of the cell , including leads, current collectors, electrodes, electrolyte, and separator, contribute to the ESR values obtained for a test cell and a full-scale packed capacitor. As a result, only a small portion of the observed resistance may be attributed to the electrode material. The energy and power density of an electrode material, for

example, have no direct relationship to those of a packaged cell and must be paired with additional information, like as the package dimensions and the mass of the other cell components, in order to be effective. (Stoller & Ruoff, 2010).

The specific capacitance of a single electrode is the capacitance per unit mass of the electrode (equation (2.5))

$$C_{sp}\left(Fg^{-1}\right) = 4 \times \frac{c}{m} \tag{2.5}$$

Where C is the two-electrode cell's measured capacitance and m is the value represents the total mass of active material present in both electrodes. . When multiplied with four, the cell's capacitance and the combined mass of two electrodes to the capacitance and mass of a single electrode. If the besieged application requires additional volume, the volume of the electrode material can be replaced by mass. Equation (2.6) is used to calculate cell capacitance using galvanostatic or constant current (CC) discharge curves, where I is the discharge current and dV/dt is determined from the gradient of the CC discharge curve.

$$C = I \Big/ \left(\frac{dV}{dt}\right) \tag{2.6}$$

The industry-accepted measurement method for determining the capacitance value for packed PCs is galvanostatic discharge. This is more closely related to how most applications apply a load on the PC. The voltage range used for testing should be comparable to that used in commercial cells and should reflect the electrochemical window of the electrolyte (from 0 V to about 1 V for aqueous electrolytes and from 0 V to 2.5–2.7 V for organic electrolytes). Hybrid cell maximum voltages will be determined by electrode materials and electrolytes. For non-faradic materials, the early portion of a discharge curve shows an IR drop due to internal resistance, while the rest of the curve is normally linear. Large departures in linearity can be seen in pseudocapacitive and hybrid

systems, which are mostly caused by changing capacitance with voltage (Conway & Pell, 2003; Elgrishi et al., 2018; Stoller & Ruoff, 2010).

It's worth noting that running a cell above its genuine maximum operating voltage can cause specific capacitance to be overestimated. Because of the non-reversible processes within the cell, cells operating at these levels will have shortened lives and low efficiency. In particular for hybrid and pseudocapacitive cells, capacitance varies with voltage; therefore, it is critical to calculate the capacitance value using the typical operating voltage range for the application (Conway & Pell, 2003; Elgrishi et al., 2018; Stoller & Ruoff, 2010). The majority of PCs will function between Vmax and approximately 0.5Vmax, and the suggested way is to apply data points from two values from the discharge curve with dV/dt = (Vmax – 0.5Vmax)/(T2 –T1).Incorporating the lower half of the voltage range into the calculations can cause the apparent capacitance to exceed what is practical for a real-world application. Low levels of discharge also result in a high number of mistakes. This is particularly true when small electrode masses are involved, with current from cell leakage, capacitance from other cell components, and faradic reactions all contributing to a growing percentage of the discharge rate indication. *I* is the average current during discharge (from Vmax to zero volts) and dV/dt is the scan rate, as calculated using equation (2.6) and CV data. Capacitance, like CC curves is affected by voltage range, scan rate, and computing method. Voltage scan rates of at least 20 to 40 mV s-1 are necessary to sustain discharge times on the order of a minute and accurately reflect the performance of a material in order to accurately reflect its performance. (Conway & Pell, 2003; Elgrishi et al., 2018; Stoller & Ruoff, 2010).

2.5 Evaluation of Devices

2.5.1 Cyclic Voltammetry (CV) and Cyclic Voltammetry Advanced (CVA)

Cyclic voltammetry (CV) is a technique that measures the current as a function of a predetermined voltage range using a reversible linear voltage sweep, referred to as the scan rate. The voltage between two SC electrodes that is applied in the case of cells with two electrodes and between a working electrode and a reference electrode in respect to cells with three electrodes. The potential in the CV begins at a fixed beginning value and increases linearly with time until it reaches a fixed final voltage. The scan is then reversed, and the potential changes proportionately linear from the final voltage to the initial voltage. The instantaneous current is measured during the cathodic and anodic sweeps to characterise the electrochemical processes. Current (A) vs. potential (V) or, in certain cases, current (A) or potential (V) vs. time (s) are shown (Theses & Khawaja, 2015; G. Wang et al., 2012; S. Zhang & Pan, 2015). CV testing with a three-electrode configuration is the most advantageous technique for examining the charge storage mechanisms of supercapacitor materials where EDLC and PC types are frequently distinct. The test results are reviewed with the ensuing CV curve in mind, which should be rectangular for EDLC. Prominent redox peaks may form in certain PC materials in a highly reversible manner.

2.5.2 Electrochemical Impedance Spectroscopy (EIS)

Electrochemical impedance spectroscopy (EIS) is a critical tool for characterising the electrochemical behaviour of SCs. It determines the impedance of a power cell in terms of frequency by superimposing a low-amplitude alternating voltage (about 5 mV) on a steady-state potential. The generated data are shown graphically using Bode plots and

Nyquist plots. While the Bode plot depicts the cell response as a function of phase angle and frequency, the Nyquist plot denotes the imaginary and real components of the cell impedances in a complex plane. Apart from the frequency response and impedance, the EIS has been utilised to characterise mechanisms for mass transit, charge transfer, and charge storage. It is used to determine the capacitance, energy, and power attributes of semiconductors. Different comparable circuits and models have been devised to distinguish the contribution of each structure component to the total impedance of a cell system. When SC devices are examined, the ESR is represented by the real components of the complex impedance at specific frequencies in the literature. However, it is important to remember that the ESR obtained from the EIS test is frequently substantially lower than the ESR obtained from the constant current charge/discharge (CCCD) test.

2.6 Electrode Materials

EDLC does not use chemical reactions to store electrical charges; rather, energy is stored by the adsorption of ions on the surface of charged electrodes. In pseudocapacitors, ultrafast redox processes occur on the electrodes' surfaces, boosting the energy density of the SC while lowering its charge-discharge speed and lifetime. The capacitance of a SC is material dependent. Two electrodes made of the same material are used in symmetrical SCs. Asymmetrical or hybrid SCs frequently have one electrode that exhibits PC and another that exhibits EDLC. This combination of the two types of capacitance is the sole reason hybrid SCs outperform ordinary pseudocapacitors in terms of efficiency and have a higher specific capacitance than EDLCs. There are a plethora of different materials that can be employed in the electrodes of the PC or EDLC. While pure EDLCs commonly use porous activated carbon (AC) electrodes, pseudocapacitors may also use electrode materials such as transition metals and conducting polymers. There is no precise

relationship between the increased specific surface area (SSA) of AC and capacitance as a result of EDLC. However, SSA is not the sole source of capacitance, encouraging research into other electrode materials (Logerais et al., 2013; Xie et al., 2016).

2.6.1 Carbon Materials

Carbon materials are the most often used electrode materials in the manufacturing of SCs in their different forms. This is because of its large surface area, low cost, availability, and well-established electrode manufacturing technology. Carbon compounds utilise the electrochemical double layer storage process at the electrode-electrolyte interface. Carbon compounds store energy via an electrochemical double layer produced at the electrode-electrolyte interface. As a result, capacitance is mostly determined by the surface area accessible to electrolyte ions. The particular surface area, pore shape and structure, pore size distribution, surface functionality, and electrical conductivity are all critical elements affecting electrochemical performance. Due to the huge surface area of carbon materials, they have a high capacity for charge accumulation at the electrode-electrolyte interface. Apart from pore size and high specific surface area, surface functionalization must be considered when rocketing specific capacitance for carbon materials. Activated carbon, carbon nanotubes, carbon aerogels, and graphene are all examples of carbon materials that have been employed as electrode materials (Iro et al., 2016; M Ali et al., 2016; H. Yang et al., 2017).

2.6.1.1 Activated Carbon

The most frequently employed electrode material is activated carbon (AC), which has a huge surface area, excellent electrical characteristics, a well-developed specific surface

area (SSA) of up to 3000 m^2 g-1, and a low cost. AC can be synthesised either physically or chemically from a variety of carbonaceous materials (e.g. wood, coal nutshell etc.). Physical activation is a technique that involves heating carbon precursors to high temperatures (700-1200 oC) in the presence of oxidising gases such as steam, CO_2, and air. While chemical activation uses activating agents such as sodium hydroxide, potassium hydroxide, zinc chloride, and phosphoric acid to treat the carbon precursors at low temperatures (400-700 °C). The porous structure of activated carbon generated via activation procedures exhibited a wide pore size distribution composed primarily of micropores (50 nm). Numerous studies have been conducted to determine the relationship between the specific capacitance and the specific surface area (SSA) of ac. Their report indicates an apparent disagreement between them. With a high SSA of around 3000 m^2 g^{-1}, a low capacitance was attained. This demonstrates that not all pores are effective during the charge buildup process. It is worth noting that excessive activation results in an increase in pore volume. This results in disadvantages such as low conductivity and material density, which result in a low energy density and a reduction in power capability (Ivandini et al., 2012; Lota & Sierczynska, n.d.; Lufrano et al., 2011; Pandolfo & Hollenkamp, 2006).

2.6.1.2 Carbon Nanotubes (CNT)

Because of their unique pore structure, mechanical and thermal resilience, and outstanding electrical characteristics, carbon nanotubes are employed as SC electrode materials. CNTs are formed during the catalytic breakdown of some hydrocarbons as shown in Figure 2.9. It is feasible to fabricate nanostructures in a variety of conformations and control their crystalline structure by fine-tuning certain parameters. In comparison to conventional carbon-based electrodes, carbon nanotubes enable a continuous charge distribution that utilises nearly all of the available surface area. Because the electrolyte

ions can migrate into the mesoporous network, CNTs have a lower ESR than AC. Additionally, they serve as an excellent support for active materials due to their high mechanical robustness and open tubular network. CNTs typically have a tiny SSA (less than 500 m^2g^{-1}), which results in a lower energy density than AC (Cheng et al., 2011; Du & Pan, 2007; J. Li et al., 2012; Pandolfo & Hollenkamp, 2006)

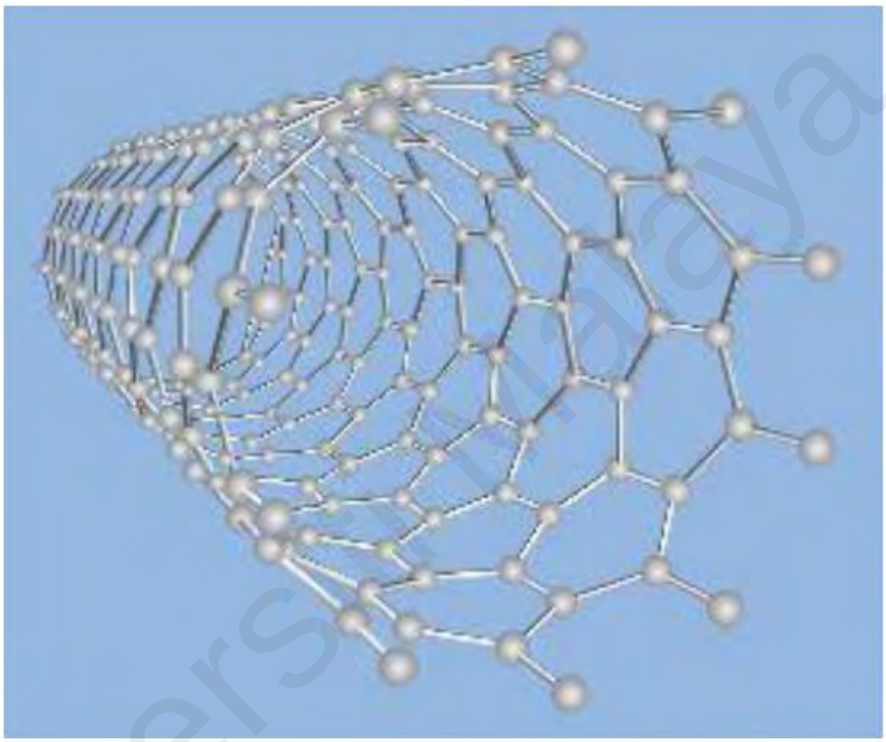

Figure 2.9 : Structure of a single walled carbon nanotube (W. D. Callister & D. G. Rethwisch, 2014)

2.6.1.3 Carbon Aerogel Derived from Biomasses

Carbon aerogel is another type of carbon that is utilised as a material for SC electrodes. It is made by pyrolyzing organic aerogels. The porosity is the result of colloidal particles mixing together. Composites, monoliths, powders, microspheres, or thin films of porous carbon are all examples of porous carbon materials. Aerogel carbon composites have been reported to have a greater surface area than AC. Carbon fibre aerogels with surface areas ranging from 1536 to 2436 m^2 g^{-1} and pores varying from 1.0 to 4.0 nm demonstrated a

high specific capacitance of 282 F g^{-1} (1 A g^{-1}) in a 6 M KOH electrolyte (Enock et al., 2017; Pandolfo & Hollenkamp, 2006)

2.6.1.4 Graphene

Figure 2.10 shows the graphene structure which is a two-dimensional substance having a layer thickness of one atom. It has distinguished itself as an extraordinary carbon material with potential for energy storage applications due to its superior electrical conductivity, chemical stability, and wide surface area. In comparison to other carbon materials such as AC, CNT, and so on, graphene is hailed as a suitable material for SC applications since its electrode material does not rely on the distribution of pores in the solid state. Graphene, a newly created material, has a greater SSA of around 2630 m^2 g^{-1}. If the entire SSA is used, it is capable of achieving a capacitance of up to 550 Fg^{-1}. Another advantage of employing graphene as an electrode material is that both of the graphene sheet's critical surfaces are exposed and easily accessible to the electrolyte. Chemical vapour deposition, micromechanical exfoliation, arch discharge, unzipping carbon nanotubes, epitaxial growth, electrochemical and chemical procedures, and intercalation methods in graphite are all methods for creating graphene (Kuilla et al., 2010; C. Liu et al., 2010; Marcano et al., 2010; H. Wang et al., 2009; Zhou et al., 2011).

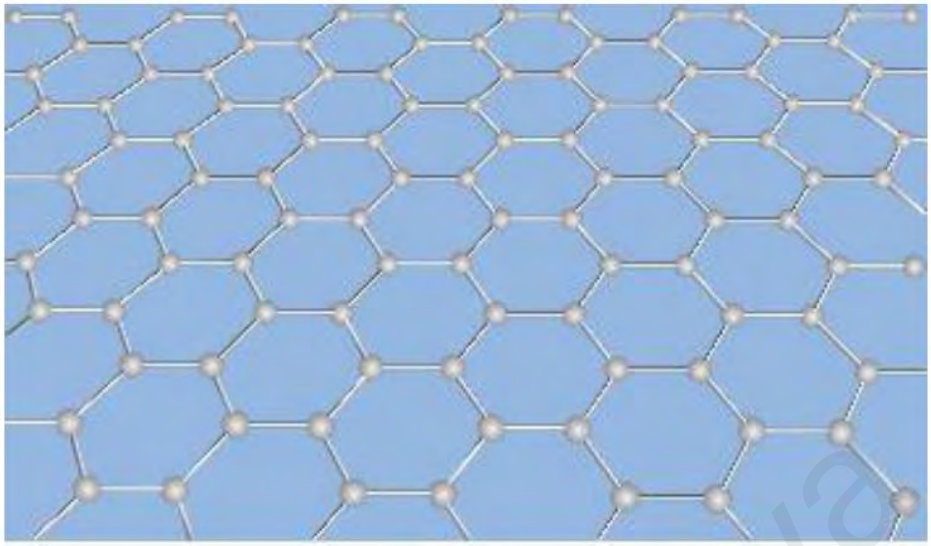

Figure 2.10: Structure of a graphene layer (W. D. Callister & D. G. Rethwisch, 2014)

2.6.2 Conducting Polymers

In comparison to carbon-based electrode materials, conducting polymers have a relatively high conductivity, capacitance, and relatively lower ESR. There are numerous electrode configurations for conducting polymers, but the n/p configuration, which consists of one negatively charged (n-doped) and one positively charged (p-doped) electrode, provides the highest energy and power densities, although the lack of n-doped conducting polymer electrode materials has prevented PCs from reaching their full potential. Charge storage and release in conducting polymers occurs via a reduction-oxidation reaction. By oxidation, also known as doping, ions are transported to the polymer's backbone, whereas by reduction, also known as de-doping, ions are released back into solution. On the other hand, this reduction-oxidation process creates mechanical stress in conducting polymers, impairing their durability over a large number of charge-discharge cycles. Among the several conducting polymers, polyaniline (PANI) is the most promising SC electrode material due to its high conductivity, ease of synthesis, outstanding energy storage capacity, and low cost. Its disadvantage is that repetitive cycles (charge/discharge process) produce swelling and shrinkage, resulting in a rapid decline of performance. To

mitigate this, PANI must be used with carbon material. This increases its stability and maximises its capacitance (Besharat et al., 2018; He et al., 2013; Marin Halper James C Ellenbogen, 2006; Sui et al., 2015; H. Wang et al., 2009).

2.6.3 Transition Metal Oxides (TMO) and Hydroxides

Metal oxides are another alternative to the materials optimization in the manufacture of electrodes SC. This is because they have a high specific capacitance and a low resistance, which simplifies the fabrication of high-energy and high-power SCs. Nickel oxide (NiO), ruthenium dioxide (RuO_2), manganese oxide (MnO_2), and iridium oxide (IrO_2) are the most frequently optimized metal oxides(Abdeladim Moftah & Ashraf Al Shetiti, 2015). They are a viable option due to their cheaper manufacturing costs and the use of a milder electrolyte. RuO_2 is a significant compound in both its amorphous and crystalline forms due to its unusual combination of features, including catalytic activity, metallic conductivity, electrochemical reduction-oxidation capabilities, chemical and thermal durability, and field emission behaviour.(S. Chen et al., 2010) Electronics, thick or thin resistors, ferroelectric films, and integrated circuit development all benefit from its use. RuO_2 is now used as an electrode material in SCs due to the benefits it offers, including a long cycle life, a wide potential window with a high specific capacitance, a highly reversible reduction-oxidation reaction, and metallic type conductivity(Acznik et al., 2014). Manganese oxide has recently sparked considerable study interest due to its extraordinary physical and chemical properties (its low cost, excellent capacitive performance in aqueous electrolytes and environmental benignity). It is used for a variety of purposes, including ion exchange, catalysis, biosensors, energy storage, and molecular adsorption (H. C. Chen et al., 2012; Jung et al., 2007; H.-Y. Wu & Wang, 2012).

To achieve good electrochemical performance, the electrode of a SC device must have a high specific capacitance. In comparison to EDL materials, advantageous pseudocapacitive materials can achieve a higher specific capacitance. Depending on the process used to prepare them, layered transition metal hydroxides exhibit a variety of flower-like lamellar structures(H. X. Wang et al., 2015). The hydroxides have a large specific area and dedicated channels, which facilitate redox reactions and contribute to their high electrochemical performance. Due to their extraordinary pseudocapacitive performance, they are particularly well suited as electrode materials for SCs, as they can display intelligent pseudocapacitive behavior (Cao et al., 2004). During the charge-discharge process, they undergo a reversible redox reaction. A high-performance electrode must satisfy the requirements for high specific capacitance, high rate capacity, and prolonged stability (Augustyn et al., 2014; Davood Nematollahi et al., 2014; Zhong et al., 2015).

2.6.4 Composites

Carbon-based composite electrodes are combined with metal oxide or conducting polymer components. As a result, it provides both physical and chemical charge storage mechanisms in a single electrode. Carbon-carbon composites, carbon-metal oxide composites, and carbon-conducting polymer composites are all examples of composite electrode materials for SCs(Cheng et al., 2011). Conducting polymers with pseudo-capacitance properties such as polyaniline, polythiophene, and polypyrrole are embedded in carbon nanomaterials with electrical double layer capacitance properties (carbon fibre, MWCNT, fullerene, and graphene) in carbon-polymer based composites(Soavi et al., 2016). Carbon material is easily merged with metal oxides (such as RuO_2, MnO_2, and Fe_2O_3) in carbon-metal oxide based composites due to its high surface area and regular

pore structure, and also the carbon material possesses both ionic and electronic conductivity of the electrode surface. As a result, the final composite material has a high density and a stable power density.(Khawula et al., 2016) Metal oxide-polymer composites are formed when metal oxides are combined with conducting polymers. This is accomplished in order to improve their electrochemical characteristics(N. Li et al., 2016). Hydrous ruthenium oxide has superior electrochemical characteristics than the other transition metal oxides (Y. Chen et al., 2012; N. Li et al., 2016; Vangari et al., 2013)

2.7 Electrolytes

Electrolytes are a critical component in electrochemical supercapacitors (ECSCs), which include electrical double-layer capacitors, pseudocapacitors, and hybrid supercapacitors(Zhong et al., 2015). These electrolytes contain ions that are used to transmit and store charge. Due to the fact that the energy density of a SC device is proportional to the capacitance and the voltage squared (refer to equation 2.3). Increases in capacitance or cell operating voltage are required to increase the energy density (Stoller et al., 2012)

As shown in equation 2.3, expanding the electrolyte's potential window, i.e., increasing the cell voltage (V), can efficiently enhance the energy density. In terms of energy density, raising the cell voltage is more efficient than increasing the electrode capacitance; this is because the energy density is related to the square of the cell voltage. As a result, optimizing novel electrolytes/solutions with broad potential windows should take precedence over developing new electrode materials. Because the aqueous electrolyte has a potential window of around 1.23 V, aqueous-based SCs typically have an operational potential window of about 1.0–1.3 V. SCs based on organic electrolytes and ionic liquids

(ILs) typically have potential windows of 2.5–2.7 and 3.5–4.0 V. Additionally, electrolytes/solutions play a critical role in determining other critical properties of SCs, such as power density, rate performance, internal resistance, cycling lifetime, operating temperature range, self-discharge, and toxicity, all of which are critical for their practical use(Ntsoenzok & FCT Nigeria, 2016).

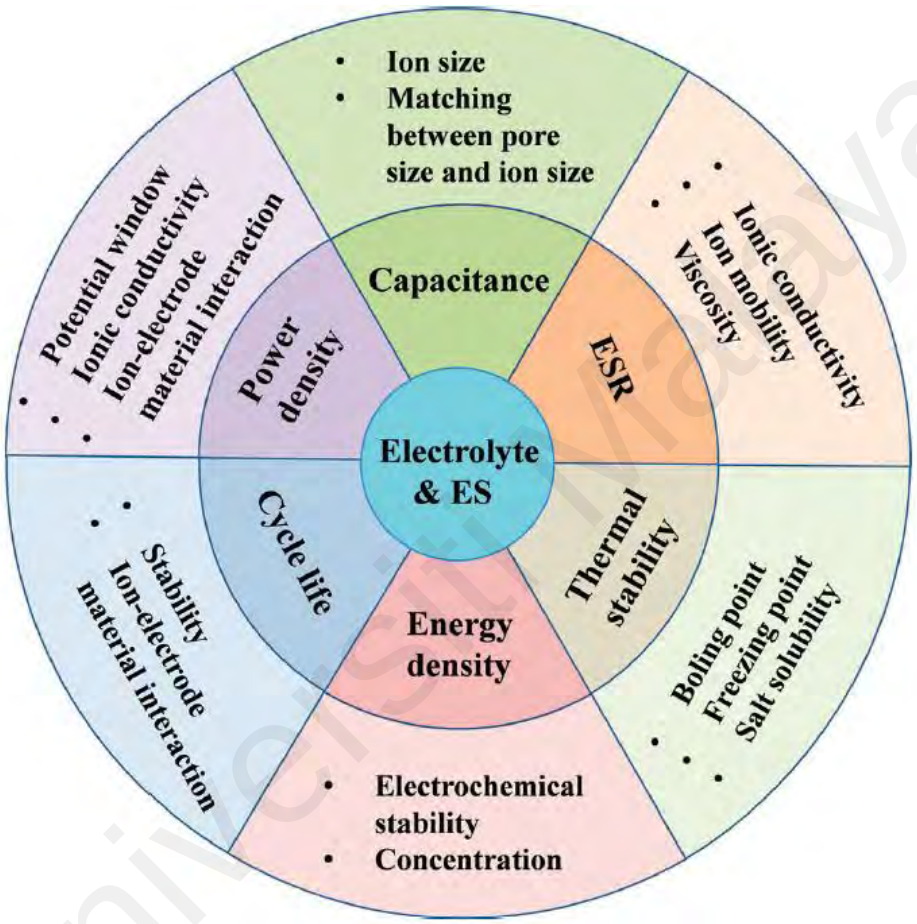

Figure 2.11 : Effects of the electrolyte on the electrochemical supercapacitor (ES) performance (Zhong et al., 2015)

The interface between the electrolyte and the electrode materials also has a significant effect on the device's performance, i.e. the precise fit between the electrolyte ion size and the pore size of the carbon electrode material has a significant effect on the achievable specific capacitance(Stoller et al., 2012). The PCs generated from carbon-based materials and TMOs are highly dependent on the electrolytes' composition. The ionic conductivity of electrolytes has a significant effect on the device's internal resistance, particularly for

organic and ionic liquid (IL) electrolytes(Zhong et al., 2015). The viscosity, boiling point, and freezing point of the electrolytes can also have a significant effect on the thermal stability of the device and thus on its working temperature range. As previously stated, gadget ageing and breakdown are caused by electrochemical deterioration of the electrolytes(Ntsoenzok & FCT Nigeria, 2016). With regards to the development of electrolytes for SC devices, a wide variety of electrolytes have been examined, including aqueous electrolytes, organic electrolytes, IL electrolytes, redox-type electrolytes, and solid or semi-solid electrolytes (Stoller et al., 2012).

In general, the requirements for a standard electrolyte are as follows: a wide potential window; high ionic conductivity; high chemical and electrochemical stability; high chemical and electrochemical inertness to other SC components such as electrodes, current collectors, and packaging; a wide operating temperature range; compatibility with the electrolyte materials; low volatility and flammability; and cost effectiveness as illustrated in Figure 2.11. Indeed, it is nearly hard for an electrolyte to satisfy all of these needs, and each electrolyte has distinct advantages and disadvantages.

To date, a large number of electrolytes have been discovered and documented in the scientific literature which in turn can be classified into three major types, as seen in Figure 2.12. Majority of the electrolytes are classified as liquid electrolytes and solid/quasisolid-state electrolytes. In general, liquid electrolytes are classed as aqueous electrolytes, organic electrolytes, and ion-liquids (ILs), whereas solid or quasi-solid state electrolytes are classified as organic and inorganic electrolytes. Currently, no perfect electrolyte has been developed that meets all of the requirements described earlier (Stoller et al., 2012; Zhong et al., 2015).

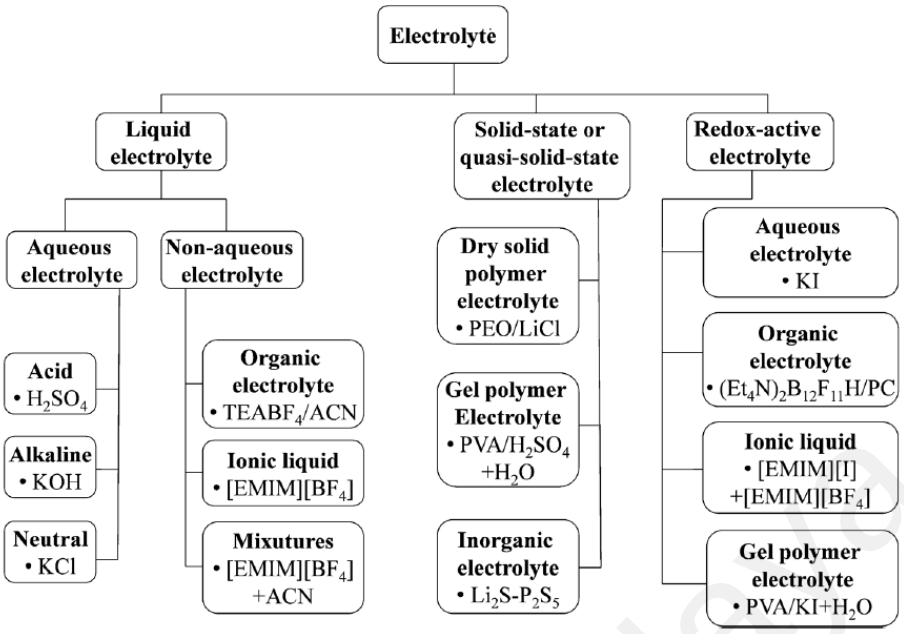

Figure 2.12 : Classification of electrolytes for electrochemical supercapacitors (Zhong et al., 2015)

2.7.1 Aqueous Electrolytes

Aqueous electrolytes have a high conductivity (approximately 0.8 S cm^{-1} for 1 M H_2SO_4 at 25 °C, for example), which is at least one order of magnitude more than the conductivity of organic and IL electrolytes(Zang et al., 2019). This is helpful because it reduces the ESR of the cell device, resulting in improved power delivery from the device. The selection criteria for aqueous electrolytes normally examine the sizes of unhydrated and hydrated cations and anions, as well as the flexibility of ions, which influences not only ionic conductivity but also the specific capacitance value(Shivakumara et al., 2014). Additionally, the electrochemical stability potential windows (ESPW) and corrosive intensity of an electrolyte should be considered. By and large, aqueous electrolytes can be classed as acid, alkaline, or neutral solutions, with H_2SO_4, KOH, and Na_2SO_4 serving as representative and most often used electrolytes, respectively (Figure 2.12). As previously noted, the primary shortcoming of aqueous electrolytes is their relatively

limited ESPW, which is constrained by water decomposition (Fic et al., 2015; Menzel et al., 2015; C. Zhao & Zheng, 2015)

2.7.2 Organic Electrolytes

Organic electrolyte-based SCs are currently dominating the commercial market due to their large working potential window, which is typically between 2.5 and 2.8 V on average. When the voltage of the operation cell is increased, it can lead to a large increase in both the energy and power densities. Additional advantages of using organic electrolytes include the utilization of less expensive materials such as aluminum for current collectors and packaging. Organic electrolytes, such as those used in commercial EDLCs, are typically made of salts that conduct electricity (e.g., tetraethylammonium tetrafluoroborate ($TEABF_4$)) dissolved in acetonitrile (CAN) or polypropylene carbonate (PC) solvents (Lim et al., 2014; Linares-Solano et al., 2012)

However, there are additional considerations to make when employing organic electrolytes for SCs. In comparison to systems that employ aqueous electrolytes, organic electrolytes are typically more expensive; have a lower specific capacitance; and have lesser conductivity. Additionally, safety issues about flammability, volatility, and toxicity raise eyebrows. Organic electrolyte requires a complex purification and assembly procedure under regulated conditions to exclude residual impurities (e.g., water) that can result in significant performance loss and serious self-discharge difficulties(Linares-Solano et al., 2012). Organic electrolyte-based supercapacitors perform similarly to aqueous electrolyte-based supercapacitors in that the nature of salts and solvents, such as ion size and ion-solvent interaction, conductivity, viscosity, and electrochemical specific

power (ESPW), all have a significant impact on the performance of the supercapacitors (Lim et al., 2014; Zhong et al., 2015).

Organic electrolytes, in general, have larger solvated ion sizes and lower dielectric constants, resulting in lower EDL capacitance values. To maximise the specific capacitance, it is critical to match the pore size of carbon materials to the size of electrolyte ions. The deterioration is due to the following factors: (1) A high cell voltage during operation may increase the oxidation of electrode materials. This occurs when the working voltage of the device exceeds the average 2.5 - 2.8 V, for example, above 3 V. This could result in gas evolution as a result of electrolyte disintegration and electrochemical oxidation of carbon. (2) Electrolyte ion intercalation or the electrochemical reaction of the organic electrolytes may also result in device degradation; and (3) finally, hard operating circumstances (e.g., high peak temperature and working voltage) may result in device degradation(C. M. Yang et al., 2007; Zhong et al., 2015). Thus, understanding how devices age and fail will aid in the creation of devices with wider voltage windows. Another disadvantage of organic electrolytes is that they have a substantially lower ionic conductivity than aqueous electrolytes. For example, the ionic conductivity of the widely used 1 M $TEABF_4$/ACN electrolyte is 0.06 S cm–1, much less than the 0.8 S cm^{-1} at 25 °C of the 30% H_2SO_4 electrolyte. Because of the low conductivity of the organic electrolyte, it has the potential to have a substantially higher ESR than electrochemical supercapacitors based on aqueous electrolyte (ESs), hence limiting the maximum power density (Dutta & De, 2016; Gupta et al., 2016)

2.7.3 Ionic Liquids

Ionic liquids are also referred to as molten salts at low or room temperatures. ILs are salts composed of cations and anions with a melting point less than 100 degrees Celsius. Typically, an IL is composed of a large asymmetric organic cation and a non-metal or metal anion. This unique combination of a certain cation and an anion results in a low melting point. ILs have generated considerable interest as alternate electrolytes for SCs due to their distinctive structures and characteristics (Zhong et al., 2015). ILs have a number of potential advantages, including excellent thermal, chemical, and electrochemical stability, low volatility, and nonflammability (Depending on the ratio of cations to anions in solution). Due to the large number (the possibilities are practically limitless) of possible combinations of cations and anions in ILs, their physical and chemical properties can be highly tailored to meet specific ES performance requirements such as operative cell voltage, operating temperature range, and ESR (related to ionic conductivity), and so on (Riva et al., 2002).

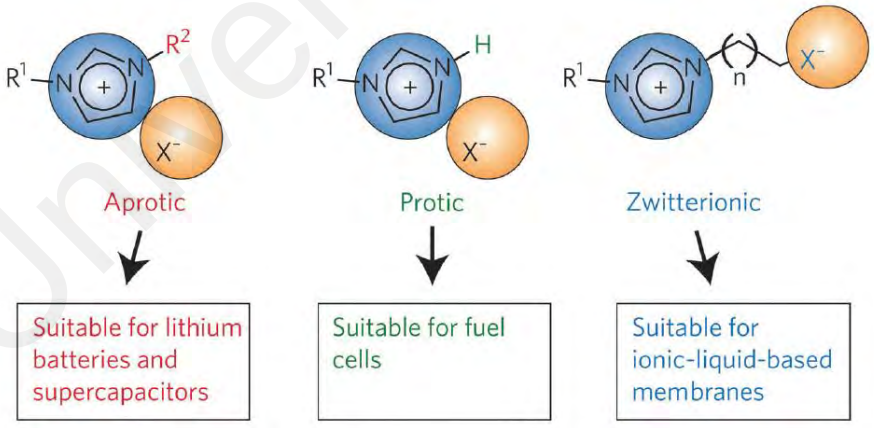

Figure 2.13: Basic types of ionic liquids: aprotic, protic and zwitterionic types (Zhong et al., 2015)

Based on their composition, ILs are classed as aprotic, protic, or zwitterionic (Fig 2.13). Imidazolium, pyrrolidinium, ammonium, sulfonium, and phosphonium cations are often

utilised ILs for SCs. Tetrafluoroborate (BF_4^-), hexafluorophosphate (PF_6^-), bis(trifluoromethanesulfonyl)imide ($TFSI^-$), bis(fluorosulfonyl)imide (FSI^-), and dicyanamide (DCA^-) are representative anions of ILs (Zhong et al., 2015).

In general, ILs based on pyrrolidinium have a larger ESPW, whereas ILs based on imidazolium can provide stronger ionic conductivity. As previously noted, the operating cell voltages of commercial organic electrolytes (e.g., ACN and PC) based EDLCs are typically limited to 2.5–2.8 V, and exceeding this limit would result in significant electrochemical degradation of organic solvents (Lewandowski & Galinski, 2007). However, numerous studies using IL-electrolyte-based SCs have demonstrated that they can achieve operative cell voltages greater than 3 V. Additionally, commercially available organic solvents (e.g., ACN) present safety concerns due to their volatile and flammable nature, particularly when used at elevated temperatures (Hatakeyama et al., 2009). Solvent-free ILs may have a benefit in terms of addressing safety concerns connected with the use of commercial organic solvents, which makes SCs based on ILs attractive for high-temperature applications (Michel Armand et al., 2009).

Regrettably, the primary disadvantages of the majority of ILs are their high viscosity, limited ionic conductivity, and high cost. These drawbacks may limit their usefulness in devices. Even though [EMIM][BF_4] electrolyte has a reasonably high ionic conductivity when compared to other ILs, its conductivity (14 mS cm^{-1} at 25 °C) is significantly less than that of $TEABF_4$/ACN (59.9 mS cm^{-1} at 25 °C) (Lewandowski & Galinski, 2007). When ILs are used in SCs devices, the rate and power performance are constrained, resulting in a loss of power density. This is because the low conductivity and viscosity of IL-based electrolytes can significantly increase the ESR values of IL-based devices (which cannot be buffered by increasing the cell voltage) (Eftekhari, 2017). Additionally, the specific capacitance of EDLC devices based on IL electrolyte is frequently less than

that of devices based on aqueous or organic electrolyte, particularly at high scan rates or charging/discharging rates. This is most likely owing to ILs' high viscosity (Fleischmann et al., 2019). To gain a better understanding of the ageing or failure mechanisms of IL electrolyte-based EDLCs, the electrochemical decomposition of ILs beyond the ESPW has been investigated using instrumental analysis techniques such as in-situ infrared and electrochemical spectroscopy, as well as in-situ XPS (Brandt et al., 2013).

2.7.4 Solid- or Quasi-Solid-State Electrolytes for ESs

The rapidly expanding demand for power for portable electronics, wearable electronics, microelectronics, printed electronics, and particularly flexible electronic devices has shifted the focus of research and development to electrochemical energy systems based on solid-state electrolytes. Solid-state electrolytes can act as both a conductor of ions and an electrode separator. The primary advantage of solid-state electrolytes is their simplicity of packing and fabrication procedures, as well as their lack of liquid leakage(Hu et al., 2018). The majority of solid-state electrolytes created for SCs are polymer electrolytes, with just a small amount of effort focusing on inorganic solid materials. Three forms of polymer-based solid electrolytes for SCs are available: gel polymer electrolytes (GPEs), solid polymer electrolytes (SPEs, also known as dry polymer electrolytes), and polyelectrolytes (Hu et al., 2018; L. Wu et al., 2013).

Consider Figure 2.14, where the SPE is composed of a polymer (for example, PEO) and a salt (for example, LiCl), with no solvent (for example, water) present. SPE has high ionic conductivity because salt ions are transported through the polymer. The GPE, on the other hand, is a polymer-based host (e.g., PVA) and an aqueous electrolyte (e.g., H_2SO_4) or a conducting salt dissolved in solvent. Essentially, the polymer acts as a matrix,

which is absorbed by the solvent in this situation. The ion transportation occurs in the solvent instead of in the polymer phase, which is quite distinct from that of the SPE. In the polyelectrolyte category, the ionic conductivity is supplied by the charged polymer chains (Zhong et al., 2015).

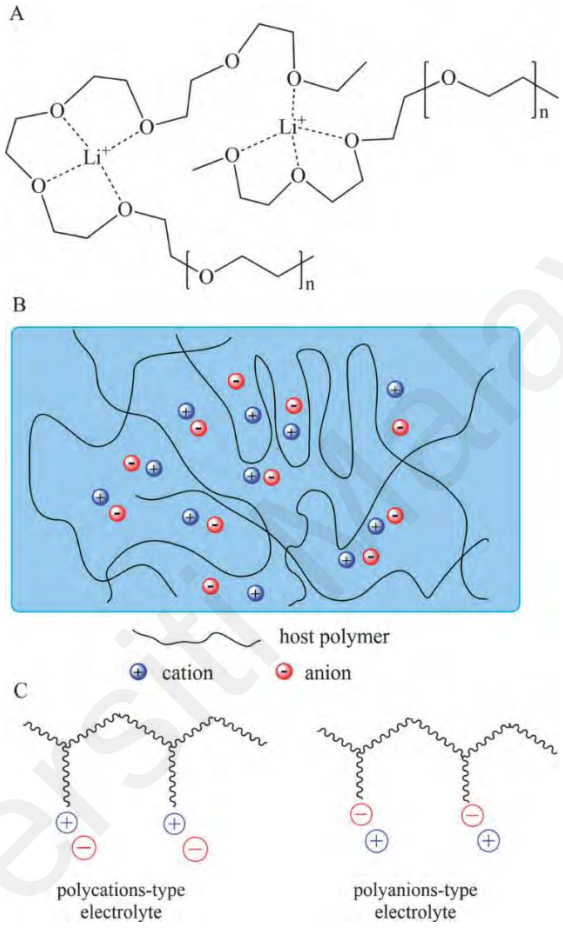

Figure 2.14 : Schematic diagrams of (a) dry solid-state polymer electrolyte (e.g., PEO/Li^+), (b) gel polymer electrolyte, and (c) polyelectrolyte (Zhong et al., 2015)

GPEs, on average, have the highest ionic conductivity among the three solid-state electrolytes. The addition of a liquid phase increases the ionic conductivity of a GPE much over that of a dry SPE. This is why it is the market leader in solid electrolyte supercapacitor products (Niu et al., 2013). However, GPEs may have a low mechanical strength and a limited operating temperature range, particularly when water is used as the

solvent. The mechanical weakness of GPEs is another significant disadvantage, since it may result in internal short circuits, posing safety concerns (Dubal et al., 2018)

While dry SPEs typically have a low ionic conductivity, they have a better mechanical strength than GPEs. The common disadvantage of these solid-state electrolytes for SCs is a small contact surface area between the solid electrolyte and the electrode material, particularly for nanoporous materials. This issue increases the ESR value, reduces the performance rate, and restricts the use of active electrode materials, resulting in a device with a low specific capacitance (Kang et al., 2016). Solid electrolytes have been employed in a variety of SC configurations, including EDLCs, PCs, and hybrid SCs with a variety of electrode materials. When creating solid-state electrolytes for SC applications, the following requirements should be taken into account: (1) high chemical, electrochemical, and thermal stability; (2) strong ionic conductivity; and (3) enough mechanical strength and dimensional stability. The reality is that no solid-sate electrolyte can meet all of these requirements. Mechanical strength and ionic conductivity frequently have a trade-off (Jeong et al., 2017; Kang et al., 2016)

2.7.4.1 Gel Polymer Electrolytes

Due to their high ionic conductivity, GPEs are currently the most extensively investigated electrolytes for solid-state SCs. GPE is made up of a polymer matrix (host polymer) and an electrolyte that is in the form of a liquid such as aqueous electrolyte, organic solvent containing conducting salt and ionic liquid (Zhong et al., 2015). The following are some previously investigated polymer matrices for the creation of GPEs. Poly(vinyl alcohol) (PVA), poly(-acrylic acid) (PAA), potassium polyacrylate (PAAK), poly(ethyl oxide) (PEO), poly(methyl methacrylate) (PMMA), poly(ether ether ketone) (PEEK), poly(acrylonitrile)-block-poly(ethylene glycol)-block-poly(acrylonitrile) (PAN-b-PEG-

b-PAN), and poly (PVDF-HFP). When water is used as the plasticizer, a hydrogel polymer electrolyte is formed. Hydrogel polymer electrolyte features three-dimensional polymeric networks that may trap water primarily via surface tension(Dubal et al., 2018). One of the most significant benefits of adopting solid-state electrolytes, such as those found in SCs, is that they enable the fabrication of pliable structures and customizable shapes for a variety of desired applications. For example, several solid-state devices have been produced using PVA-based hydrogels, including flexible, stretchy, flexible micro-, printable micro-, on-chip micro-, 3D micro-, yarn, wire, or fiber-shaped, transparent, ultrathin, and weaveable SCs (Kang et al., 2016).

2.7.5. Hydrogel electrolytes

Hydrogels is unique because of their three-dimensional crosslinked polymer meshwork structure, they have a proclivity for absorbing huge volumes of water and bonding it together while maintaining the network structure in its swollen state. The existence of polar hydrophilic components in hydrogels is responsible for the presentation of such occurrences in them such as SO_3H, OH, NH_2, COOH, and $CONH_2$ as branching groups throughout the polymer network. Water absorption is a characteristic of hydrogels that is determined by the hydrophilicity of connected groups, swelling media, and crosslinked bonding strength. Crosslinking regulates water absorption and contributes to the network structure remaining swollen (Abad et al., 2003; Ahmed, 2015; Ali & Zaidi, 2005; Bhattarai et al., 2010). Crosslinkers are critical for secondary interactions with biological tissues, as are hydrophilic groups involved in water uptake (Nie et al., 2019). Due to their semi-solid phase and intrinsic flexibility, hydrogels have recently garnered considerable attention for energy storage and conversion applications. The disadvantages of conventional energy storage and conversion technologies include their high weight, mechanical rigidity, and unsustainable nature. Additionally, because commercially available devices involve liquid electrolytes, there is the issue of device leakage. Due to

the organic nature of liquid electrolytes, they are expensive and potentially dangerous to humans. As a result, these devices incorporate hydrogel electrolytes. Hydrogel electrolytes are semi-solid, biocompatible, biodegradable, and cost-effective. Together with the inherent flexibility, these properties are critical for practical applications in energy storage devices, particularly supercapacitors (Huang et al., 2017). Electrochemical devices made of hydrogels become flexible, stretchable, and elastic, allowing them to function while being stretched, bent, folded, and twisted. These features significantly outperform those of conventional electrochemical devices. Additionally, hydrogels are self-healing, a vital characteristic for wearable and portable electronic devices. The capacity of the gadgets to self-heal or manage damage makes them ideal for smart and light-weight electronics (Huang et al., 2015; Z. Wang et al., 2018).

The substitution of water for organic solvents as a plasticizer in gel-polymer electrolytes significantly reduces the device's cost (Choudhury et al., 2009; Pal et al., 2019). The hydrogel-polymer electrolyte is a gel-polymer-carrying water electrolyte (Bashir et al., 2020). Due to hydrogels' unique ability to conduct ions with dimensional stability, a variety of energy storage devices have been constructed employing hydrogels as electrolytes. Batteries and supercapacitors are incorporated. Indeed, due to the presence of a liquid phase, gel-polymer electrolytes have a higher ionic conductivity than solid-state electrolytes. Numerous polymer hosts have been investigated in order to construct polymer hydrogel electrolytes. Chitosan, sodium alginate, agar, cellulose, starch, poly (ethylene oxide) (PEO), poly (acrylic acid) (PAA), poly (acrylamide), poly (ether ether ketone) (PEEK), and poly (vinyl alcohol) (PVA) are a few examples (Alipoori et al., 2020; Fang et al., 2019a; Y. Guo et al., 2018; Han et al., 2020; Y. Khan et al., 2020; Saborío et al., 2019; Willfahrt et al., 2019; H. Yang et al., 2019; L. Yang et al., 2020; H. Zhang et al., 2020).

Chen et al. investigated six distinct forms of PVA-based hydrogels in conjunction with six distinct electrolytes, including H_2SO_4, KOH, NaOH, NaCl, H_3PO_4, and KCl, in order to develop supercapacitors with graphene-based electrodes. The results revealed that when all PVA-based hydrogels are compared, the PVA-H_3PO_4 hydrogel electrolytes have the best capacitive performance. Electrochemical measurements were used to obtain this comparison. In comparison to the other ions in gel electrolytes (K^+, Na^+, Cl^- and OH^-), the H^+ ion has the shortest ionic radius, contributing to the high capacitance of PVA/H_3PO_4. The radius of the ions is proportional to how quickly and easily they can diffuse through the electrode. At similar molar concentrations, H_3PO_4 produces significantly more unbounded ions than NaOH or NaCl. Thus, PVA-H_3PO_4 hydrogel electrolytes exhibit the highest specific capacitance of all salt electrolytes investigated (Chen et al., 2014) . Due to their size-controlled morphology, biodegradability, and biocompatibility, chitosan-based hydrogel electrolytes are receiving growing interest. Yang et al. recently synthesised carboxylated chitosan-g-poly (acrylamide)/lithium sulphate hydrogel electrolytes by covalent crosslinking. Hydrogel electrolytes demonstrated increased ionic conductivity (1.74 x 10^{-2} S/cm) and mechanical strength. Sandwiched hydrogel electrolytes between carbon electrodes generated 8.7 W h/kg of energy and 350.3 W/kg of power over a wide potential range of 0 to 1.4 V.

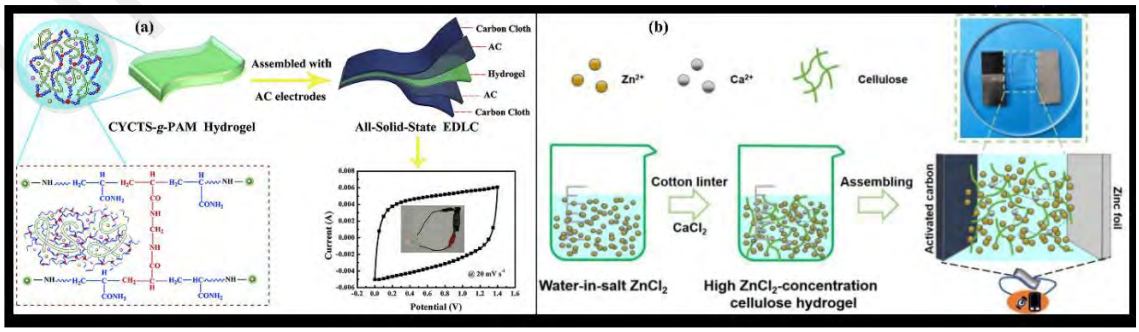

Figure 2.15 : (a) Synthesis and supercapacitor assembly containing prepared covalently carboxylated chitosan hydrogel electrolytes (Yang et al., 2019). (b) Synthesis of physically crosslinked cellulose hydrogel electrolytes and zinc ion hybrid supercapacitor assembly (Yang et al., 2020).

The manufacturing and assembly of a supercapacitor using the produced hydrogel electrolytes are depicted in Figure 2.15a (H. Yang et al., 2019). Yang et al. demonstrated the use of biodegradable cellulose-based hydrogel electrolytes containing highly concentrated zinc chloride in zinc ion hybrid supercapacitors. The supercapacitors had a specific capacitance of 193 mA h g^{-1}, an energy density of 192 W h kg^{-1}, and a power density of 16,976Wkg^{-1}, and they remained stable and worked at a temperature of 20 C. Figure 2.15b (L. Yang et al., 2020) illustrates the synthesis of the hydrogel electrolytes and the hybrid supercapacitor structure. Additionally, all-in-one supercapacitor production is a novel process that involves very close contact between the electrodes and electrolytes. To create an asymmetric supercapacitor, we employed biodegradable cellulose hydrogels crosslinked with epichlorohydrin at low temperatures as electrolytes and nitrogen-doped graphene hydrogels as electrodes. The supercapacitor demonstrated a rate capability of 89.5 percent at a current density of 16 A/g and a capacitance retention of 93.9 percent after 5000 charge/discharge cycles (H. Wang et al., 2019).

2.8 Prior Works on Polymer Electrolyte Based Electrochemical Capacitors

Hezhen Yang et al. (Tan et al., 2009) produced a flexible GPE film with good conductivity based on green biopolymer-carboxylated chitosan via solution casting and hydrochloric acid crosslinking for all-solid-sate SCs. To prepare the carboxylated chitosan hydrogel (CCH) film, carboxylated chitosan powder (1.0 g) was dissolved in deionized water (10 ml) at room temperature while stirring magnetically to form carboxylated chitosan casting solution. After allowing the solution to settle for a few minutes to remove any air bubbles, coat casting on the glass plate was performed. Spin coating was utilised to produce the casting solution as a film, and spin coating at a speed of 500 rpm/min for 6 seconds was employed to control the film thickness. Finally, the

glass plate containing the solution was cross-linked for 6 hours in hydrochloric acid solution, resulting in a CCH film with a thickness of 0.532 mm. The transparent and flexible CCH film exhibited a number of desirable properties, including strong ionic conductivity, high electrolyte absorption capacity, and high flexibility. The resulting carboxylated chitosan hydrogel sheet exhibited a high electrolyte absorption rate of 742.0 weight percent and a maximum ionic conductivity of 8.69 S cm^{-1}. The device demonstrated excellent electrochemical performance, with a specific capacitance of 45.9 Fg1 at 0.5 A g^{-1}. Within the 0–0.9 V potential window, the maximum energy density of the constructed EDLC was 5.2 Wh kg^{-1} at a power density of 226.6 Wkg^{-1} and a high power density of 2206.5 Wkg1 at 1.9 Wh kg^{-1} (Tan et al., 2009).

Shengmei Chen et al. (Ito et al., 2007) demonstrated for the first time a flexible solid-state zinc ion hybrid supercapacitor (ZHS) based on co-polymer derived hollow carbon spheres (HCS) as the cathode material, polyacrylamide (PAM) hydrogel as the polymer electrolyte, and deposited zinc on carbon cloth as the anode material. The polyacrylamide (PAM) hydrogel electrolyte was prepared using an in-situ polymerization process. Under vigorous stirring, 80 mM zinc sulphate ($ZnSO_4$) was typically dissolved in 40 mL deionized (DI) water. Then, under vigorous magnetic stirring at 40 °C, 10 g of acrylamide was added to the aforementioned solution. Following that, 2 mg of N, N'-methylenebisacrylamide was added to the aforesaid solution as cross-linkers and 50 mg of potassium persulfate was added as an initiator. The solution was then maintained at 40 °C for 2 hours. For 30 minutes, the mixed solution was degassed and enclosed under a nitrogen environment to remove any dissolved oxygen. Finally, the $ZnSO_4$ PAM film formed following a two-hour free-radical polymerization at 70 oC. A flexible solid-state ZHS with a maximum discharge capacity of 86.8 mAh g^{-1} and an energy density of 59.7 Wh kg^{-1} is available. Additionally, it has exceptional cycling stability, retaining 98 percent of its capacity after 15,000 cycles at a current density of 1.0 Ag^{-1}. The solid-state

ZHS is customizable enough to withstand varied deformations such as squeezing, twisting, and folding due to the flexible electrodes and electrolyte (Ito et al., 2007).

Huili L. et al. created ultra-stretchable and better healable supercapacitors based on a double cross-linked hydrogel electrolyte (Lee et al., 2001). They described a nanocomposite hydrogel composed of a copolymer poly(2-acrylamido-2-methylpropane sulfonic acid-co-N,N-dimethylacrylamide) (poly(AMPS-co-DMAAm)) that was cross-linked using Laponite (a synthetic hectorite-type clay) and graphene oxide as double linkers (GO). To generate the poly(AMPS-co-DMAAm)/Laponite/GO nanocomposite hydrogels, the monomers AMPS and DMAAm were co-polymerized in situ in the presence of GO and Laponite dispersion. To create a homogenous dispersion, 0.32 g, 2.5 wt percent GO was dispersed in 7.8 mL deionized water with continuous stirring for 20 minutes. This was followed by 30 minutes of ultrasonic vibration. Then, 0.16 g Laponite was added to the GO suspension and the mixture was agitated for 15 minutes. The AMPS (0.38 g), DMAAm (1.05 mL), and initiator potassium persulfate (KPS; 0.01 g) were added one at a time and stirred for 15 minutes. Finally, a catalyst of N,N,N′,N′-tetramethylethylenediamine (TEMED; 10 L) was combined with stirring for 5 minutes to generate the precursor. Transfer of the precursor into a handmade mould was followed by 24 hours of in-situ free radical co-polymerization at ambient temperature. The hydrogel films were cut into appropriate shapes (thickness ranging from 0.8 to 1.5 mm) for characterisation or usage in supercapacitors. The resulting hydrogel has good mechanical stretchability (tensile strength of 34 KPa and stretchability of 1173 percent), great ionic conductivity, and exceptional healability. Not only do supercapacitors constructed with this hydrogel as the gel electrolyte exhibit an ultrahigh mechanical stretchability of 1000 percent, but they also exhibit repeated healable performance when exposed to infrared light and heating. Additionally, the broken/healed supercapacitor exhibits an extremely high stretchability of up to 900 percent with only a little performance degradation of 15%.

This lauded hydrogel electrolyte may be easily functionalized by incorporating other functional components, and it can also be extended for application in various multifunctional portable and wearable energy devices (Lee et al., 2001). Sandra A. Alexandre et al. (2019) produced a highly sticky poly(ionic liquid) and a commercial ionic liquid (PIL/IL) gel polymer electrolyte for application in flexible solid state SCs. They demonstrated the preparation of a novel gel polymer electrolyte (GPE) with significant adhesive properties in their work by combining a synthesised poly(ionic liquid) composed of poly(1-vinyl-3-propylimidazolium bis(fluorosulfonyl)imide) (poly(VPIFSI)) and a commercial ionic liquid composed of 1-ethyl-3-methyl imidazolium bis(fluorosulf (EMIFSI). Two phases were used to produce the polymeric ionic liquid poly(1-vinyl-3-propylimidazolium bis(fluorosulfonyl)imide) poly(VPIFSI). To begin, the IL monomer VPIBr was directly polymerized to form the poly(ionic liquid) 1-vinyl-3-propylimidazoliumbromide-poly (VPIBr). The second stage involves the modification of the produced poly(ionic liquid) via an ion exchange reaction between the poly(VPIBr) and the lithium bis(fluorosulfonyl)imide (LiFSI) (PVIFSI). The PIL/IL-GPE was made using the solution casting process and contained poly(VPIFSI) as the host polymer in concentrations of 30, 50, and 70% by weight of IL. Separately, 0.5 g of poly(VPIFSI) was dissolved fully in 5 mL of acetone for 8 hours. The solution was then added in corresponding amounts of EMIFSI ionic liquid and stirred until a homogenous solution was obtained.The effect of the PIL/IL-GPE (50 wt.% IL) on the properties of a flexible solid state SC was investigated using electrochemical impedance spectroscopy (EIS), cyclic voltammetry (CV), and the galvanostatic charge/discharge technique, which enables synchronous measurements or determination of the cell voltage and positive and negative electrode potentials. The adhesive PIL/IL-GPE has a high conductivity, a good interaction between the PIL matrix and the IL liquid phase that prevents leakage and hence ensures safety, and the gel electrolyte adheres and wetts well to the electrode

surface. All of these outstanding qualities have been combined to create a device with increased rate capability and cyclability that exhibits little change in the cell's specific capacitance, energy density, or power density when folded (Ono et al., 2000). Pankaj Tuhania et al. (2012) created a novel ionic liquid (IL)-doped solid polymer electrolyte based on poly (vinylidene fluoride-co-hexafluoropropylene) as the host polymer (PVDF-HFP) and a low-viscosity dopant, 1-ethyl-3-methylimidazolium thiocyanate, enabling effective electrochemical double- (EDLC). Through the solution casting procedure, pure and IL-doped electrolyte films were created. To make IL-doped films, PVDF-HFP was dissolved in acetone for 2 hours using a magnetic stirrer and a directly chosen amount of IL was added to maintain the required ratio (by weight) in PVDF-HFP films. To obtain a homogeneous viscous solution of polymer-IL, the mixture was stirred overnight with a magnetic stirrer. The resultant solution was dried at room temperature in polypropylene petri dishes, followed by vacuum drying to remove any leftover acetone (if any), resulting in freestanding films of pure PVDF-HFP and IL-doped films. Conductivity measurements, electrochemical stability window (ESW) studies, optical microscopy, and Fourier transform infrared (FTIR) spectroscopy were used to characterise the films. Finally, they constructed a device utilising an IL-doped sheet with the highest conductivity as the electrolyte material. Electrochemical impedance spectroscopy of the polymer electrolyte doped with ionic liquid demonstrated a sixfold increase in the conductivity behaviour of the electrolyte films due to IL doping. A linear sweep voltammetric research and examination of the electrolyte films demonstrated a stable electrochemical range of 3.6 V. Polarized optical microscopy of the produced films revealed a decrease in crystallinity as a result of the IL doping. The FTIR spectroscopy analysis confirms the film's composite origin. The greatest conductivity value obtained is 2.65 mS cm^{-1} for an 80 percent ionic-doped solution. Additionally, the constructed EDLC demonstrates a specific capacitance of 2.36 Fg^{-1} (Yoo, 2012).

CHAPTER 3 : EXPERIMENTAL PROCEDURE AND CHARACTERIZATION TECHNIQUES

3.1 Production of the various hydrogel electrolyte and electrode material

This chapter discusses the materials that were used in this study. The second section discusses the sample preparation and characterisation procedures. The construction of the electrode is discussed in detail in the following part, and the final section discusses the manufacturing and characterization of the EDLC and hydrogel electrolytes.

3.1.1 Materials

N-hydroxymethylacrylamide (NHMA), ammonium persulfate (APS), sodium montmorillonite, carbon black (super P), poly (vinylidene fluoride) having molecular weight of 534, 000 g/mol were purchased from Sigma Aldrich, USA. N-Methyl-2-pyrrolidone (purity ≥ 99.5%) and activated carbon (particle size = 5 - 20 μm, surface area = 1800 – 2000 m^2/g) were obtained from Kuraray Chemical Co., Ltd. (Japan) and Merck (Germany), respectively. Lithium trifluoromethanesulfonate (LiTF) was obtained from Cross Organic, Malaysia. Deionized water was used throughout the experiment.

3.1.2 Preparation of hydrogel electrolyte

Hydrogels were created with the use of free radicals. In this process, N-hydroxymethylacrylamide (NHMA) was polymerized in the presence of clay sodium montmorillonite utilising ammonium persulfate (APS) as a free radical initiator. The monomer, APS, and clay combination was heated to 110°C and stirred continuously until a viscous hydrogel formed. Under conditions of heating at the temperature of 110 °C with continuous stirring, sulphate anion free radicals were produced from ammonium persulfate (APS), which worked as a free radical initiator. The heating is continuously

done until the reactants form a semi solid form. The radicals then extracted protons from water molecules, generating hydroxyl free radicals. Due to the presence of the vinyl group, these hydroxyl free radicals created free radicals of N-hydroxymethylacrylamide, which resulted in polymerization of N-hydroxymethylacrylamide and so the propagation reaction was initiated. Sodium montmorillonite was used as a crosslinking agent in this polymerization. Thus, the polymer chains connected to the clay platelets created a physically crosslinked network structure that was stable. Additionally, LiTF was used to create hydrogel electrolytes. Li^+ ions and sulfonate anions reacted ionically with the polymer's hydroxyl, -NH, and C=O groups (N-hydroxymethylacrylamide). The structure of the hydrogel produced was in a transparent semi-solid form and has the elasticity intact in the structure. The technique of production of hydrogel electrolyte is depicted in Figure 3.1.

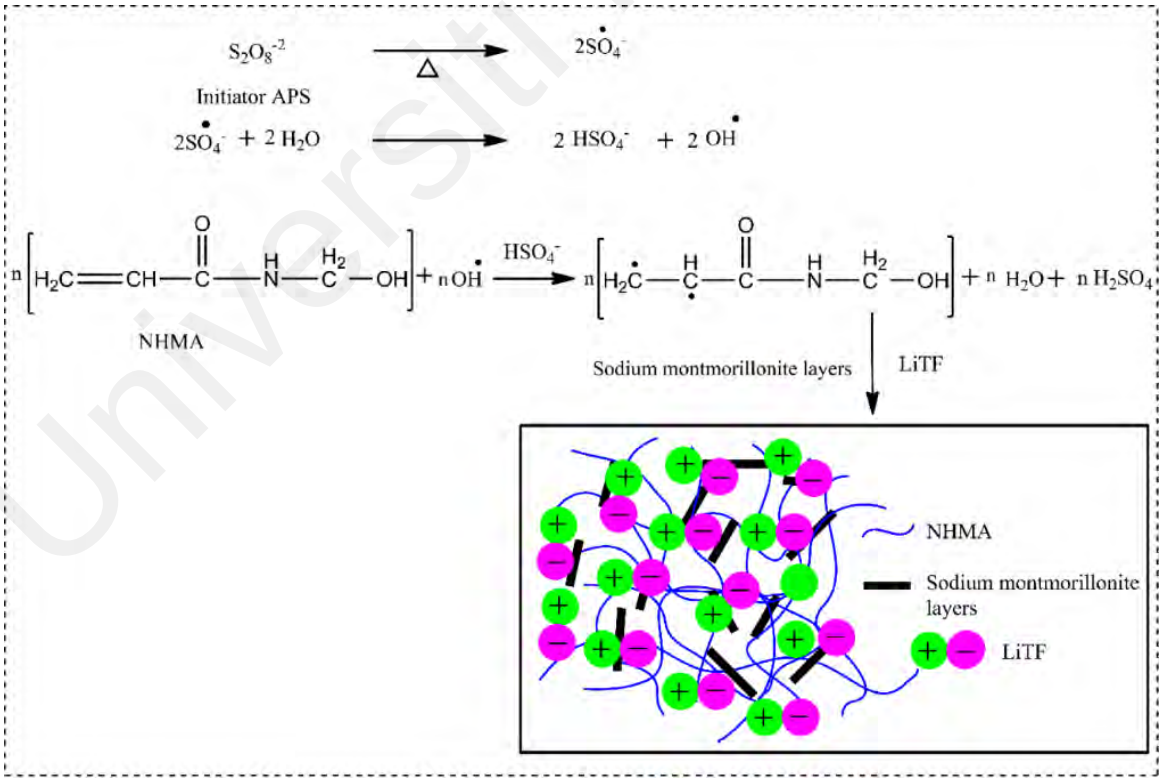

Figure 3.1 : Mechanism of synthesized hydrogel electrolyte

Similarly, hydrogel electrolytes were made using the same procedure by adding lithium trifluoromethanesulfonate salt at various quantities (LiTF). The electrolytes produced from poly (N-hydroxymethylacrylamide) were described and used for electrochemical research. Table 3.1 summarises the procedure for synthesising hydrogel electrolytes.

Table 3.1 : Synthesis scheme of hydrogel electrolytes.

Formulation	NHMA (mg)	Clay (mg)	APS (mg)	Salt (mg)
NHMA	1000	0.3	5	0
NHMA 1	900	0.3	5	100
NHMA 2	800	0.3	5	200
NHMA 3	700	0.3	5	300
NHMA 4	600	0.3	5	400

3.2 Material Charaterisation

3.2.1 Characterisation

Fourier-transform infrared spectroscopy (FTIR), X-ray diffraction (XRD), and Field emission scanning electron microscopy (FESEM) were used to characterise the physicochemical properties of hydrogel electrolytes. FTIR analysis was used to observe the structural characterization and functional group identification of hydrogel electrolytes before and after synthesis, utilising a Perkin Elmer spectrometer with a resolution of 1 cm^{-1} in the range of 4000 cm^{-1} to 500 cm^{-1}. Transmittance FTIR spectra were acquired. The crystalline and amorphous properties of hydrogel electrolytes were investigated using X-ray diffraction analysis. XRD was performed in this work using an X-ray diffractometer equipped with Cu K radiation (1.5406 Å) at a voltage of 40 kV and a current of 30 mA.. The surface morphology and porosity of the hydrogel electrolyte are critical properties that affect ionic conductivity and ion transport.

As a result, we investigated these properties using field emission scanning electron microscopy (FEG-400). Prior to all of these studies, the hydrogel and hydrogel electrolytes were freeze-dried.

3.3 Electrochemical Analysis

3.3.1 Electrochemical Impedance Spectroscopy (EIS) Studies

The ionic conductivity of hydrogel electrolytes was determined using an impedance spectroscopic instrument, the Hioki 3532-50 LCR HiTESTER, at frequencies ranging from 50 Hz to 5 MHz and temperatures ranging from 25 to 100 °C. This was accomplished by storing samples in a sample container. Stainless steel blocking electrodes were used to install this holder. The bulk resistance was determined using the hydrogel electrolytes' complicated impedance graphs (Cole-Cole plot). The ionic conductivity (σ) of the hydrogel electrolytes was determined using the area of the blocking electrodes [A (cm^2)], the bulk resistance of the hydrogel electrolytes [R_b (Ω)], and the thickness of the hydrogel electrolytes [L (cm)], as specified in equation 3.1.

$$\sigma = \frac{L}{R_b A} \tag{3.1}$$

3.4 Preparation of electrode material

Carbon slurry was used to produce the working electrode (active material). This slurry was made in N-methyl-2-pyrrolidone solvent by adding activated carbon, carbon black, and poly (vinylidene fluoride) binder in the proportions of 80:10:10. This mixture was stirred continuously for 24 hours at room temperature to ensure homogeneity. Following that, the slurry was coated on graphite electrodes and cured overnight at 90 degrees Celsius.

Weighing the graphite electrodes before and after coating with active material and drying provided the mass of the active material. The difference in mass was considered as the active material mass, which in this experiment was 0.8 mg.

3.5 Symmetric Supercapacitor Cell Fabrication and Supercapacitor Performance Studies

Symmetric supercapacitor cells were constructed by sandwiching hydrogel electrolytes between two activated carbon coated electrodes and subjected to CV and GCD using a Gamry interface 1000 potentiostat. CV measurements were made at scan rates of 5, 10, 20, 30, 40, 60, 70, 80, 90, and 100 mV/s in the 0-1.0 V potential region. Additionally, GCD was detected at current densities ranging between 200 and 500 mA/g. The specific capacitance (C_{sp}) of EDLC was determined using the following equations 3.2 and 3.3 from CV and GCD readings.

$$C_{sp(CV)} = \frac{A}{\Delta V v m} \tag{3.2}$$

$$C_{sp(GCD)} = \frac{I \Delta t}{\Delta V m} \times 2 \tag{3.3}$$

Where A is the integral area of the CV loop, V denotes the potential window, v denotes the scan rate in V/s, m denotes the mass of active material on both electrodes in gram (g), I denotes the discharge current in ampere (A), and t denotes the discharge time in second (s) following the IR drop. The following equations 3.4 and 3.5 were used to compute the specific energy (E; W h/kg) and specific power (P; W/kg) respectively.

$$E = \frac{1}{2} C_{sp(GCD)} \times (\Delta V)^2 \times \frac{1000}{3600} \tag{3.4}$$

$$P = \frac{E}{\Delta t} \tag{3.5}$$

CHAPTER 4 :RESULTS AND DISCUSSION

4.1. Introduction

In this work, hydrogel has been synthesized as mentioned in Chapter 3. The samples have been further characterized to evaluate the performance properties. To understand the self-healing properties, a cut-heal test was used to visually illustrate the stimulus-free self-healing tendency. The hydrogel's capacity for self-healing was then evaluated qualitatively based on whether each separated component was adhering back. The hydrogel was cut to break on, the two fractured parts were brought into touch, the hydrogel self-healed after two hours, and the specimen was then cut once again. It was pulled from each side, and the hydrogel showed good mechanical strength. This is a result of the interaction between polymers that occurred during the polymerization process.

4.1.1. Fourier transform infrared (FTIR)

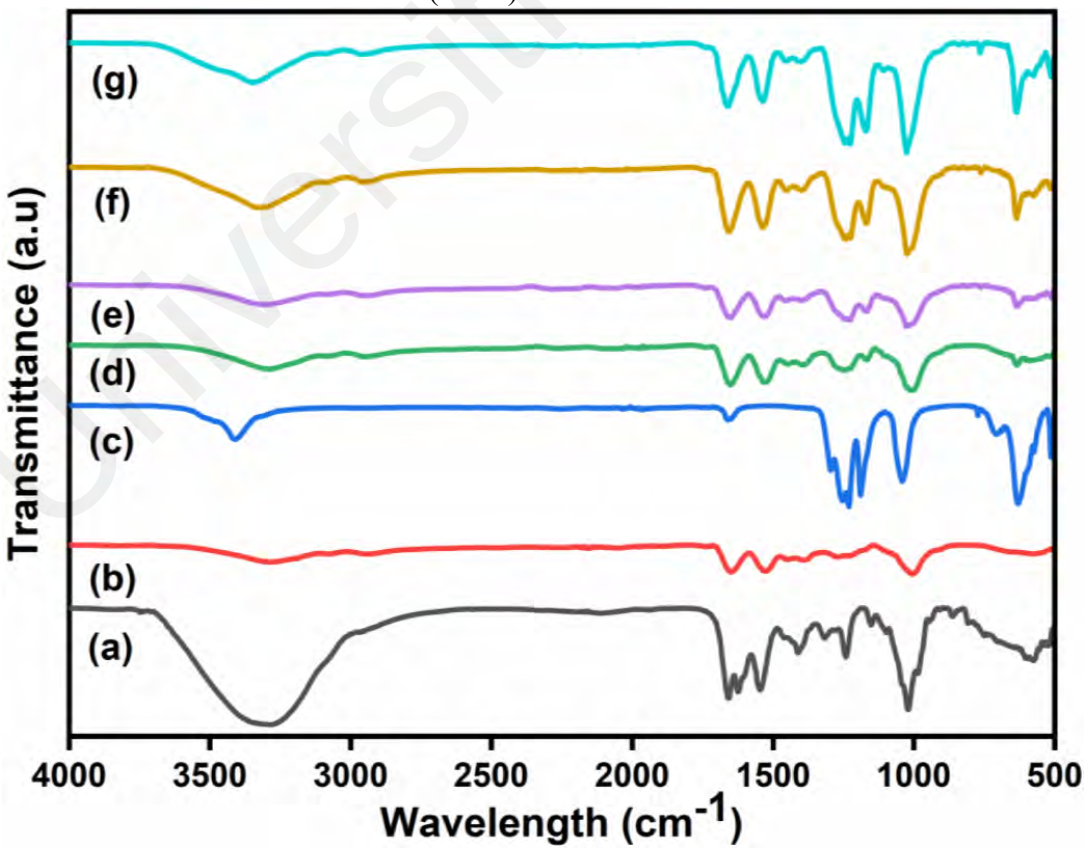

Figure 4.1 :FTIR spectra of a) N-hydroxymethylacrylamide, b) NHMA hydrogel, c) LiTF, d) NHMA1, e) NHMA2, f) NHMA3, and g) NHMA4.

The FTIR spectra of N-hydroxymethylacrylamide, NHMA hydrogel, LiTF, NHMA1, NHMA2, NHMA3, and NHMA4 hydrogel electrolytes are shown in Figure 4.1 (a-g).

The peaks at 3310 cm^{-1} in the spectrum of N-hydroxymethylacrylamide indicate the presence of an O-H stretching vibration. At 1660 cm^{-1}, the absorption is attributed to the amide group. The C=C, C-N stretching vibration, C-H deformation, and C-O stretching vibrations are represented by the peaks at 1610 cm^{-1}, 1543 cm^{-1}, 1404 cm^{-1}, and 1240 cm^{-1}, respectively. The spectrum of LiTF is shown in Figure 4.1 (c), with three significant peaks at 1230 cm^{-1}, 1185 cm^{-1}, and 1030 cm^{1}, corresponding to the stretching vibration of C-F, antisymmetric stretching of C-F, and stretching vibration of S=O. (sulfonate) respectively. The FTIR spectrum of NHMA hydrogel is shown in Figure 4.1(b).

The NHMA peaks are plainly visible in this spectrum; the peak at 3408 cm^{-1} corresponds to the O-H stretching vibration, while the peak at 1656 cm^{-1} corresponds to the amide group. The peak at 1610 cm^{-1} indicating the existence of C=C in NHMA has completely vanished. The removal of the C=C peak and the subsequent shifting of the peak indicate the successful development of the hydrogel. Additionally, the NHMA peaks at 1256 cm^{-1} exhibited the C-O stretching vibration of NHMA. Additionally, Figure 4.1 depicts the spectra of hydrogel electrolytes containing LiTF (NHMA1, NHMA2, NHMA3, and NHMA4 in d, e, f, & g respectively). These spectra demonstrate the presence of NHMA functional groups as well as LiTF, with the exception of NHMA's C=C group and a peak shift to 1648 cm^{-1} due to electrostatic interaction and the formation of H-bonds between the polymer and salt. Additionally, practically all of the peaks of N-hydroxymethylacrylamide and LiTF can be seen in these spectra, indicating that hydrogel electrolytes containing LiTF were successfully prepared.(Silvaraj et al., 2021)

4.1.2. X-ray diffraction (XRD)

The phase structure of NHMA hydrogels NHMA1, NHMA2, NHMA3, and NHMA4 was investigated using XRD analysis. Figure 4.2 illustrates the XRD diffractograms. Only two

large peaks at 9.7° and 22.4° are visible in the diffractogram of NHMA hydrogel, indicating the network's amorphous structure. Due to the strong hydrogen bonds and polar intra- and intermolecular interactions, these peaks could be ascribed to a long-range chain order (Khan,et al.,, 2020). The diffractogram of the NHMA1 hydrogel electrolyte demonstrated that LiTF was properly exfoliated in the hydrogel. LiTF is a crystalline salt characterised by several sharp peaks indicating a highly crystalline structure.

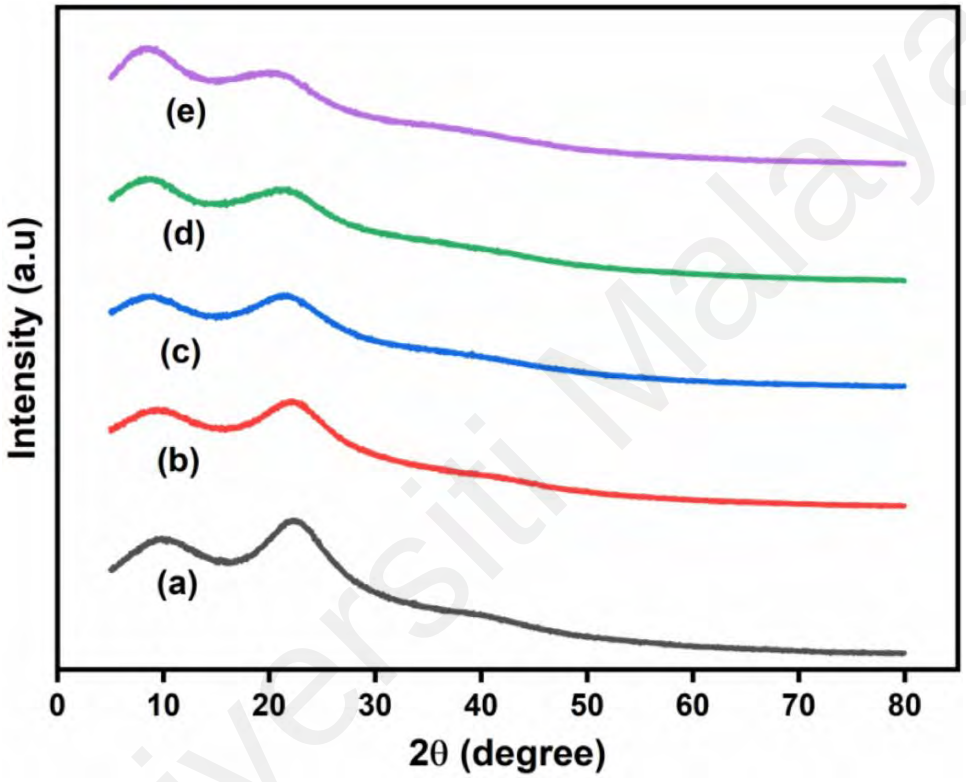

Figure 4.2 : XRD diffractograms of a) NHMA hydrogel, b) NHMA1, c) NHMA2, d)NHMA3, and e) NHMA4.

According to the literature, LiTF has sharp peaks at 16.27°, 19.5 °, 22.24 °, 31.98 °, 39.65 °, and 48.35 ° (N.B. Sahli, 2012). However, the diffractogram of NHMA1 does not have a peak for LiTF. This result is consistent with the interaction of polymer with LiTF, which revealed the hydrogel's amorphous structure and complete salt complexation with the polymer matrix. As a result, we can conclude that LiTF dissociate in a suitable manner within the hydrogel network. The XRD diffractograms of NHMA2, NHMA3, and NHMA4 exhibited similar tendencies to those of NHMA1. These findings imply that

LiTF dissociates and diffuses inside the hydrogel network. The interaction of salt and polymer accentuated the amorphous aspect of the material. Second, the ionisation of salt resulted in an increase in the hydrogel electrolytes' ionic conductivity. Ions could freely migrate throughout the amorphous network structure. However, the trend of NHMA4 was marginally altered. The initial peak at 8.6o was slightly displaced from its original position of 9.7^{o} in NHMA, indicating an interaction between the polymer and LiTF, while the peak's intensity rose in comparison to NHMA1, NHMA2, and NHMA3. This increase in intensity is a result of the reassociation of Li^{+} and TF ions as the concentration of the hydrogel electrolyte increases.

4.2.3 Morphology Study

The morphology of freeze-dried hydrogels and hydrogel electrolytes was examined using a field emission scanning electron microscope (FESEM), which offers structural information.The internal morphology of the hydrogels, as illustrated in Figure 4.3, demonstrates the morphology's dependence on the composition. As illustrated in Figure 4.3, the NHMA hydrogel formed a highly porous three-dimensional network with a regular pore structure. The pores are larger, and the dispersion is extremely uniform.

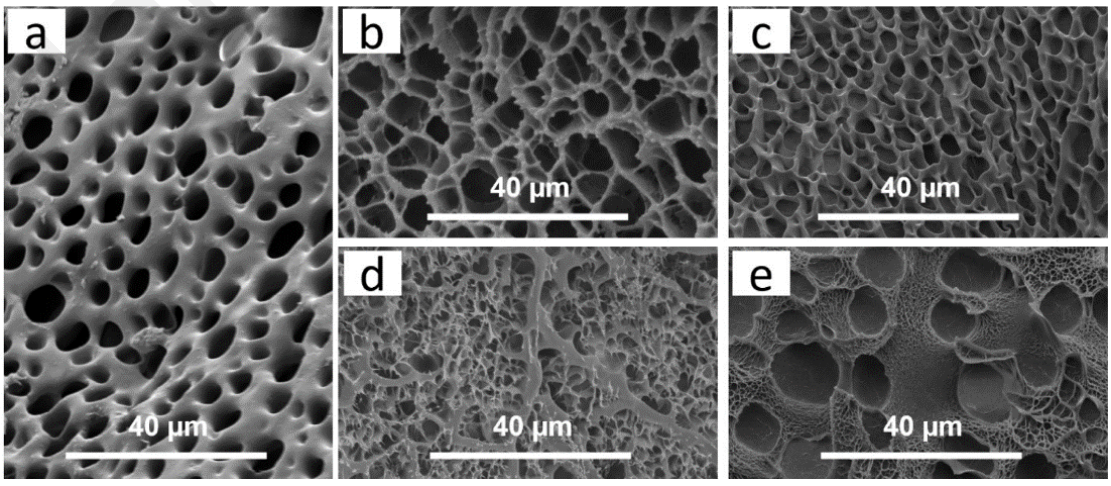

Figure 4.3 : Surface morphology images of a) NHMA, b) NHMA1, c) NHMA2, d) NHMA3, and e) NHMA4.

The large and homogeneous pore size is due to the development of an interconnected three-dimensional network with precise monomer, initiator, and crosslinking ratios. Additionally, uniform pore size can be produced by heating the mixture at a steady rate. This densely coupled porous network can maintain a high-water content (Wang et al., 2020). However, when lithium trifluoromethanesulfonate (LiTF) was added to produce hydrogel electrolytes, the surface shape and pore size changed. The hydrogel electrolytes' pore size, distribution of pore size, and surface morphology altered significantly from the pristine NHMA hydrogel, owing to the creation of novel physical and ionic interactions between the host polymer and the lithium trifluoromethanesulfonate (LiTF). The surface became rough, and the pore size decreased. The roughness on the surface is related to the polymer's decreased crystallinity, while the reduction and irregularity in pore size are attributable to the novel interactions between poly (N-hydroxymethylacrylamide) and LiTF. Figure 4.3 (b-e) illustrates the surface roughness and pore size fluctuation clearly. As can be seen, the addition of salt increased the density of the polymer network by interconnecting the pores (Hamzah et al., 2012). In aqueous media, the polymer containing C=O, OH, NH, and methyl groups decomposed into Li^+ ion and trifluoromethanesulfonate anion. The dissociation of the salt created topological disorder, and the Li^+ ion interacted with the C=O, NH, and OH groups, whilst the salt anion interacted with the methyl group. These interactions intensified as the salt concentration grew from 10% to 40% (NHMA1, NHMA2, NHMA3, and NHMA4), and the pore size became compact and gradually decreased as the salt level increased (H. Wang et al., 2019; N. Zhao et al., 2019). The hydrogel electrolytes' interconnected pores promoted ionic transport between the electrode and electrolyte. In the absence of a blocking phase, the transport of ions throughout the hydrogel electrolyte network increased the ionic conductivity of hydrogel electrolytes through the interconnected pores (Fang et al., 2019b; Fan et al., 2018). The mobility of ions increased from 10% to 30% salt, and the

ionic conductivity increased as well (J. Khan et al., 2020; Zhu et al., 2012). Though the pores almost vanished after 40% salt was added due to the creation of a dense network and the utilisation of available space. Due to the high salt content, agglomeration occurred, and the restricted flow of ions resulted in a decrease in ionic conductivity (Y. Khan et al., 2020).

4.2 Electrochemical impedance spectroscopy (EIS)

Ionic conductivity is the fundamental and critical property of electrolytes utilised in energy storage devices. Electrical impedance spectroscopy was used to determine the ionic conductivity of the hydrogel electrolytes. Ionic conductivity plots against temperature are shown in Figure 4.4, Figure 4.5 and Figure 4.6 .

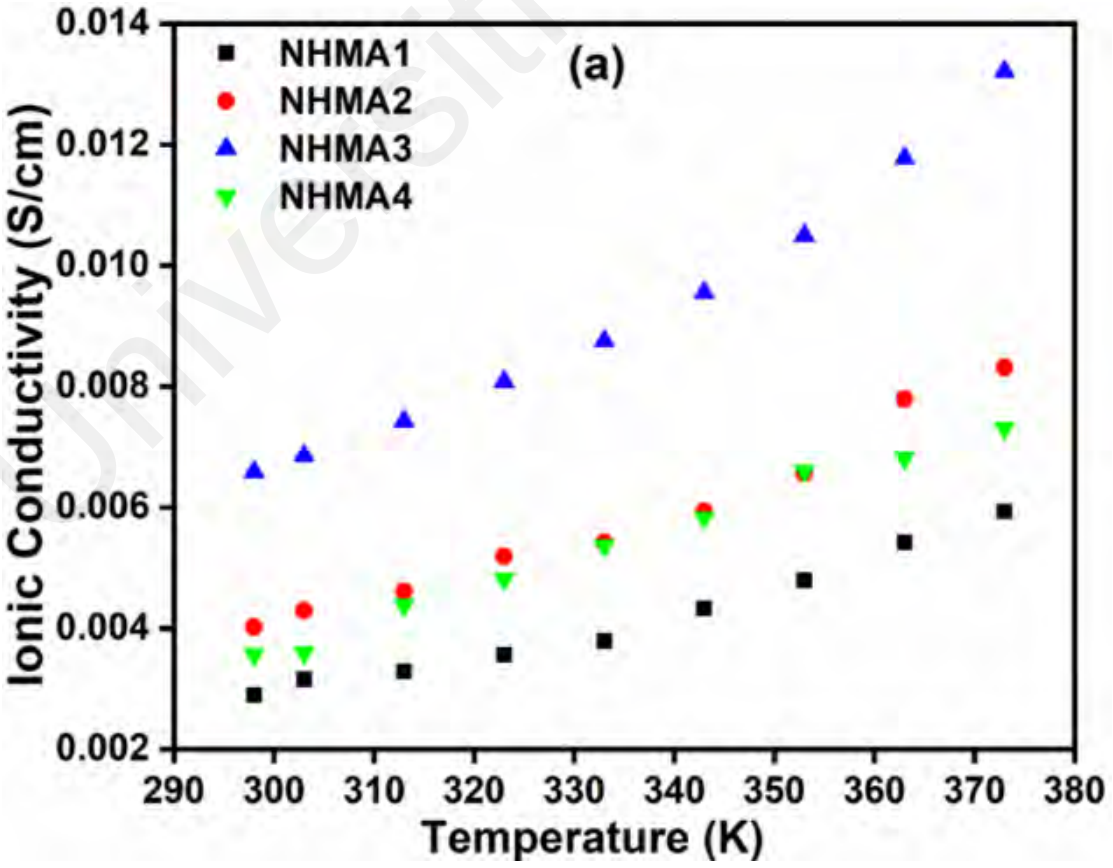

Figure 4.4 : Ionic conductivity against temperature

The results demonstrated that adding salt had an effect on ionic conductivity. Increases in the concentration of LiTF in the hydrogel electrolyte increased the ionic conductivity. The hydrogel electrolyte containing 10 wt.% LiTF (NHMA1) demonstrated a low ionic conductivity (2.9×10^{-3} S cm^{-1}) and a high bulk resistance. The poor ionic conductivity was due to a limited number of charge carriers, but the ionic conductivity improved with increasing salt content, as demonstrated by 4.01×10^{-3} S cm^{-1} and 6.6×10^{-3} S cm^{-1}, respectively, for NHMA2 and NHMA3 hydrogel electrolytes. The increase in ionic conductivity was caused by the flow of ions across the polymer chains, which was aided by the polymer segmental motion's great amplitude.

Thus, segmental motion either enables ions to hop between sites or creates a conduit for them to go. The addition of 40% LiTF to the NHMA4 hydrogel electrolyte decreased the ionic conductivity to 3.6×10^{-3} S cm^{-1}. This drop was caused by the salt association and a reduction in the amount of space available for the salt ions to freely move. Salt ions could form neutral pairs, and the presence of an excess of ions resulted in increased resistance in the ion's migration toward the corresponding electrodes.

The association between logarithmic ionic conductivity and inverse absolute temperature for NHMA1, NHMA2, NHMA3, and NHMA4 is depicted in Figure 4.5. These findings established the existence of a direct relationship between ionic conductivity and temperature. With increasing temperature, the ionic conductivity of NHMA1, NHMA2, NHMA3, and NHMA4 increased. This rise was caused by an increase in charge carrier mobility. These results are consistent with the Arrhenius rule, owing to the close proximity of the regression value to unity. The increase in ionic conductivity as a function of temperature may be due to polymer expansion and the development of more space. Additionally, charge carriers obtained sufficient energy to overcome the activation energy. As a result, they began jumping to the empty gaps created by the expanding

polymer. Following that, the transfer of free ions throughout the polymer chain increased ionic conductivity (Chong et al., 2016).

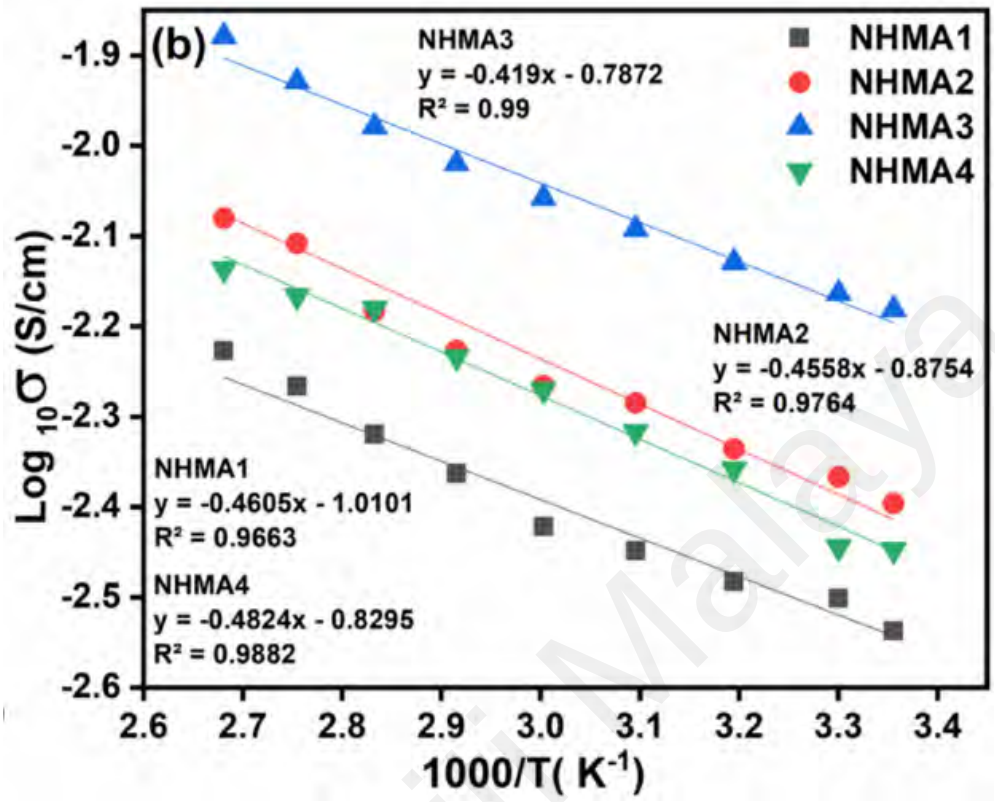

Figure 4.5 : logarithmic ionic conductivity vs inverse absolute temperature for NHMA1, NHMA2, NHMA3 and NHMA4,

Activation energy also revealed that NHMA3 has a higher conductivity than NHMA1 (0.091 eV) and NHMA2 (0.089 eV), owing to its lower activation energy of 0.085 eV, however NHMA4 has a lower ionic conductivity and a higher activation energy (0.095 eV) than NHMA3. Increased heat energy (temperature) also results in increased potential and mechanical energy, which facilitates the polymer's dynamic segmental motion. Bond rotations result in segmental motion due to the polymer chain's fast internal modes, which favour inter- and intra-chain ion hopping, increasing the degree of conductivity via free routes. The activation energy was determined using the equation 4.1:

$$\sigma = \sigma_o e^{\frac{-Ea}{kT}} \qquad (4.1)$$

Where is the ionic conductivity, o is the pre-exponential factor, E_a is the activation energy, k is the Boltzmann constant, and T is the absolute temperature.

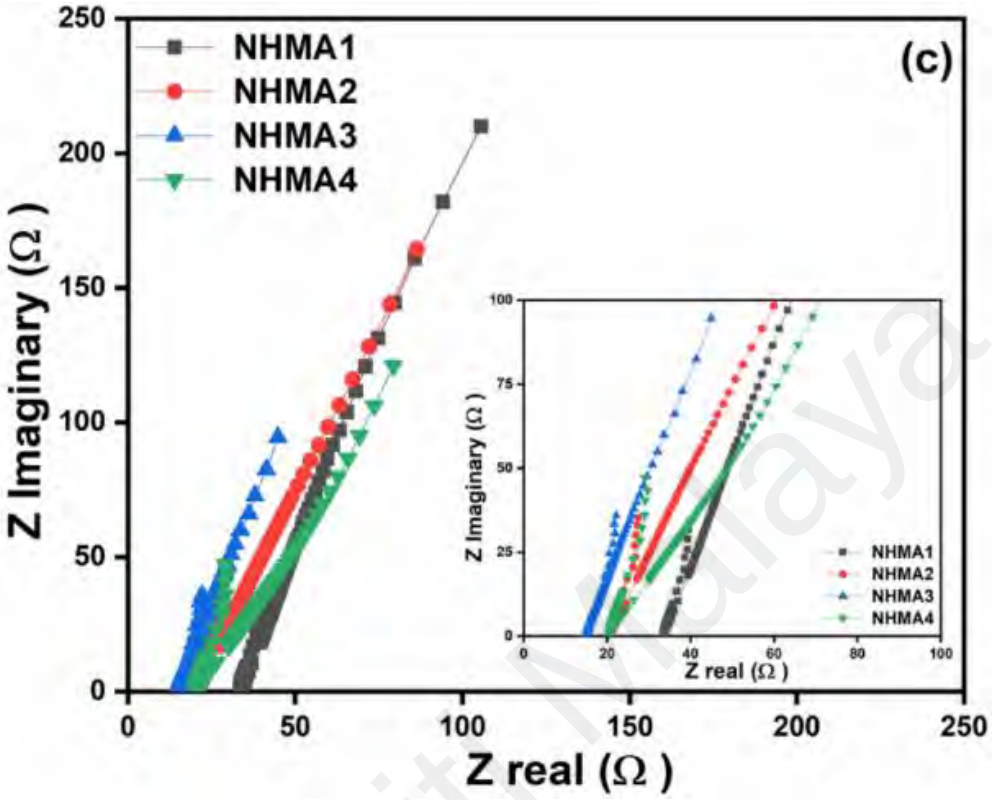

Figure 4.6 : Real vs imaginary impedance spectroscopy.

The Nyquist plots of the NHMA1, NHMA2, NHMA3, and NHMA4 hydrogel electrolytes are shown in Figure 4.6. The Nyquist plot is composed of two regions: a low frequency zone indicating capacitive properties, and a high frequency region with an arc indicating the electrolyte's equivalent series resistance (ESR). The semicircle is incomplete due to the low ESR caused by the rapid passage of charge carriers at the electrode-electrolyte interface. The charge carriers in the system are the mobile ions that were responsible for the electrolyte's total electrical conductivity. Additionally, excellent connections are formed at the interface between the electrodes and the polymer electrolytes (Ng et al., 2015). Vertical lines parallel to the imaginary axis at low frequencies depict the electrolyte's internal charge resistance, the electrode's intrinsic resistance, the

electrode/electrolyte contact interfacial resistance, and the current collector.(Chang & Park, 2006)

The ideal electrolyte exhibits a vertical line parallel to the imaginary axis. However, these hydrogel electrolytes do not exhibit a straight line parallel to the imaginary axis, and the angle of this line is depending on the composition of the hydrogel. At low frequencies, the charge transfer in NHMA3 was shown to be more vertical than that of other hydrogel electrolytes in this work. This ideal vertical line in the case of NHMA3 indicates that ions have a significantly lower diffusion resistance, which favours electrolyte permeation and increases the ion transfer kinetics and maximum number of free ions, implying that ions have rapid and smooth transportation in the hydrogel electrolyte, as well as faster diffusion at the electrode surface and a better capacitive characteristic (Chong et al., 2018). Additionally, the hydrogel electrolyte has a higher proportion of water due to the porous polymer network structure, and the ion transport is essentially identical to that of a liquid, with cations and anions migrating towards the corresponding electrodes across the polymer network (Fang et al., 2019).

4.3 Cyclic voltammetry

CV analysis is the most logical way for determining the capacitive properties of materials utilised in energy storage devices. The electrochemical performance of the supercapacitor devices as produced was determined using a symmetric two-electrode arrangement with approximately 2 mm thick hydrogel electrolytes sandwiched between graphite electrodes. CV was investigated in the potential range 0-1 V at scan speeds ranging from 5 mV/s to 100 mV/s, as illustrated in Figure 4.7 (a-d). The CV curves of hydrogel electrolytes exhibit quasi-rectangular and symmetrical forms, showing higher electrolyte wettability, reduced charge transfer resistance, superior electrolyte ion transport, and relatively perfect capacitive behaviour of supercapacitor due to its high ionic conductivity.

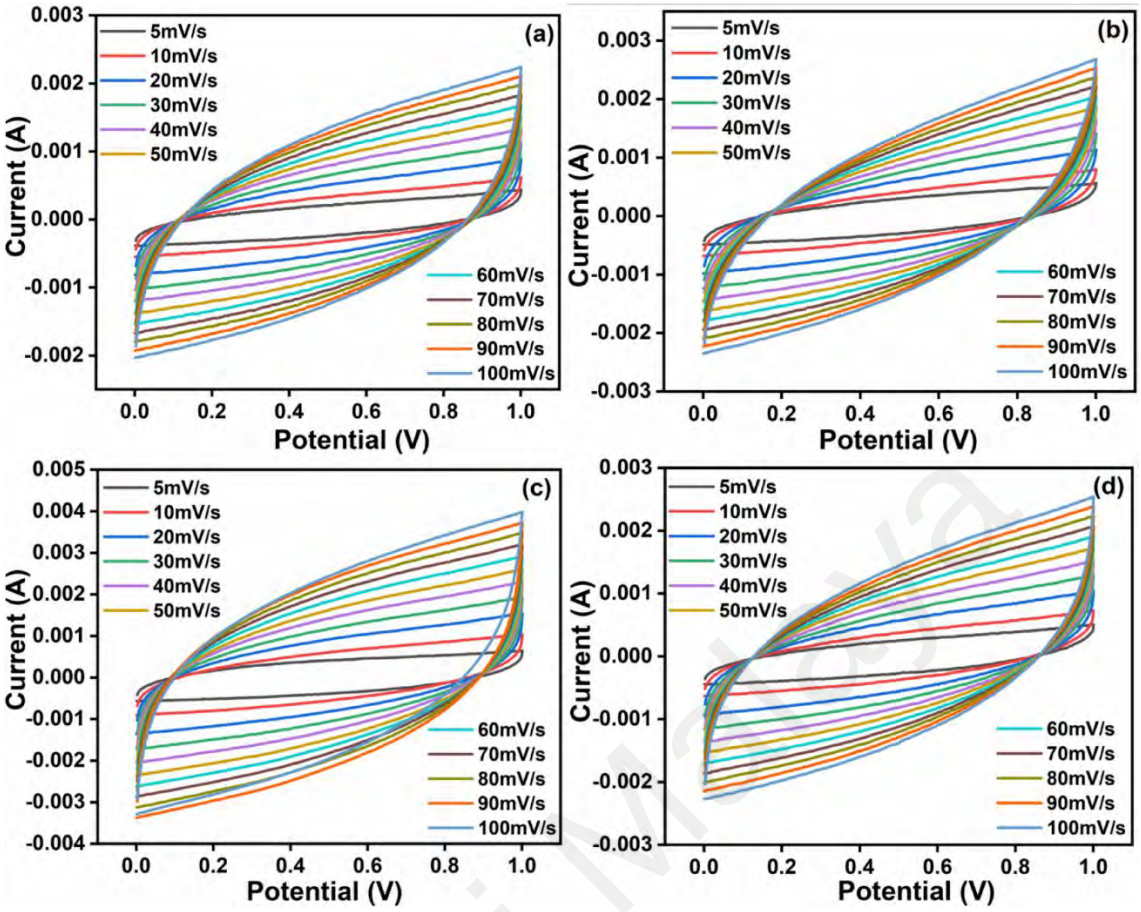

Figure 4.7 : Cyclic Voltammetry curves of a), AC/NHMA1/AC, b) AC/NHMA2/AC, c) AC/NHMA3/AC, and d) AC/NHMA4/AC.

Interestingly, synthetic hydrogel electrolytes exhibit an outstanding double layer capacitive characteristic, as seen by their CV curves being rectangular in shape and exhibiting no oxidation or reduction peak. CV curves at various scan rates indicated an optimal rate capability and polarisation at high scan rates. The voltammogram maintained its rectangular form to the maximum extent possible when the scan rate was increased, and the current value was observed to grow as the scan rate was increased. The currents (I) appear to be quite steady and remain unchanged during cycling, indicating that the ions entrapped in the hydrogel electrolytes move smoothly. However, hydrogel electrolytes were unable to preserve the whole rectangular CV curve shape at higher scan rates, and their specific capacitance also dropped as the scan rate increased. The distortion

of the rectangular shape and decrease in specific capacitance with increasing scan rate were caused by an incomplete electrode/electrolyte interaction, decreased electrolyte adhesion to the electrode, increased contact resistance, and a delay in reverse adsorption of ions at the electrode/electrolyte interface, a phenomenon dubbed the "Electrolyte Starvation Effect" (Li et al., 2021; Wang et al., 2018). Due to the imperfect interaction and decreased diffusion of electrolyte ions to the electrode materials as a result of the shorter ion diffusion time, the active electrode materials were unable to be utilised, which lowered the kinetics of double layer development. Additionally, these factors contributed to the decrease in charge storage behaviour (Liu et al., 2020). Additionally, these curves distinguished the effect of salt content on hydrogel electrolytes' performance. At 5 mV/s, AC/NHMA1/AC exhibited a tiny CV area and a low specific capacitance of 94.54 F/g. Due to the increase in ionic transport, AC/NHMA2/AC had a larger CV area and a specific capacitance of 121.11F/g at 5 mV/s than AC/NHMA1/AC. The addition of LiTF to AC/NHMA3/AC at a concentration of 30% led in an increase in CV area and specific capacitance of 165.19 F/g at 5 mV/s. This is because LiTF is completely dissociated within the NHMA3 hydrogel that was utilised to produce AC/NHMA3/AC.

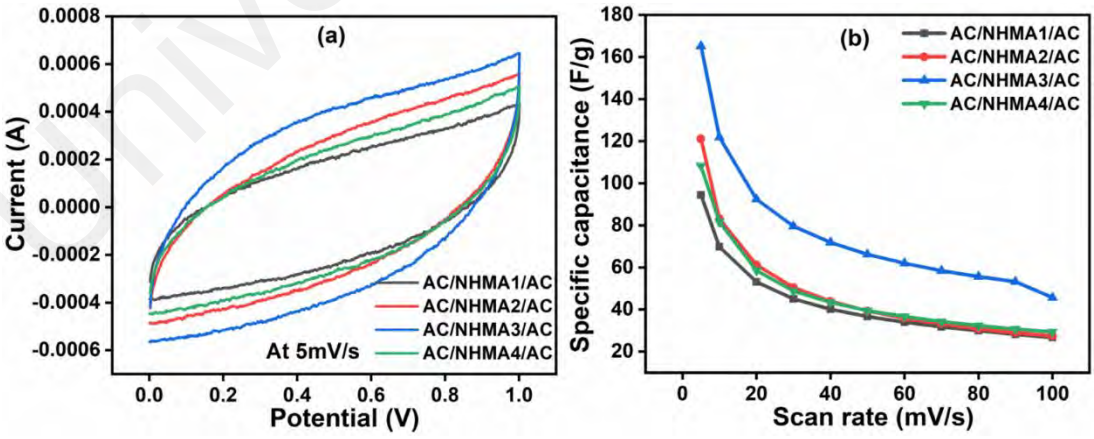

Figure 4.8 : a) Comparison of CV curves of hydrogel electrolytes at 5 mV/s and b) presents the relationship between scan rate and specific capacitance.

The specific capacitance of the AC/NHMA4/AC cell, on the other hand, was reduced to 108.21 F/g at 5 mV/s due to the salt association in NHMA4. The salt association increased the internal resistance to ion movement, lowering the ionic conductivity of the hydrogel electrolyte and the cell's electrochemical performance. It is well established that the conductivity of a hydrogel matrix is affected by the dissolution of a homogenous salt. The overall performance of all cells at 5 mV/s is compared in Figure 4.8, as is the relationship between scan rate and specific capacitance (a & b).

4.4. Galvanic charge discharge (GCD)

Galvanic charge discharge was used to further study the electrochemical performance of the devices generated from the hydrogel electrolytes. The galvanic charge discharge experiment was conducted at current densities ranging from 200 to 500 mA/g. Figure 4.9 illustrates the results of the galvanic charge discharge (a-d). The two identical galvanostatic curves had highly symmetric triangular shapes with a minimal internal resistance (IR) drop, indicating an excellent reversible capacitance characteristic and low internal resistance. Additionally, Figure 4.10 shows the specific capacitance of the cells at various current densities and a comparison of the cells' GCD curves (a & b). Charge discharge curves are linear, indicating perfect contact between electrode and electrolyte and confirming the optimum EDLC behavior. The devices' curves were identical regardless of charge discharge duration or specific capacitance. The results indicated that the devices' charge discharge and specific capacitance were depending on the current density and composition of their hydrogel electrolytes. All devices created with hydrogel electrolytes had a higher charge discharge and specific capacitance at low current densities and a lower charge discharge and specific capacitance at high current densities.

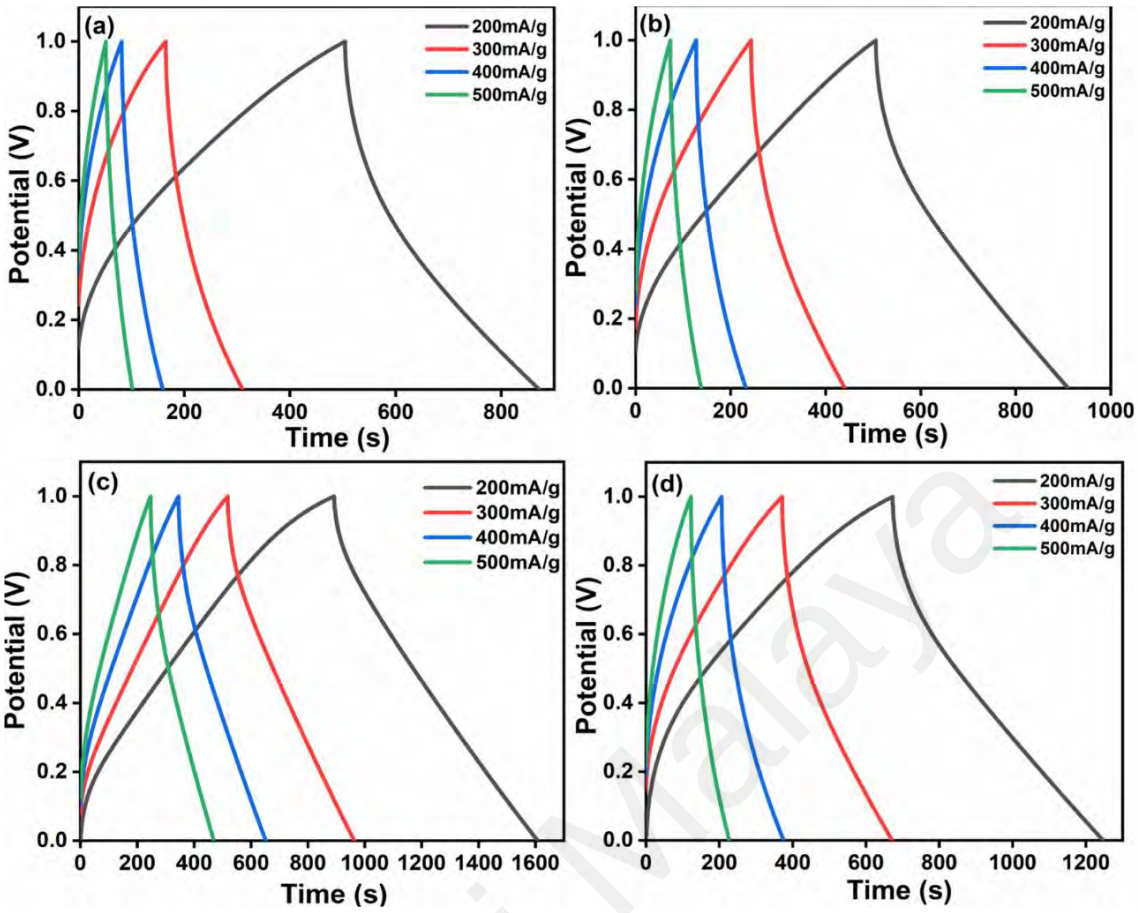

Figure 4.9 :GCD curves of a), AC/NHMA1/AC, b) AC/NHMA2/AC, c) AC/NHMA3/AC, and d) AC/NHMA4/AC.

The discharge time and specific capacitance of the devices decreased as the current density increased. This is because the ions from the hydrogel electrolyte do not have enough time to permeate the porous structure of AC at high current rates. At low current rates, the ions can enter the internal surfaces of the AC, resulting in a prolonged discharge duration (Bidin et al., 2018). Additionally, the time required to discharge the charge varied according to the composition of the hydrogel electrolytes. Due to the low LiTF content in AC/NHMA1/AC, the discharge time and specific capacitance were short. At a current density of 200 mA/g, the specific capacitance, specific energy, and specific power of AC/NHMA1/AC were 123.64 F/g, 17.19 W h/kg, and 56.3 W/kg, respectively. As with AC/NHMA2/AC and AC/NHMA3/AC, the discharge duration and specific capacitance increased as the LiTF content rose. At a current density of 200 mA/g, the specific

capacitance, specific energy, and specific power of AC/NHMA2/AC were 167.05 F/g, 22.35 W h/kg, and 196.36 W/kg, respectively. The increased discharge time and specific capacitance were caused by the increased ion transport compared to the previous device. Specific capacitance, specific energy, and specific power rose further as the salt concentration of AC/NHMA3/AC increased. This cell measured 287.96 F/g of specific capacitance, 39.63 W h/kg of specific energy, and 199.16 W/kg of specific power. The worse performance of the AC/NHMA1/AC and AC/NHMA2/AC in comparison to the AC/NHMA3/AC is due to the lower conductivity, which results in a decrease in IR. Additionally, this cell had a tiny IR drop due to the electrolyte's strong ionic conductivity and low resistivity, and typically, coulombic efficiency decreased as the quantity of ions transported increased. This cell demonstrates the electrolyte's excellent conductivity, as well as a higher charge rate and reversibility of electrode/electrolyte interaction. This is the same scenario as was noticed in CV. However, increasing the LiTF concentration resulted in a decrease in discharge time and specific capacitance, as seen by the results of AC/NHMA4/AC, which contains 40% LiTF. At a current density of 200 mA/g, the specific capacitance, specific energy, and specific power of AC/NHMA4/AC were 231.81 F/g, 31.71 W h/kg, and 198.56 W/kg, respectively. This is because there is reduced dissociation of LiTF contents and the creation of complex ion aggregations, which slow down ionic transport. Figure 4.10 illustrates the comparison of GCD curves and specific capacitance vs current density (a & b).

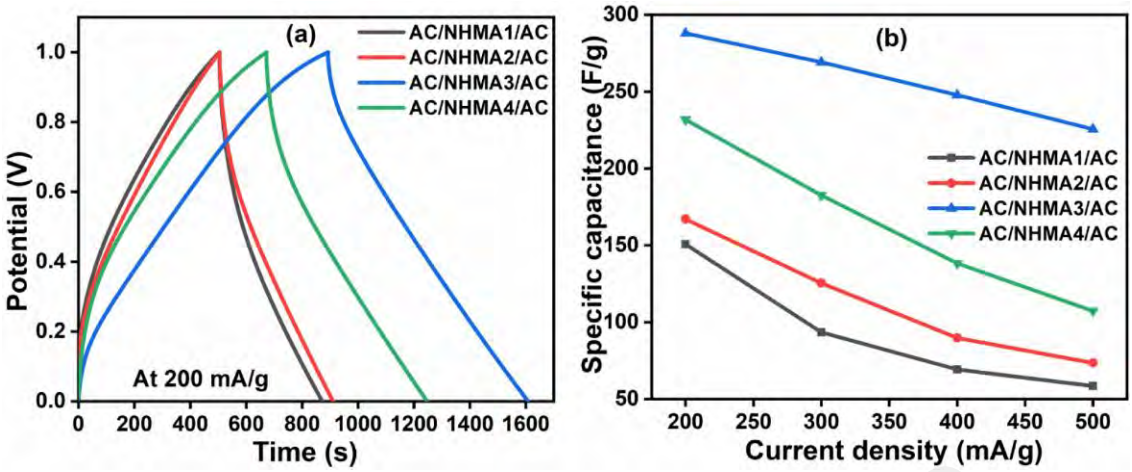

Figure 4.10 a) Comparison of GCD curves of all cells, b) the relationship between specific capacitance and current density.

The Ragone plot of all four cells is shown in Figure 4.11 (a), revealing an inverse relationship between specific energy and specific power. AC/NHMA3/AC produced a maximum of 39.63 W h/kg of specific energy and 199.16 W/kg of specific power. This cell maintained a specific energy density of 30.92 W h/kg while delivering a specific power density of 496.9 W/kg. The acquired specific energy is more than that reported in the current literature on supercapacitor hydrogel electrolytes (Bashir et al., 2020; Y. Guo et al., 2018; Na et al., 2019; Park et al., 2019; Peng et al., 2019). Table 4.1 compares the performance of previously reported supercapacitors made on hydrogel electrolytes to our findings. Longevity and consistent performance of the constructed supercapacitor are crucial factors in today's competitive economy. As a result, the cyclic stability of the manufactured supercapacitor was determined using galvanic charge-discharge measurements at a fixed current density of 5 A/g in a potential window ranging from 0 to 1 V, and the results are plotted and presented in Figure 4.11. (b).

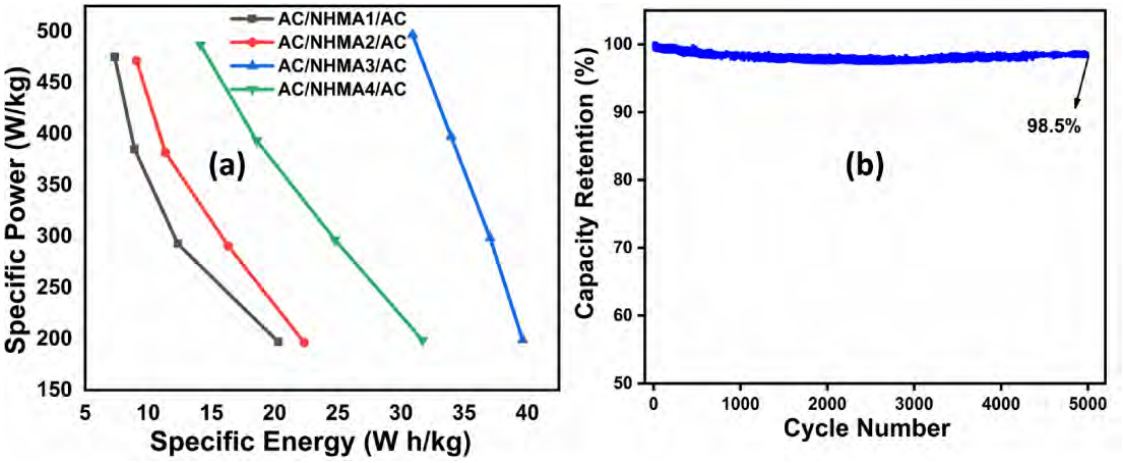

Figure 4.11 : a) Ragone plot of AC/NHMA1/AC, AC/NHMA2/AC, AC/NHMA3/AC and AC/NHMA4/AC, and b) Life cycle of AC/NHMA3/AC.

After 5000 cycles, the stability study revealed a coherent charge-discharge time and the supercapacitor kept 98.5 percent capacitance. The supercapacitor was constructed using porous carbon electrodes and a hydrogel electrolyte, as is well known.

Supercapacitors made of carbon typically have a long cycle life. The minor drop in capacitance, on the other hand, was almost certainly caused by the loss of charges initially held at the interfaces associated with the weakly connected surface groups on the porous carbon electrodes (Pandey & Hashmi, 2013). The supercapacitor cell's remarkable cycling stability was based on the following factors: (a) The first and most important element is the hydrogel electrolyte's ionic conductivity, which facilitated the rapid and smooth passage of ions during cyclic charge-discharge, resulting in an increase in energy density and power density. (b) Secondly, the porous character of the carbon electrode material encouraged increased wettability, which increased electrolyte ion accessibility to electrode materials. (c) Meso/microporous carbon electrode materials with a high surface area and hydrogel electrolyte architectures dramatically improved electrode/electrolyte interaction and electrolyte ion diffusion within the porous carbon network. (d) The improved capacitive performance was due to the well-balanced

electrode/electrolyte interaction and dispersion of electrolyte ions. Micropores in the electrode materials provided a significant amount of specific surface area that served as an ion reservoir, ensuring charge storage capability, while the abundant mesopores increased the size of the ions transport channel, enabling rapid ion transport at high current density, and the fabricated supercapacitor retained excellent capacitance retention after a lengthy cyclic study (Feng et al., 2018).

Table 4.1 : Performance comparison of supercapacitors comprised of hydrogel electrolytes.

Material	Capacitance	Specific Energy	Specific Power	Charge carriers and Solvent	Ionic conductivity	Preparation Method	Reference
Poly (acrylic acid) PAA crosslinked with Fe3+ ions hydrogel electrolyte	87.4 F/g at 0.5 A/g current density	×	×	KCl aq. solution	0.09 S/cm	Fe3+/PAA hydrogel synthesized by radical polymerization, and the ionic crosslinking mechanism, followed by the addition of potassium persulfate	(Y. Guo et al., 2016)
Poly (acrylic acid) PAA crosslinked with waterborne polyurethane (WPU)	94.6 mF/cm^2 at 1 mA/cm^2	13.14 µWh/ cm^2	0.5 mW/ cm^2	KOH aq. solution	9.6×10^{-2} S/cm	Free radical polymerization of acrylic acid followed by cross linking with WPU	(J. A. Wang et al., 2018)
Copper oxide-poly (acrylic acid) (CuO-PAA) hybrid thin films	136 F/g at 500◦C annealed temperature	x	x	H2SO4 aq. solution	×	C uCl2. 6H2O and PAA solutions were mixed to form ionically crosslinked and thin films were prepared by spin coating. Thin films were annealed at 200, 300, and 400 ◦C to form CuO-PAA phase and soaked in H2SO4	(Shaikh, Pawar, Moholkar, et al., 2011)
Influence of acrylic acid on ethylene carbonate/dimethyl carbonate/lithium trifluoromethanesulfonimide (LiTFSI) based liquid electrolyte	15.25 F/g at 50 mA/g	X	x	LiTFSI salt and dimethyl carbonate plasticizer	2.24×10^{-3} S/cm	Solution mixing of acrylic acid, ethylene carbonate, and LiTFSI for 48 hours at room temperature	(Nadiah et al., 2017)
Lignin hydrogel electrolyte film	129.23 F/g at 0.5 A/g	4.49 Wh/kg	252 W/ kg	3.3 M KOH aq. solution	0.01×10^{-3} S/cm	Lignin solution was prepared in 3.3 M KOH and PEGDGE was added at 1.2 mmol glignin 1 . Lignin hydrogel films were formed by pouring into the molds	(Park et al., 2019)
Double network lignin hydrogel electrolyte film	190 F/g at 0.25 A/g	15.24 Wh/kg	2157.3 W /kg	x	0.08 S/cm	Lignin and PEGDGE were dissolved in 1M NaOH and heated at 50 ◦C to form single network hydrogel. This hydrogel was soaked in 1M H2SO4 for 12 hours to prepare double network hydrogel	(T. Liu et al., 2020)
Dual crosslinked poly acrylic acid and vinyl hybrid silica nanoparticles (VSNPs-PAA) polyelectrolyte	106 F/g at 5mA/g	X	X	H3PO4 aq. solution	x	Acrylic acid was crosslinked using VSNPs via solution polymerization and soaked in H3PO4	(Huang et al., 2015)
Poly (acrylic acid) (PAA), (LiTFSI) salt and titania (TiO2) electrolyte membrane	28.56 F/g	X	X	LiTFSI solution	8.36×10^{-4} S/cm	PAA, LiTFSI and TiO2 solutions were mixed, and sonicated. Thin films of this solution were formed via solution casting	(Liew et al., 2016)
CuO–poly (acrylic acid) (CuO-PAA) thin film electrolyte	65 F/ g	X	x	H2SO4 aq. Solution	X	C uCl2. 6H2O and PAA solutions were mixed to form ionically crosslinked and thin films were prepared by spin coating and annealed at 400 ◦C to form CuOPAA thin film and soaked in H2SO4	(Shaikh, Pawar, Tarwal, et al., 2011)
Poly (acrylic acid-co-acrylamide) crosslinked by divalent cobalt ions electrolyte	134.1 F/g at 0.5 A/g	X	X	KCl aq. solution	0.0175 S/cm	Hydrogel was prepared via inter and intramolecular hydrogen bonding and ionic crosslinking of Co2+ and carboxylate ions. The dried hydrogel was soaked in KCl solution	(Dai et al., 2019)
Polyacrylic acid crosslinked by methacrylated graphene oxide (MGO-PAA) electrolyte	3.6 F/g at 0.1 A/g	x	X	H2SO4 aq. solution	7.16 S/m	Acrylic acid crosslinked by methacrylated graphene oxide via solution polymerization and soaked in H2SO4 to form polyelectrolyte	(Jin et al., 2018)
Poly (acrylamide)/agar hydrogel electrolyte crosslinked via MBA	92 F/g at 0.125 A/g	X	x	LiCl aq. solution	0.013 S/cm	Free radical polymerization through ultraviolet irradiation	(Fang et al., 2019a)
Polyvinyl alcohol-methacrylate/poly (acrylamide) double network hydrogel electrolyte	185.1 F/g at 0.25 A/g	16.1 Wh/kg	1432.8 W /kg	H2SO4 aq. solution	0.48 S/m	Single network hydrogel was prepared under UV light and then immersed in acrylamide and N,Nmethylenebisacrylamide and 1M H2SO4 solution and heated at 60 ◦C to form double network hydrogel electrolyte.	(Z. Liu et al., 2020)
Poly (acrylic acid) hydrogel electrolytes crosslinked via MBA	132 F/g at 50 mA/g	18.36 Wh/kg	1000 W/ kg	LiCLO4 aq. solution	x	Free radical polymerization	(Y. Khan, Bashir, Hina, Ramesh, Ramesh, & Lahiri, 2020)
Poly (acrylic acid) hydrogel electrolytes crosslinked via MBA	144.65 F/g at 0.5 A/g	19.54 Wh/kg	493.29 W /kg	CaCl2 aq. solution	10.4×10^{-3} S/cm	Free radical polymerization	(Y. Khan, Bashir, Hina, Ramesh, Ramesh, Mujtaba, et al., 2020b)
Poly (acrylamide) physically crosslinked hydrogel electrolytes	157 F/g at 50 mA/g	21.59 W h/Kg	493.29 W /kg	Lithium trifluoro methane sulfonate	9.34×10^{-3} S/cm	Free radical polymerization	(Hina et al., 2020)
Poly (N-hydroxymethylacrylamide) physically crosslinked hydrogel electrolytes	287.96 F/g at 200 mA/g	39.63 W h/Kg	199.16 W/kg	Lithium trifluoro methane sulfonate	6.6×10^{-3} S/cm	Free radical polymerization	Our work

CHAPTER 5 : CONCLUSION AND FUTURE PERSPECTIVES

5.1. Conclusion

Hydrogel electrolytes for supercapacitors were effectively synthesised via a free radical polymerization method with varying concentrations of LiTF salt (10%, 20%, 30%, and 40%). The hydrogel electrolytes produced were characterised using FTIR, XRD, and FESEM. The ionic conductivity analysis found that the hydrogel electrolyte containing 30% LiTF (NHMA3) had the highest ionic conductivity (6.6×10^{-3} S cm^{-1}) and the lowest activation energy (0.085 eV) when compared to other hydrogel electrolytes. This demonstrated that NHMA3 was superior to the other hydrogel electrolytes in terms of Li^+ ion transfer. The observed results demonstrate that all hydrogel electrolytes adhered to the Arrhenius theory.

Additionally, the produced hydrogel electrolytes were evaluated for their performance in supercapacitors equipped with activated carbon-coated graphite electrodes. The specific capacitance value was determined using cyclic voltammetry and galvanostatic charge-discharge analysis, and it reveals that NHMA3 has the highest value, measuring 165.19 F/g at 5 mV/s and 287.96 F/g at 200 mA/g, respectively. At a current density of 200 mA/g, this cell produced the most specific energy (39.63 W h/kg) at a specific power of 199.16 W/kg. As a result, the AC/NHMA3/AC electrolyte demonstrated the highest capacitance properties when compared to the other hydrogel electrolytes prepared, demonstrating that 30% LiTF is the optimal salt concentration for the cell's maximal electrochemical performance. After 5000 consecutive charge-discharge cycles at a current density of 5 A/g, this supercapacitor cell preserved 98.5 percent capacitance.

5.2. Future perspectives

The goal of this research was to see if a self-healing hydrogel electrolyte might be used instead of aqueous or ionic liquid electrolytes in electrochemical supercapacitor applications. FTIR, XRD, and SEM were used in the hydrogel electrolyte characterization process. Transmission electron microscopy (TEM) can be used to visualize hydrogels and generate a highly magnified image, Nuclear Magnetic Resonance (NMR) can be used to determine the molecular structure of the hydrogel at the atomic level, and differential scanning calorimetry (DSC) can be used to determine the material's thermal stability and operating temperature range. Furthermore, adjustments should be performed to increase the device's operating voltage window. This is accomplished by altering the proportions/ratios of the electrolyte elements while varying the salt content. A more effective hydrogel electrolyte for EDLC will also be possible with a different salt incorporation to the hydrogel. As a result, more room would be available for the device's capacitance and energy density values to be increased. Even though large power densities may be achieved using hydrogel electrolytes, literature shows that the equivalent series resistance of EDLCs using hydrogel polymer electrolytes is still considerable. Efforts and future research could be aimed at lowering the ESR of the EDLC device in order to achieve higher power density.

REFERENCES

Abad, L. V., Relleve, L. S., Aranilla, C. T., & dela Rosa, A. M. (2003). Properties of radiation synthesized PVP-kappa carrageenan hydrogel blends. *Radiation Physics and Chemistry*, *68*(5), 901–908.

Abdeladim Moftah, & Ashraf Al Shetiti. (2015). Review of Supercapacitor Technology. *International Journal of Computer Science and Electronics Engineering (IJCSEE)*, *3*(3), 2320 - 4028.

Acznik, I., Lota, K., Sierczynska, A., & Lota, G. (2014). Carbon-Supported Manganese Dioxide as Electrode Material For Asymmetric Electrochemical Capacitors. In *International Journal of Electrochemical Science* 9(5), 2518-2534.

Ahmed, E. M. (2015). Hydrogel: Preparation, characterization, and applications: A review. In *Journal of Advanced Research*. Elsevier B.V. , *6*(2), 105–121.

Alexandre, S. A., Silva, G. G., Santamaría, R., Trigueiro, J. P. C., & Lavall, R. L. (2019). A highly adhesive PIL/IL gel polymer electrolyte for use in flexible solid state supercapacitors. *Electrochimica Acta*, *299*, 789–799.

Alipoori, S., Mazinani, S., Aboutalebi, S. H., & Sharif, F. (2020). Review of PVA-based gel polymer electrolytes in flexible solid-state supercapacitors: Opportunities and challenges. *Journal of Energy Storage*, *27*(3), 346 - 358.

Ali, S. W., & Zaidi, S. A. R. (2005). Synthesis of copolymeric acrylamide/potassium acrylate hydrogels blended with poly(vinyl alcohol): Effect of crosslinking and the amount of poly(vinyl alcohol) on swelling behavior. *Journal of Applied Polymer Science*, *98*(5), 1927–1931.

Augustyn, V., Simon, P., & Dunn, B. (2014). Pseudocapacitive oxide materials for high-rate electrochemical energy storage. In *Energy and Environmental Science* (Vol. 7, Issue 5, pp. 1597–1614). Royal Society of Chemistry.

Bashir, S., Omar, F. S., Hina, M., Numan, A., Iqbal, J., Ramesh, S., & Ramesh, K. (2020). Synthesis and characterization of hybrid poly (N, N-dimethylacrylamide) composite hydrogel electrolytes and their performance in supercapacitor. *Electrochimica Acta*, *332*(7), 499 – 513.

Bashir, S., Teo, Y. Y., Ramesh, S., & Ramesh, K. (2018). Synthesis and characterization of karaya gum-g- poly (acrylic acid) hydrogels and in vitro release of hydrophobic quercetin. *Polymer*, *147*, 108–120.

Béguin, F., Presser, V., Balducci, A., & Frackowiak, E. (2014). Carbons and electrolytes for advanced supercapacitors. *Advanced Materials*, *26*(14), 2219–2251.

Besharat, S. F., Manteghian, M., & Abdollahi, M. (2018). Study of Polypyrrole/Graphene Oxide Nanocomposite Structural and Morphological Changes Including Porosity. *Polymer Science - Series B*, *60*(5), 664–674.

Bhattarai, N., Gunn, J., & Zhang, M. (2010). Chitosan-based hydrogels for controlled, localized drug delivery. In *Advanced Drug Delivery Reviews* (Vol. 62, Issue 1, pp. 83–99).

Bidin, M. Z., Hon Ming, N., Omar, F. S., Ramesh, K., & Ramesh, S. (2018). Solid terpolymer electrolyte based on poly(vinyl butyral-co-vinyl alcohol-co-vinyl acetate) incorporated with lithium salt and tetraglyme for EDLCs. *Journal of Applied Polymer Science*, *135*(8), 45902.

Brandt, A., Pohlmann, S., Varzi, A., Balducci, A., & Passerini, S. (2013). Ionic liquids in supercapacitors. *MRS Bulletin*, *38*(7), 554–559.

Cao, L., Xu, F., Liang, Y. Y., & Li, H. L. (2004). Preparation of the novel nanocomposite Co(OH)2/ultra-stable Y zeolite and its application as a supercapacitor with high energy density. *Advanced Materials*, *16*(20), 1853–1857.

Chang, B. Y., & Park, S. M. (2006). Integrated description of electrode/electrolyte interfaces based on equivalent circuits and its verification using impedance measurements. *Analytical Chemistry*, *78*(4), 1052–1060.

Cheng, Q., Tang, J., Ma, J., Zhang, H., Shinya, N., & Qin, L. C. (2011). Graphene and carbon nanotube composite electrodes for supercapacitors with ultra-high energy density. *Physical Chemistry Chemical Physics*, *13*(39), 17615–17624.

Chen, H. C., Chen, K. J., Wang, C. H., Lin, C. C., Yeh, C. C., Tsai, H. H., Shih, M. H., Kuo, H. C., & Lu, T. C. (2012). A novel randomly textured phosphor structure for highly efficient white light-emitting diodes. *Nanoscale Research Letters*, *7*(1), 1–5.

Chen, Q., Li, X., Zang, X., Cao, Y., He, Y., Li, P., Wang, K., Wei, J., Wu, D., & Zhu, H. (2014). Effect of different gel electrolytes on graphene-based solid-state supercapacitors. *RSC Advances*, *4*(68), 36253–36256.

Chen, S.-M., Mani, V., Ramiah, S., Ramachandran, R., & Saraswathi, R. (2014). Recent Advancements in Electrode Materials for the High-performance Electrochemical Supercapacitors: A Review metal hexacyanoferrate View project Recent Advancements in Electrode Materials for the High-performance Electrochemical Supercapacitors: A Review. In *Article in International Journal of Electrochemical Science* (Vol. 9), 4072 – 4085.

Chen, S., Zhu, J., Wu, X., Han, Q., & Wang, X. (2010). Graphene oxide-Mno2 nanocomposites for supercapacitors. *ACS Nano*, *4*(5), 2822–2830.

Chen, Y., Zhang, X., Zhang, H., Sun, X., Zhang, D., & Ma, Y. (2012). High-performance supercapacitors based on a graphene-activated carbon composite prepared by chemical activation. *RSC Advances*, *2*(20), 7747–7753.

Chong, M. Y., Liew, C. W., Numan, A., Yugal, K., Ramesh, K., Ng, H. M., Chong, T. v., & Ramesh, S. (2016). Effects of ionic liquid on the hydroxylpropylmethyl cellulose (HPMC) solid polymer electrolyte. *Ionics*, *22*(12), 2421–2430.

Chong, M. Y., Numan, A., Liew, C. W., Ng, H. M., Ramesh, K., & Ramesh, S. (2018). Enhancing the performance of green solid-state electric double-layer capacitor incorporated with fumed silica nanoparticles. *Journal of Physics and Chemistry of Solids*, *117*, 194–203.

Choudhury, N. A., Sampath, S., & Shukla, A. K. (2009). Hydrogel-polymer electrolytes for electrochemical capacitors: An overview. In *Energy and Environmental Science* (Vol. 2, Issue 1, pp. 55–67).

Conway, B. E., & Pell, W. G. (2003). Double-layer and pseudocapacitance types of electrochemical capacitors and their applications to the development of hybrid devices. *Journal of Solid State Electrochemistry*, *7*(9), 637–644.

Dai, L. xin, Zhang, W., Sun, L., Wang, X. huo, Jiang, W., Zhu, Z. wen, Zhang, H. bin, Yang, C. cai, & Tang, J. (2019). Highly Stretchable and Compressible Self-Healing P(AA-co-AAm)/$CoCl_2$ Hydrogel Electrolyte for Flexible Supercapacitors. *ChemElectroChem*, *6*(2), 467–472.

Davood Nematollahi, Saeideh Mahdinia, Peiman Karimi, Hamid Salehzadeh, & Sajad Kaihani. (2014). A green electrochemical method for the synthesis of new N,N'- diphenylbenzene-1,4-diamine derivatives. *RSC Advances*, *5*(37), 29209–29213.

Dubal, D. P., Chodankar, N. R., Kim, D. H., & Gomez-Romero, P. (2018). Towards flexible solid-state supercapacitors for smart and wearable electronics. In *Chemical Society Reviews* (Vol. 47, Issue 6, pp. 2065–2129). Royal Society of Chemistry.

Du, C., & Pan, N. (2007). Carbon Nanotube-Based Supercapacitors. *Nanotech. L. & Bus.*, *4*(1), 813 - 822.

Dutta, S., & De, S. (2016). Few layered vanadyl phosphate nano sheets-MWCNT hybrid as an electrode material for supercapacitor application. *AIP Conference Proceedings*, *1728*(4), 2122 - 2146.

Eftekhari, A. (2017). Supercapacitors utilising ionic liquids. In *Energy Storage Materials* (Vol. 9, pp. 47–69). Elsevier B.V.

Elgrishi, N., Rountree, K. J., McCarthy, B. D., Rountree, E. S., Eisenhart, T. T., & Dempsey, J. L. (2018). A Practical Beginner's Guide to Cyclic Voltammetry. *Journal of Chemical Education*, *95*(2), 197–206.

Enock, T. K., King'ondu, C. K., Pogrebnoi, A., & Jande, Y. A. C. (2017). Status of Biomass Derived Carbon Materials for Supercapacitor Application. *International Journal of Electrochemistry*, *2017*, 1–14.

Fang, L., Cai, Z., Ding, Z., Chen, T., Zhang, J., Chen, F., Shen, J., Chen, F., Li, R., Zhou, X., & Xie, Z. (2019). Skin-Inspired Surface-Microstructured Tough Hydrogel Electrolytes for Stretchable Supercapacitors. *ACS Applied Materials and Interfaces*, *11*(24), 21895–21903

Fan, W., Li, N. W., Zhang, X., Zhao, S., Cao, R., Yin, Y., Xing, Y., Wang, J., Guo, Y. G., & Li, C. (2018). A Dual-Salt Gel Polymer Electrolyte with 3D Cross-Linked Polymer Network for Dendrite-Free Lithium Metal Batteries. *Advanced Science*, *5*(9), 3401 - 3437.

Feng, L., Wang, K., Zhang, X., Sun, X., Li, C., Ge, X., & Ma, Y. (2018). Flexible Solid-State Supercapacitors with Enhanced Performance from Hierarchically Graphene Nanocomposite Electrodes and Ionic Liquid Incorporated Gel Polymer Electrolyte. *Advanced Functional Materials*, *28*(4), 2891 - 2905.

Feng, X., Yi, J., Zhang, W., Niu, Y., & Xu, L. (2019). A redox poly(ionic liquid) hydrogel: Facile method of synthesis and electrochemical sensing. *Journal of Applied Polymer Science*, *136*(42), 1521 - 1546.

Fic, K., Meller, M., & Frackowiak, E. (2015). Interfacial Redox Phenomena for Enhanced Aqueous Supercapacitors. *Journal of The Electrochemical Society*, *162*(5), A5140–A5147.

Fleischmann, S., Widmaier, M., Schreiber, A., Shim, H., Stiemke, F. M., Schubert, T. J. S., & Presser, V. (2019). High voltage asymmetric hybrid supercapacitors using lithium- and sodium-containing ionic liquids. *Energy Storage Materials*, *16*, 391–399.

Gao, Q. , Wang, W., Dong, F., Du, L., & Deng, Y. (2013). Optimizing carbon /carbon supercapacitors in aqueous and organic electrolytes. *Phys. Chem. Chem. Phys.* 2013, 15, 8692 - 8699.

Guo, L., Ma, W. bin, Wang, Y., Song, X. Z., Ma, J., Han, X. D., Tao, X. Y., Guo, L. T., Fan, H. L., Liu, Z. S., Zhu, Y. B., & Wei, X. Y. (2020). A chemically crosslinked hydrogel electrolyte based all-in-one flexible supercapacitor with superior performance. *Journal of Alloys and Compounds*, *843*(5), 2431 - 2458.

Guo, Y., Zheng, K., & Wan, P. (2018). A Flexible Stretchable Hydrogel Electrolyte for Healable All-in-One Configured Supercapacitors. *Small*, *14*(14), 1539-1548.

Guo, Y., Zhou, X., Tang, Q., Bao, H., Wang, G., & Saha, P. (2016). A self-healable and easily recyclable supramolecular hydrogel electrolyte for flexible supercapacitors. *Journal of Materials Chemistry A*, *4*(22), 8769–8776.

Gupta, K., Liu, T., Kavian, R., Chae, H. G., Ryu, G. H., Lee, Z., Lee, S. W., & Kumar, S. (2016). High surface area carbon from polyacrylonitrile for high-performance electrochemical capacitive energy storage. *Journal of Materials Chemistry A*, *4*(47), 18294–18299.

Hamzah, H., Razali, H., Yusri, M., Rahman, A., Fahmi, E. M., Ahmad, A., Nazeri, N. N. M., Hamzah, H., & Rahman, M. Y. A. (2012). Effect of $LiBF_4$ Salt Concentration on the Properties of Poly (Ethylene Oxide)-Based Composite Polymer Electrolyte Doped photoanode and doped counter electrode for DSSC View project Effect of $LiBF_4$ Salt Concentration on the Properties of Poly(Ethylene Oxide)-Based Composite Polymer Electrolyte. In *Article in International Journal of Electrochemical Science*, *7*(7) , 5798-5804.

Han, L., Huang, H., Fu, X., Li, J., Yang, Z., Liu, X., Pan, L., & Xu, M. (2020). A flexible, high-voltage and safe zwitterionic natural polymer hydrogel electrolyte for high-energy-density zinc-ion hybrid supercapacitor. *Chemical Engineering Journal*, *392*(9), 1238-1251.

Hatakeyama, Y., Okamoto, M., Torimoto, T., Kuwabata, S., & Nishikawa, K. (2009). Small-angle X-ray scattering study of Au nanoparticles dispersed in the ionic liquids 1-alkyl-3-methylimidazolium tetrafluoroborate. *Journal of Physical Chemistry C*, *113*(10), 3917–3922.

He, P., Yang, K., Wang, W., Dong, F., Du, L., & Deng, Y. (2013). Reduced graphene oxide-$CoFe_2O_4$ composites for supercapacitor electrode. *Russian Journal of Electrochemistry*, *49*(4), 359–364.

Hina, M., Bashir, S., Kamran, K., Ramesh, S., & Ramesh, K. (2020). Synthesis and characterization of self-healable poly (acrylamide) hydrogel electrolytes and their application in fabrication of aqueous supercapacitors. *Polymer*, *210*(1), 58854-58861.

Huang, Y., Zhong, M., Huang, Y., Zhu, M., Pei, Z., Wang, Z., Xue, Q., Xie, X., & Zhi, C. (2015). A self-healable and highly stretchable supercapacitor based on a dual crosslinked polyelectrolyte. *Nature Communications*, *6*(3),12502-12508.

Huang, Y., Zhong, M., Shi, F., Liu, X., Tang, Z., Wang, Y., Huang, Y., Hou, H., Xie, X., & Zhi, C. (2017). An Intrinsically Stretchable and Compressible Supercapacitor Containing a Polyacrylamide Hydrogel Electrolyte. *Angewandte Chemie - International Edition*, *56*(31), 9141–9145.

Hu, X., Chen, Y., Hu, Z., Li, Y., & Ling, Z. (2018). All-Solid-State Supercapacitors Based on a Carbon-Filled Porous/Dense/Porous Layered Ceramic Electrolyte. *Journal of The Electrochemical Society*, *165*(7), A1269–A1274.

IEA (2019, July), World Energy Outlook 2019, IEA, Paris International Energy Outlook 2019, Retrieved on 13th November 2021 from https://www.iea.org/reports/world-energy-outlook-2019.

Iro, Z. S., Subramani, C., & Hafeez, H. Y. (2016). Study of asymmetric hybrid supercapacitor using carbon and metal oxides as electrode materials. *Indian Journal of Science and Technology*, *9*(29), 1-6.

Ito, T., Yeo, Y., Highley, C. B., Bellas, E., & Kohane, D. S. (2007). Dextran-based in situ cross-linked injectable hydrogels to prevent peritoneal adhesions. *Biomaterials*, *28*(23), 3418–3426.

Ivandini, T. A., Syarif, N., Tribidasari, I., & Wibowo, W. (2012). Direct synthesis carbon/Metal oxide composites for electrochemical capacitors electrode. *International Transaction Journal of Engineering, Management, & Applied Sciences & Technologies*, *3*(1), 21-34

Jeong, H. T., Du, J. F., & Kim, Y. R. (2017). Development of Flexible Energy Storage Device by Using Polymer Electrolyte Based on Ionic Liquid. *ChemistrySelect*, *2*(21), 6057–6061.

Jin, X., Sun, G., Yang, H., Zhang, G., Xiao, Y., Gao, J., Zhang, Z., & Qu, L. (2018). A graphene oxide-mediated polyelectrolyte with high ion-conductivity for highly stretchable and self-healing all-solid-state supercapacitors. *Journal of Materials Chemistry A*, *6*(40), 19463–19469.

Jung, K.-D., Gujar, T. P., Kim, W.-Y., Puspitasari, I., & Joo, O.-S. (2007). Electrochemically Deposited Nanograin Ruthenium Oxide as a Pseudocapacitive Electrode. In *International Journal of Electrochemical Science*, *2*(1), 666 – 673.

Kang, Y. J., Yoo, Y., & Kim, W. (2016). 3-V Solid-State Flexible Supercapacitors with Ionic-Liquid-Based Polymer Gel Electrolyte for AC Line Filtering. *ACS Applied Materials and Interfaces*, *8*(22), 13909–13917.

Khan, J., Alexander, A., Ajazuddin, Saraf, S., & Saraf, S. (2020). Biomedical applications of interpenetrating polymer network gels. In *Interpenetrating Polymer Network: Biomedical Applications* (pp. 289–312). Springer Singapore.

Khan, Y., Bashir, S., Hina, M., Ramesh, S., Ramesh, K., & Lahiri, I. (2020). Effect of Salt Concentration on Poly (Acrylic Acid) Hydrogel Electrolytes and their Applications in Supercapacitor. *Journal of The Electrochemical Society*, *167*(10), 9828-9836.

Khan, Y., Bashir, S., Hina, M., Ramesh, S., Ramesh, K., Mujtaba, M. A., & Lahiri, I. (2020). Effect of Charge Density on the Mechanical and Electrochemical Properties of Poly (acrylic acid) Hydrogel Electrolytes Based Flexible Supercapacitors. *Materials Today Communications*, *25*(3), 2856-2870.

Khawula, T., Khawula, T. N. Y., Raju, K., Franklyn, P. J., Sigalas, I., & Ozoemena, K. I. (2016). Symmetric pseudocapacitors based on molybdenum disulfide (MoS2)-modified carbon nanospheres: correlating physicochemistry and synergistic interaction on energy storage. *Journal of Materials Chemistry*, *4*(17), 6411 – 6425.

Kö Tz, R., & Carlen, M. (2000). Principles and applications of electrochemical capacitors. In *Electrochimica Acta* , *45*(15-16), 2483 – 2498.

Kuilla, T., Bhadra, S., Yao, D., Kim, N. H., Bose, S., & Lee, J. H. (2010). Recent advances in graphene based polymer composites. In *Progress in Polymer Science (Oxford)* (Vol. 35, Issue 11, pp. 1350–1375). Elsevier Ltd.

Lee, K. Y., Alsberg, E., & Mooney, D. J. (2001). Degradable and injectable poly(aldehyde guluronate) hydrogels for bone tissue engineering. *Journal of Biomedical Materials Research*, 56(2), 228–233.

Lewandowski, A., & Galinski, M. (2007). Practical and theoretical limits for electrochemical double-layer capacitors. *Journal of Power Sources*, *173*(2 SPEC. ISS.), 822–828.

Liew, C.-W., Ng, H. M., Numan, A., & Ramesh, S. (2016). Poly(Acrylic acid)–Based Hybrid Inorganic–Organic Electrolytes Membrane for Electrical Double Layer Capacitors Application. *Polymers*, *8*(5), 179.

Li, G., Zhang, X., Sang, M., Wang, X., Zuo, D., Xu, J., & Zhang, H. (2021). A supramolecular hydrogel electrolyte for high-performance supercapacitors. *Journal of Energy Storage*, *33*(1), 4976-4983.

Li, H., Lv, T., Sun, H., Qian, G., Li, N., Yao, Y., & Chen, T. (2019). Ultrastretchable and superior healable supercapacitors based on a double cross-linked hydrogel electrolyte. *Nature Communications*, *10*(1), 282-286.

Li, J., Cheng, X., Shashurin, A., & Keidar, M. (2012). Review of Electrochemical Capacitors Based on Carbon Nanotubes and Graphene. *Graphene*, *01*(01), 1–13.

Lim, E., Kim, H., Jo, C., Chun, J., Ku, K., Kim, S., Lee, H. I., Nam, I. S., Yoon, S., Kang, K., & Lee, J. (2014). Advanced hybrid supercapacitor based on a mesoporous niobium pentoxide/carbon as high-performance anode. *ACS Nano*, *8*(9), 8968–8978.

Linares-Solano, A., Lillo-Ródenas, M. A., Marco-Lozar, J. P., Kunowsky, M., & Romero-Anaya, A. J. (2012). NaOH And KOH For Preparing Activated Carbons Used In Energy And Environmental Applications. *International Journal of Energy, Environment and Economics, 20*(4), 59-91.

Li, N., Tang, S., & Meng, X. (2016). Preparation of Pt-GO composites with high-number-density Pt nanoparticles dispersed uniformly on GO nanosheets. *Progress in Natural Science: Materials International*, *26*(2), 139–144.

Liu, C., Yu, Z., Neff, D., Zhamu, A., & Jang, B. Z. (2010). Graphene-based supercapacitor with an ultrahigh energy density. *Nano Letters*, *10*(12), 4863–4868.

Liu, T., Ren, X., Zhang, J., Liu, J., Ou, R., Guo, C., Yu, X., Wang, Q., & Liu, Z. (2020). Highly compressible lignin hydrogel electrolytes via double-crosslinked strategy for superior foldable supercapacitors. *Journal of Power Sources*, *449*(1), 1633-1643.

Liu, Z., Zhang, J., Liu, J., Long, Y., Fang, L., Wang, Q., & Liu, T. (2020). Highly compressible and superior low temperature tolerant supercapacitors based on dual chemically crosslinked PVA hydrogel electrolytes. *Journal of Materials Chemistry A*, *8*(13), 6219–6228.

Logerais, P.-O., Riou, O., Camara, M. A., & Durastanti, J.-F. (2013). Study of Photovoltaic Energy Storage by Supercapacitors through Both Experimental and Modelling Approaches. *Journal of Solar Energy*, *2013*, 1–9.

Lota, K., & Sierczynska, A. (2013). Effect of aqueous electrolytes on electrochemical capacitor capacitance. *Chemik*, *67*(11), 1138–1145

Lufrano, F., Staiti, P., Calvo, E. G., Juárez-Pérez, E. J., Menéndez, J. A., & Arenillas, A. (2011). Carbon Xerogel and Manganese Oxide Capacitive Materials for Advanced Supercapacitors. In *International Journal of Electrochemical Science*, *6*(1), 596 – 612.

Lu, N., Zhang, X., Na, R., Ma, W., Zhang, C., Luo, Y., Mu, Y., Zhang, S., & Wang, G. (2019). High performance electrospun Li+-functionalized sulfonated poly(ether ether ketone)/PVA based nanocomposite gel polymer electrolyte for solid-state electric double layer capacitors. *Journal of Colloid and Interface Science*, *534*, 672–682.

M Ali, G. A., Yusoff, M. M., & Feng Chong, K. (2016). *Graphene: Electrochemical Production And Its Energy Storage Properties*. Journal of Engineering and Applied Science, *11*(16), 9712-9717.

Marcano, D. C., Kosynkin, D. v., Berlin, J. M., Sinitskii, A., Sun, Z., Slesarev, A., Alemany, L. B., Lu, W., & Tour, J. M. (2010). Improved synthesis of graphene oxide. *ACS Nano*, *4*(8), 4806–4814.

Marin Halper James C Ellenbogen, V. S. (2006). *Supercapacitors: A Brief Overview. Mitre Nanosyst. Gr*.

Mayer, S. T., Pekala, R. W., & Kaschmitter, J. L. (1993). The Aerocapacitor: An Electrochemical Double-Layer Energy-Storage Device. *Journal of The Electrochemical Society*, *140*(2), 446–451.

Meng, J., Guo, H., Niu, C., Zhao, Y., Xu, L., Li, Q., & Mai, L. (2017). Advances in Structure and Property Optimizations of Battery Electrode Materials. In *Joule* (Vol. 1, Issue 3, pp. 522–547). Cell Press.

Menzel, J., Fic, K., & Frackowiak, E. (2015). Hybrid aqueous capacitors with improved energy/power performance. *Progress in Natural Science: Materials International*, *25*(6), 642–649.

Michel Armand, Frank Endres, Douglas R. MacFarlane, Hiroyuki Ohno, & Bruno Scrosati. (2009). Ionic-liquid materials for the electrochemical challenges of the future. *Nature Materials*, *8*, 621–629.

Miller, J. R., & Simon, P. (2008). Materials science: Electrochemical capacitors for energy management. In *Science* (Vol. 321, Issue 5889, pp. 651–652).

Nadiah, N. S., Omar, F. S., Numan, A., Mahipal, Y. K., Ramesh, S., & Ramesh, K. (2017). Influence of acrylic acid on ethylene carbonate/dimethyl carbonate based liquid electrolyte and its supercapacitor application. *International Journal of Hydrogen Energy*, *42*(52), 30683–30690.

Na, R., Liu, Y., Lu, N., Zhang, S., Liu, F., & Wang, G. (2019). Mechanically robust hydrophobic association hydrogel electrolyte with efficient ionic transport for flexible supercapacitors. *Chemical Engineering Journal*, *374*, 738–747.

N.B. Sahli. (2012). Effect of lithium triflate salt concentration in methyl cellulose-based solid polymer electrolytes. *IEEE Colloquium on Humanities, Science and Engineering (CHUSER),2012,* pp. 739-742

Ng, H. M., Ramesh, S., & Ramesh, K. (2015). Exploration on the P(VP-co-VAc) copolymer based gel polymer electrolytes doped with quaternary ammonium iodide salt for DSSC applications: Electrochemical behaviors and photovoltaic performances. *Organic Electronics*, *22*, 132–139.

Nie, J., Pei, B., Wang, Z., & Hu, Q. (2019). Construction of ordered structure in polysaccharide hydrogel: A review. In *Carbohydrate Polymers* (Vol. 205, pp. 225–235). Elsevier Ltd.

Niu, Z., Dong, H., Zhu, B., Li, J., Hng, H. H., Zhou, W., Chen, X., & Xie, S. (2013). Highly stretchable, integrated supercapacitors based on single-walled carbon nanotube films with continuous reticulate architecture. *Advanced Materials*, *25*(7), 1058–1064.

Noori, A., El-Kady, M. F., Rahmanifar, M. S., Kaner, R. B., & Mousavi, M. F. (2019a). Towards establishing standard performance metrics for batteries, supercapacitors and beyond. In *Chemical Society Reviews , 48*(5), 1272-1341.

Ntsoenzok, P. E., & FCT Nigeria, A. (2016). *Activated Carbon From Plant-Biomass Waste Materials As Promising Electrodes For Supercapacitor Applications*. *Carbon , 144*(1), 185–192.

Ono, K., Saito, Y., Yura, H., Ishikawa, K., Kurita, A., Akaike, T., & Ishihara, M. (2000). Photocrosslinkable chitosan as a biological adhesive. *Journal of Biomedical Materials Research , 49*(2), 289-295

Pal, B., Yang, S., Ramesh, S., Thangadurai, V., & Jose, R. (2019). Electrolyte selection for supercapacitive devices: A critical review. *Nanoscale Advances*, *1*(10), 3807–3835.

Pandey, G. P., & Hashmi, S. A. (2013). Performance of solid-state supercapacitors with ionic liquid 1-ethyl-3-methylimidazolium tris(pentafluoroethyl) trifluorophosphate based gel polymer electrolyte and modified MWCNT electrodes. *Electrochimica Acta*, *105*, 333–341.

Pandolfo, A. G., & Hollenkamp, A. F. (2006). Carbon properties and their role in supercapacitors. In *Journal of Power Sources*, *157*(1), 11-27.

Park, J. H., Rana, H. H., Lee, J. Y., & Park, H. S. (2019). Renewable flexible supercapacitors based on all-lignin-based hydrogel electrolytes and nanofiber electrodes. *Journal of Materials Chemistry A*, *7*(28), 16962–16968.

Peng, H., Lv, Y., Wei, G., Zhou, J., Gao, X., Sun, K., Ma, G., & Lei, Z. (2019). A flexible and self-healing hydrogel electrolyte for smart supercapacitor. *Journal of Power Sources*, *431*, 210–219.

Poy, S. Y., Bashir, S., Omar, F. S., Saidi, N. M., Farhana, N. K., Sundararajan, V., Ramesh, K., & Ramesh, S. (2020). Poly (1-vinylpyrrolidone-co-vinyl acetate) (PVP-co-VAc) based gel polymer electrolytes for electric double layer capacitors (EDLC). *Journal of Polymer Research*, *27*(3).

Rajeshwar, K. (1993). Electrochemistry of semiconductors and electronics processes and devices. *Advanced Materials*, *5*(3), 225 -226

Riva, A., Zanetti, M., Braglia, M., Camino, G., & Falqui, L. (2002). Thermal degradation and rheological behaviour of EVA/montmorillonite nanocomposites. *Polymer Degradation and Stability*, *77*(4), 349-357.

Saborío, M. G., Svelic, P., Casanovas, J., Ruano, G., Pérez-Madrigal, M. M., Franco, L., Torras, J., Estrany, F., & Alemán, C. (2019). Hydrogels for flexible and compressible free standing cellulose supercapacitors. *European Polymer Journal*, *118*, 347–357.

Shaikh, J. S., Pawar, R. C., Moholkar, A. v., Kim, J. H., & Patil, P. S. (2011). CuO-PAA hybrid films: Chemical synthesis and supercapacitor behavior. *Applied Surface Science*, *257*(9), 4389–4397.

Shaikh, J. S., Pawar, R. C., Tarwal, N. L., Patil, D. S., & Patil, P. S. (2011). Supercapacitor behavior of CuO-PAA hybrid films: Effect of PAA concentration. *Journal of Alloys and Compounds*, *509*(25), 7168–7174.

Shivakumara, S., Kishore, B., Penki, T. R., & Munichandraiah, N. (2014). Symmetric supercapacitor based on partially exfoliated and reduced graphite oxide in neutral aqueous electrolyte. *Solid State Communications*, *199*, 26–32.

Silvaraj, D. S., Bashir, S., Hina, M., Iqbal, J., Gunalan, S., Ramesh, S., & Ramesh, K. (2021). Tailorable solid-state supercapacitors based on poly (N-hydroxymethylacrylamide) hydrogel electrolytes with high ionic conductivity. *Journal of Energy Storage*, *35*, 500-513..

Soavi, F., Bettini, L. G., Piseri, P., Milani, P., Santoro, C., Atanassov, P., & Arbizzani, C. (2016). Miniaturized supercapacitors: key materials and structures towards autonomous and sustainable devices and systems. *Journal of Power Sources*, *326*, 717–725.

Stoller, M. D., Murali, S., Quarles, N., Zhu, Y., Potts, J. R., Zhu, X., Ha, H. W., & Ruoff, R. S. (2012). Activated graphene as a cathode material for Li-ion hybrid supercapacitors. *Physical Chemistry Chemical Physics*, *14*(10), 3388–3391.

Stoller, M. D., & Ruoff, R. S. (2010). Best practice methods for determining an electrode material's performance for ultracapacitors. In *Energy and Environmental Science* , *3*(9), 1294 – 1301.

Sui, L., Tang, S., Dai, Z., Zhu, Z., Huangfu, H., Qin, X., Deng, Y., & Haarberg, G. M. (2015). Supercapacitive behavior of an asymmetric supercapacitor based on a Ni(OH)2/XC-72 composite. *New Journal of Chemistry*, *39*(12), 9363–9371.

Tan, H., Chu, C. R., Payne, K. A., & Marra, K. G. (2009). Injectable in situ forming biodegradable chitosan–hyaluronic acid based hydrogels for cartilage tissue engineering. *Biomaterials*, *30*(13), 2499–2506.

Taylor, K., Silver, L., & Cornibert, S. (2019). "Smartphone Ownership Is Growing Rapidly around the World, but Not Always Equally." *Pew Research Center*, (Vol. 5).

Theses, G., & Khawaja, M. (2015). Synthesis and Fabrication of Graphene/ Conducting Polymer/Metal Oxide Nanocomposite Materials for Supercapacitor Applications. *Nanomaterials*, *10*(1), 554-557.

Tiruye, G. A. (2016). Application Of Ionic Liquids, Innovative Polymer Electrolytes And Novel Carbonaceous Materials *In Sensors & Actuators, B: Chemical, 298(4)*, 1613-1617.

Vangari, M., Pryor, T., & Jiang, L. (2013). Supercapacitors: Review of Materials and Fabrication Methods. *Journal of Energy Engineering*, *139*(2), 72–79.

Wang, B., Li, J., Hou, C., Zhang, Q., Li, Y., & Wang, H. (2020). Stable Hydrogel Electrolytes for Flexible and Submarine-Use Zn-Ion Batteries. *ACS Applied Materials & Interfaces*, *12*(41), 46005–46014.

Wang, D., Yu, L., He, B., & Wang, L. (2018). A high-performance carbon-carbon(C/C) quasi-solid-state supercapacitor with conducting gel electrolyte. *International Journal of Electrochemical Science*, *13*(3), 2530–2543.

Wang, G., Zhang, L., & Zhang, J. (2012). A review of electrode materials for electrochemical supercapacitors. *Chemical Society Reviews*, *41*(2), 797–828.

Wang, H., Hao, Q., Yang, X., Lu, L., & Wang, X. (2009). Graphene oxide doped polyaniline for supercapacitors. *Electrochemistry Communications*, *11*(6), 1158–1161.

Wang, H., Wu, J., Qiu, J., Zhang, K., Shao, J., & Yan, L. (2019). In situ formation of a renewable cellulose hydrogel electrolyte for high-performance flexible all-solid-state asymmetric supercapacitors. *Sustainable Energy and Fuels*, *3*(11), 3109–3115.

Wang, H. X., Zhang, W., Chen, H., & Zheng, W. T. (2015). Towards unlocking high-performance of supercapacitors: From layered transition-metal hydroxide electrode to redox electrolyte. In *Science China Technological Sciences* (Vol. 58, Issue 11, pp. 1779–1798). Springer Verlag.

Wang, J. A., Lu, Y. T., Lin, S. C., Wang, Y. S., Ma, C. C. M., & Hu, C. C. (2018). Designing a Novel Polymer Electrolyte for Improving the Electrode/Electrolyte Interface in Flexible All-Solid-State Electrical Double-Layer Capacitors. *ACS Applied Materials and Interfaces*, *10*(21), 17871–17882.

Wang, Z., Li, H., Tang, Z., Liu, Z., Ruan, Z., Ma, L., Yang, Q., Wang, D., & Zhi, C. (2018). Hydrogel Electrolytes for Flexible Aqueous Energy Storage Devices. In *Advanced Functional Materials* (Vol. 28, Issue 48). Wiley-VCH Verlag.

W. D. Callister, & D. G. Rethwisch. (2014). Materials Science and Engineering 9th Edition. *Journal of Computer Science and Engineering, 12(3),231 -245.*

Willfahrt, A., Steiner, E., Hötzel, J., & Crispin, X. (2019). Printable acid-modified corn starch as non-toxic, disposable hydrogel-polymer electrolyte in supercapacitors. *Applied Physics A 2019 125:7*, *125*(7), 1–10.

Winter, M., & Brodd, R. J. (2004). What are batteries, fuel cells, and supercapacitors? *Chemical Reviews*, *104*(10), 4245–4269.

Wu, H.-Y., & Wang, H.-W. (2012). Electrochemical Synthesis of Nickel Oxide Nanoparticulate Films on Nickel Foils for High-performance Electrode Materials of Supercapacitors. In *International Journal of Electrochemical Science ,7*(2), 4405 – 4417.

Wu, L., Li, R., Guo, J., Zhou, C., Zhang, W., Wang, C., Huang, Y., Li, Y., & Liu, J. (2013). Flexible solid-state symmetric supercapacitors based on MnO2 nanofilms with high rate capability and long cyclability. *AIP Advances*, *3*(8), 194-203.

Xie, Y., Sheng, X., Xie, D., Liu, Z., Zhang, X., & Zhong, L. (2016). Fabricating graphene hydrogels with controllable pore structure via one-step chemical reduction process. *Carbon*, *109*, 673–680.

Yang, C. M., Kim, Y. J., Endo, M., Kanoh, H., Yudasaka, M., Iijima, S., & Kaneko, K. (2007). Nanowindow-regulated specific capacitance of supercapacitor electrodes of single-wall carbon nanohorns. *Journal of the American Chemical Society*, *129*(1), 20–21.

Yang, H., Ji, X., Tan, Y., Liu, Y., & Ran, F. (2019). Modified supramolecular carboxylated chitosan as hydrogel electrolyte for quasi-solid-state supercapacitors. *Journal of Power Sources*, *441*(1), 181-196.

Yang, H., Kannappan, S., Pandian, A. S., Jang, J. H., Lee, Y. S., & Lu, W. (2017). Graphene supercapacitor with both high power and energy density. *Nanotechnology*, *28*(44), 347-353.

Yang, L., Song, L., Feng, Y., Cao, M., Zhang, P., Zhang, X. F., & Yao, J. (2020). Zinc ion trapping in a cellulose hydrogel as a solid electrolyte for a safe and flexible supercapacitor. *Journal of Materials Chemistry A*, *8*(25), 12314–12318.

Yoo, H. S. (2012). Photo-cross-linkable and thermo-responsive hydrogels containing chitosan and Pluronic for sustained release of human growth hormone (hGH). *Journal of Biomaterials Science, Polymer Edition*, *18*(11), 1429–1441.

Zang, X., Shen, C., Sanghadasa, M., & Lin, L. (2019). High-Voltage Supercapacitors Based on Aqueous Electrolytes. In *ChemElectroChem* (Vol. 6, Issue 4, pp. 976–988). Wiley-VCH Verlag.

Zeng, J., Dong, L., Sha, W., Wei, L., & Guo, X. (2020). Highly stretchable, compressible and arbitrarily deformable all-hydrogel soft supercapacitors. *Chemical Engineering Journal*, *383*(7), *1106-1114*.

Zhang, H., Niu, W., & Zhang, S. (2020). Extremely stretchable, sticky and conductive double-network ionic hydrogel for ultra-stretchable and compressible supercapacitors. *Chemical Engineering Journal*, *387(1)*, 6112-6125.

Zhang, R. (2016). *A Study Of Flexible Supercapacitors: Design, Manufacture And Testing*. *The Journal of the Mexican Chemical Society*, *63*, 155–163.

Zhang, S., & Pan, N. (2015). Supercapacitors performance evaluation. In *Advanced Energy Materials* (Vol. 5, Issue 6). Wiley-VCH Verlag.

Zhao, C., & Zheng, W. (2015). A review for aqueous electrochemical supercapacitors. *Frontiers in Energy Research* (Vol. 3, Issue May). Frontiers Media S.A.

Zhao, N., Wu, F., Xing, Y., Qu, W., Chen, N., Shang, Y., Yan, M., Li, Y., Li, L., & Chen, R. (2019). Flexible Hydrogel Electrolyte with Superior Mechanical Properties Based on Poly(vinyl alcohol) and Bacterial Cellulose for the Solid-State Zinc-Air Batteries. *ACS Applied Materials and Interfaces*, *11*(17), 15537–15542.

Zhong, C., Deng, Y., Hu, W., Qiao, J., Zhang, L., & Zhang, J. (2015). A review of electrolyte materials and compositions for electrochemical supercapacitors. In *Chemical Society Reviews* (Vol. 44, Issue 21, pp. 7484–7539). Royal Society of Chemistry.

Zhou, W., Liu, J., Chen, T., Tan, K. S., Jia, X., Luo, Z., Cong, C., Yang, H., Li, C. M., & Yu, T. (2011). Fabrication of Co3O4-reduced graphene oxide scrolls for high-performance supercapacitor electrodes. *Physical Chemistry Chemical Physics*, *13*(32), 14462–14465.

Zhu, A., Shi, Z., Jin, J., Li, G., & Jiang, J. (2012). Synthesis and properties of polyacrylamide-based conducting gels with enhanced mechanical strength. *Journal of Macromolecular Science, Part B: Physics*, *51*(11), 2183–2190.